Be on Your Guard: Options Markets and Safety-Related Small Maturity Phenomena

Gurdip Bakshi[1], John Crosby[2], Xiaohui Gao[3], and Jorge W. Hansen[4]

[1]Fox School of Business, Temple University, gurdip.bakshi@temple.edu
[2]Strome College of Business, Old Dominion University, acrosby@odu.edu
[3]Fox School of Business, Temple University, xiaohui.gao.bakshi@temple.edu
[4]Aarhus University and the Danish Finance Institute, jh@econ.au.dk

May 26, 2025

Abstract

To analyze small maturity phenomena related to safety in markets, we develop a model to explain observable patterns: a positive correlation between the returns of out-of-the-money (OTM) Treasury bond futures calls and S&P 500 stock puts, lack of correlation between the returns of OTM bond puts and stock calls, and a decrease in the VVIX/VIX ratio during times of market stress. The estimated model is based on a theory of bivariate jump distributions for the bond's upside (downside) and the stock's downside (upside) supported by two stochastic jump intensities and is validated empirically by small maturity findings that encompass 15 variables.

Keywords: Matched small maturity options on S&P 500 index and options on Treasury bond futures; bivariate jump distributions; stochastic jump intensity rates; estimated models

Revised draft: May 2025. Seminar participants at Aarhus University, Copenhagen Business School, the University of Maryland, Old Dominion University, Temple University, Midwestern Finance Association, EFA, Cancun, and Montreal meetings provided useful feedback. We acknowledge helpful discussions with Torben Andersen, Fousseni Chabi-Yo, Andrew Chen, Tim Christensen, Jaroen Dalderop, Dobrislav Dobrev, Andrey Ermolov, Steve Heston, Yuan Hu, Pete Kyle, Mark Loewenstein, Juan Londono, Dmitriy Muravyev, Valery Polkovnichenko, Matt Pritzker, Tobias Sichert, Min Wei, Lai Xu, Jinming Xue, Zhaowei Zhang, and Wei Zhou.

1 Introduction

This paper provides insights into small maturity phenomena by exploiting advancements in the simultaneous trading of seven-day (Friday to Friday) and one-day (Thursday to Friday) expiry options on Treasury bond futures and the S&P 500 stock index. A novel aspect is the time-matching of option payoffs for small maturity options across bond and stock markets.

This development on the data front allows us to analyze option prices and synchronous payoffs observed across four separate markets: Treasury bond futures, the S&P 500 index, options on the Treasury bond futures, and options on the S&P 500 index. These markets are instrumental to understanding the trading behaviors, changes in asset allocations, pricing, and concerns of bond and stock investors over a small horizon. Over the course of 630 weekly option expiration cycles from January 28, 2011, to February 24, 2023, we examine state-contingent returns pertinent to small maturity. This joint time-series of state-contingent returns on bond and stock has not yet been studied. To integrate market-wide small maturity phenomena, we combine this data with small maturity options on VIX futures.

A. Unique characteristics of state-contingent returns of bond and stock. Our investigation examines the connection between bond and stock markets and their respective option markets, in addition to providing evidence on their determinants and joint pricing. A key finding is the strong positive correlation between returns to buying OTM calls on bond and OTM puts on stock, contrasting the much weaker correlation between returns to buying puts on bond and calls on stock.

We develop a model that incorporates simultaneous down and up price jumps in stock and bond markets, which aligns with our empirical results. Furthermore, we provide an economic explanation for the documented small maturity phenomena: Investors solicit protection against both downward stock movements and upward bond movements. During times of market stress, both forms of protection are in demand, likely due to investors seeking safer investments. Our findings are reinforced by this explanation, with evidence to support it.

Our analysis indicates that there is a need for jumps in both directions in bond futures prices to explain the observed small maturity pattern of option returns. Extant models that derive bond futures prices do not incorporate this feature. Therefore, our findings from options and stock-bond associations may challenge these models in terms of both explaining and incorporating them.

B. Reconciling gaps in prevailing theories by modeling two Poisson processes, each with stochastic intensity rates. Our model accounts for the tendency of bond prices to jump up when stock prices jump down. Additionally, when stock prices jump up, bond prices are allowed to jump down, but the association is weaker than when stock prices jump down. The intensity rate of down (up) jumps in stock is associated with bad (good) news. Our premise of simultaneous price jumps is supported by the empirical specification exercises advocated by Barndorff-Nielsen and Shephard (2006) and Dumitru and Urga (2012).

In the context of small maturity option expirations, the properties of state-contingent returns can be attributed to the structure of price jumps in stock and bond. We model these discontinuities through the marginal and bivariate distributions of down (up) and up (down) jumps in stock (bond). The real-world and risk-neutral jump measures are modeled to respect empirical observations.

Our theory aligns with state-contingent stock and bond returns that can change with market conditions, necessitating stochastic intensity rates. We model these influences on the returns of stock and bond options using two — as opposed to one or four — Poisson processes, each with a stochastic intensity rate. Providing a rationale for our approach, we show that the Merton (1976) model, modified to have a single stochastic jump intensity, cannot generate imperfect small maturity correlations between state-contingent returns of stock and bond.

The essence of our approach is that the returns of bond calls can be positively correlated with those of stock puts. This small maturity relationship can be attributed to flight-to-quality effects, which are evident during market declines. The asymmetrical correlation between the state-contingent returns of bond and stock — constructed using Friday-to-Friday (7DTE) and Thursday-to-Friday (1DTE) options — is our salient modeling aspect and has not been previously explored.

C. Benchmarking our data, findings, and estimated model to the literature. Our modeling approach formulates option prices, correlations between state-contingent returns, and volatilities. This approach — utilized in our estimation procedure — assumes that stock prices can jump down or up according to an exponential distribution, as can bond prices but in the opposite direction.

We examine the applicability of the model through empirical exercises. We use weekly puts and calls on bond and stock, along with intraday calculated seven-day realized volatilities and VIX data

from Treasury bond futures and S&P 500 index. We find that the model reasonably represents the data, revealing evidence in favor of simultaneous (negatively correlated) jumps in bond and stock.

Our framework introduces two novelties for small maturity options. First, it takes into account the risks associated with price jumps, recognizing their significant role in generating option values. Second, it acknowledges that diffusive volatility is not as relevant for small maturity options (as framed in Aït-Sahalia (2004), Bollerslev and Todorov (2011), Aït-Sahalia and Jacod (2012), Andersen, Fusari, and Todorov (2017), and Bakshi, Crosby, and Gao (2022)). Specifically, we examine conditions that reveal a potential correlation between buying bond calls and buying stock puts, which implies the need to incorporate jump intensities of two types, namely, "bad news" and "good news." Previous research has investigated weekly options on the S&P 500 index, but there is a gap in knowledge about weekly options on bond futures (see Bakshi, Crosby, Gao, and Hansen (2023)).

Unlike our investigation, extant studies do not consider state-contingent returns constructed from small maturity options or the impact of simultaneous price jumps in stock and bond markets. By utilizing the Ang and Chen (2002) method to reveal asymmetric exceedance correlations, we convey further understanding of small maturity data. Studies examining the low-frequency relationship between stock and bond returns include, among others, Baele, Bekaert, and Inghelbrecht (2010), David and Veronesi (2013), Wachter (2013), and Campbell, Pflueger, and Viceira (2020).[1]

D. Empirical findings and small maturity phenomena. A substantive finding of our study is the robust positive correlation between returns from buying OTM call options on bond and OTM put options on stock, compared to the weaker and statistically insignificant correlation between returns from buying OTM put options on bond and OTM call options on stock. Bolstering confidence, this idea remains consistent in a bootstrap exercise that pairwise compares correlation magnitudes.

These findings suggest that there is a common factor, likely a bad news jump factor with a stochastic intensity rate, that is a major influencer of (a) price increases in bond, (b) price decreases in stock, and (c) OTM call option prices on bond and OTM put option prices on stock. We also observe evidence of a second common factor, a good news jump factor, which drives price

[1]We add to the understanding of the stock, bond, and traded volatility markets by addressing theories of small maturity contingent claims by incorporating simultaneous jumps in the context of estimated models. Furthermore, we identify the characteristics of state-contingent returns of bond and stock and the link to safety phenomena in these markets. Our approach stands out from studies, such as those of Connolly, Sun, and Stivers (2005), Andersen, Bollerslev, Diebold, and Vega (2007), Campbell, Sunderam, and Viceira (2017), Baele, Bekaert, Inghelbrecht, and Wei (2020), Cieslak and Pang (2021), Ermolov (2022), and Kozak (2022).

decreases in bond and increases in stock, but with a smaller average magnitude. This perspective is supported by our findings on the relationship between the option payoffs standardized by the underlier price on the upside (downside) of bond and on the downside (upside) of stock markets.

E. Empirical consistency of the estimated model with small maturity phenomena. In this study, we propose a four-state variable model that incorporates both stochastic volatility and stochastic jump intensity rates for stock and bond contingent claims. Our goal is to improve upon existing models, which do not take into account priced down and priced up risks. To estimate this model, we use the Kalman filter in combination with quasi-maximum likelihood.

Through our study, we make empirical contributions by demonstrating that our model is able to generate realistic bond and stock return volatilities. Moreover, the model shows a quantitative agreement with both seven-day bond VIX and stock VIX, indicating that our model aligns with risk-neutral volatilities and embedded risk premiums. Furthermore, our model captures the characteristics of the joint cross-section of stock and bond options, which have not been considered by previous models. Overall, our approach takes us a step closer to better understanding and addressing multiple aspects — 15 data variables — of the Treasury bond futures and stock markets.

We also evaluate the model's performance with regard to the behavior of the small maturity VVIX to stock VIX ratio. This ratio reflects the relative cost of hedging against upside market volatility (via small maturity calls on VIX futures) compared to downside S&P 500 index protection (via small maturity stock index puts). This exercise is significant for two reasons. First, it allows us to understand how well the model quantitatively captures the ratio of VVIX to stock VIX during times of market stress. Second, the derived VVIX values are informative about the model's internal consistency. Hence, validating these model aspects is pertinent and informative.

Setting a bar for model consistency, we further assess the model's ability to forecast small maturity correlations between stock and bond returns. Our estimated model is compatible with negative values for the stock-bond correlation, aligning with essential features of associations between stock and bond option payoffs.

Our framework offers a way for evaluating and distinguishing between models. Previous literature has not analyzed small maturity patterns of state-contingent claims of bond and stock, joint drivers of options on bond and the S&P 500 index, and the intersection of volatilities of bond and

stock returns. This makes our estimated model a contribution to the field, offering an economically meaningful perspective on the relationship between small maturity stock and bond returns, with implications for both small maturity asset pricing and economic analysis.

2 The nature of small maturity phenomena in markets

Our empirical investigation centers on the relationship between short maturity options on the Treasury bond futures and those on the S&P 500 stock index (augmented later by small maturity options on traded stock volatility). We consider data of correlations between option excess returns on both bond and stock. Four distinct pairs are examined: $(\mathbb{r}^{\mathbf{b},\,\text{call}}, \mathbb{r}^{\mathbf{s},\,\text{put}})$, $(\mathbb{r}^{\mathbf{b},\,\text{put}}, \mathbb{r}^{\mathbf{s},\,\text{call}})$, $(\mathbb{r}^{\mathbf{b},\,\text{put}}, \mathbb{r}^{\mathbf{s},\,\text{put}})$, and $(\mathbb{r}^{\mathbf{b},\,\text{call}}, \mathbb{r}^{\mathbf{s},\,\text{call}})$. The first option return in every pair represents the bond ($\mathbf{b}$), while the second represents the stock ($\mathbf{s}$). The options under analysis have a small maturity — seven-day or one-day — and standardized moneyness connected to option deltas, δ, of $\pm$ 20 (OTM) or $\pm$7 (deeper OTM). Of the correlations that are analyzed, only the $(\mathbb{r}^{\mathbf{b},\,\text{call}}, \mathbb{r}^{\mathbf{s},\,\text{put}})$ pair exhibits a significantly positive correlation, while the remaining three are weaker and/or statistically indistinct from zero.

Our empirical results motivate the development of a continuous-time model to explain and understand the joint dynamics of bond and stock returns. This model captures features of stochastic volatility and simultaneous upward and downward jumps in the prices of bond and stock. One possible explanation for the documented correlation pattern is the higher cost — relative to the expected payoff — for protective measures in times of market stress, as well as a preference for safer investments during periods of volatile market conditions. This model recognizes mechanisms influencing the observed small-maturity option relationships.

Weekly options on futures on the 10-year Treasury bond and the S&P 500 index are actively traded on the Chicago Mercantile Exchange and the Chicago Board of Options Exchange, respectively. The novelty is that these options expire each Friday (PM-settled), allowing us to address questions related to asymmetry of state-contingent returns, for both the Treasury bond futures and the S&P 500 index, in addition to properties of their correlations.

The prices of stock (cum-dividend) are represented by S_t and the prices of futures on the stock by $F_t^{\mathbf{s}}$. Similarly, $F_t^{\mathbf{b}}$ represents the futures price on bond. The matched sample of weekly expiring options on futures on the 10-year Treasury bond and the S&P 500 spans the period of January 28,

2011, to February 24, 2023, with 630 cycles. We denote the stock (bond) option strike price by $K^{\mathbf{s}}$ ($K^{\mathbf{b}}$).

At the beginning of weekly expiration cycles (Friday initiation), we focus on options on stock, where OTM puts (calls) are associated with moneyness $k^{\mathbf{s}} \equiv \frac{K^{\mathbf{s}}}{S_t} < 1$ ($k^{\mathbf{s}} > 1$). We adopt the same approach for options on bond futures (i.e., $k^{\mathbf{b}} \equiv \frac{K^{\mathbf{b}}}{F_t^{\mathbf{b}}}$), considering strikes — by enforcing comparable deltas — that account for the higher stock volatility than bond volatility. For example, the weekly return volatility for 10-year bond futures is 0.7%, compared to 2.24% for the S&P 500.

The impact of downward and upward price jumps and perceptions of tail risks in the stock and bond markets can be inferred through OTM state-contingent returns. We compute the excess returns of buying OTM options on stock with fixed-option delta, denoted $\delta^{\mathbf{s}}$, as follows:

$$\mathbb{r}^{\mathbf{s},\,\text{put}}_{\{t\to t+\Delta\}}[k^{\mathbf{s}}] = \frac{[K^{\mathbf{s}} - S_{t+\Delta}]^+}{\text{put}_t[K^{\mathbf{s}}]} - R_t^{\text{rf}}, \text{ where strike } K^{\mathbf{s}} \text{ corresponds to } \delta^{\mathbf{s}} \text{ of } -20 \text{ or } -7 \text{ and} \quad (1)$$

$$\mathbb{r}^{\mathbf{s},\,\text{call}}_{\{t\to t+\Delta\}}[k^{\mathbf{s}}] = \frac{[S_{t+\Delta} - K^{\mathbf{s}}]^+}{\text{call}_t[K^{\mathbf{s}}]} - R_t^{\text{rf}}, \text{ where strike } K^{\mathbf{s}} \text{ corresponds to } \delta^{\mathbf{s}} \text{ of } 20 \text{ or } 7. \quad (2)$$

The option holding period is from t to $t+\Delta$, where Δ is the time to maturity of the option, and $\text{put}_t[K]$ ($\text{call}_t[K]$) is the price of a put (call) with strike K. Additionally, $[a]^+ \equiv \max(a, 0)$ and R_t^{rf} is the gross risk-free return over Δ (known at time t).

Accounting for differences in return volatilities across stock and bond, we similarly compute the returns of buying OTM options on bond futures with fixed delta $\delta^{\mathbf{b}}$. These bond option returns — following equations (1) and (2) — are denoted by $\mathbb{r}^{\mathbf{b},\,\text{put}}_{\{t\to t+\Delta\}}[k^{\mathbf{b}}]$ and $\mathbb{r}^{\mathbf{b},\,\text{call}}_{\{t\to t+\Delta\}}[k^{\mathbf{b}}]$.

Table 1 (Panels A and B) displays the characteristics of these 7DTE option returns in both Treasury bond and stock markets. Dollar open interest and volume associated with these small maturity options is sizable. The returns of both 20 and 7 delta call options for bond futures and stock are not pairwise significantly different, as shown by the stationary bootstrap confidence intervals (Panel C of Table 1). Moreover, the average excess returns of OTM puts on bond are less negative than those on stock. These findings suggest consistent investor behavior in the bond and stock markets, as manifested in the shared signs of average state-contingent returns.

To set the stage for discussing the correlations between stock and bond option returns, we first employ the modeling of the conditional joint distribution of stock and bond returns in Ang and Chen

(2002). Their methodology targets exceedance return correlations benchmarked to the bivariate normal distribution based on sigma event thresholds and without using options data. Adopting their approach over the extended sample period of January 5, 1990, to February 23, 2023 (1,781 observations), we report exceedance correlation statistics for seven-day stock and bond futures returns in Table 2. The meaning of reported H^- (Ang and Chen (2002, equation (15), page 464)) in row (a) is that conditional on the downside pairing of $\log(F^{\mathbf{s}}_{t+\Delta}/F^{\mathbf{s}}_t)$ and $\{-\log(F^{\mathbf{b}}_{t+\Delta}/F^{\mathbf{b}}_t)\}$, the correlations differ from the bivariate normal counterparts by 23%. This H^- statistic for negative sigma thresholds significantly differs from H^+ of 18% for positive sigma thresholds in row (b).

The bootstrap p-value for $\mathrm{H}^- < \mathrm{H}^+$ is 0.02, which is reinforced by the two-sided p-value of 0.07 using the test of Hong, Tu, and Zhou (2006, equation (8)). To summarize, the consequential finding — with respect to our analysis of protective measures — is asymmetric return correlation effects over small maturity: Losses on stock declines are accompanied by gains on rising Treasury bond futures (as mirrored by losses on the short Treasury bond futures position).

Our principal innovation is uncovering the relationship between the returns of OTM calls on bond and OTM puts on stock. For this exercise, we calculate the following sample correlations:

$$\rho[\delta^{\mathbf{b}},\ \delta^{\mathbf{s}}] \text{ corresponds to the return correlation with } \delta^{\mathbf{b}}(\delta^{\mathbf{s}}) \text{ of } 20\ (-20) \text{ and } 7\ (-7).$$

Our approach, which is based on small-maturity option returns, is in line with the method used by Hong, Tu, and Zhou (2006, equation (9)) and is effective in analyzing the characteristics of state-contingent correlations between stock and bond returns.

In Table 3 (column I), the full sample correlations of 7DTE call returns on bond and 7DTE put returns on stock range from 0.28 to 0.47, whereas the mean 52-week rolling correlations range from 0.25 and 0.43. These correlations are significantly positive, as evidenced by the stationary bootstrap confidence intervals (displayed in square brackets).

These findings can be interpreted as quantifying the impact of de-risking strategies. Specifically, they suggest that investors tend to reallocate their portfolios from riskier stocks to more secure bonds during weeks marked by significant stock market declines. In times of volatility, many investors choose to shift their focus to Treasuries, which offer both quality and liquidity. Thus, calls

on bond are desirable and offer a layer of protection when stocks perform poorly. This relationship is evident through the positive correlation between the returns of OTM bond calls and stock puts.

Emphasizing this part of our analysis, we next construct data on options with even smaller maturity given by 1DTE. We note that our estimation approach is based on asymptotics as $\Delta \to 0$, where the effects of diffusive return volatility diminish and price jumps become the determining factor in shaping OTM option prices. Thus, examining 1DTE options is aligned with the underlying premise of our investigation. We utilize 630 daily expiration cycles, with each cycle occurring every week from Thursday PM initiation to Friday PM expiration,[2] rather than from Friday to Friday. Compatible with our findings, Table 3 (column II) shows that the full sample correlations of 1DTE call returns on bond and 1DTE put returns on stock are positive and range from 0.20 to 0.25.

Table 3 (Panel B) shows the correlations between the returns of buying OTM puts on bond and buying OTM calls on stock. Specifically,

$$\rho[\delta^{\mathbf{b}},\ \delta^{\mathbf{s}}] \text{ corresponds to the return correlation with } \delta^{\mathbf{b}}(\delta^{\mathbf{s}}) \text{ of } -20\ (20) \text{ and } -7\ (7).$$

In comparison to Table 3 (Panel A), the correlations in Panel B are noticeably lower, and the bootstrap confidence intervals bracket zero. Equally relevant to the big picture, our findings in Table 3 (Panels C and D) demonstrate near-zero correlations between returns of OTM puts (calls) of bond and returns of OTM puts (calls) of stock.

In support of our arguments, we perform a bootstrap exercise aimed to determine whether the correlation between $(\mathbb{r}^{\mathbf{b},\ \text{call}}, \mathbb{r}^{\mathbf{s},\ \text{put}})$ for a specific delta is statistically higher than the correlations among the other three option return pairs: $(\mathbb{r}^{\mathbf{b},\ \text{put}}, \mathbb{r}^{\mathbf{s},\ \text{call}})$, $(\mathbb{r}^{\mathbf{b},\ \text{put}}, \mathbb{r}^{\mathbf{s},\ \text{put}})$, and $(\mathbb{r}^{\mathbf{b},\ \text{call}}, \mathbb{r}^{\mathbf{s},\ \text{call}})$. Stationary bootstrap p-values generated in Table 4 (Panel A) imply that the correlations between the returns of bond calls and stock puts are generally higher, in comparison with the remaining pairs of option returns and delta configurations. The substantive message is that stock and bond markets are more interconnected when there are upward jumps in bond and downward jumps in stock.

We acknowledge that our analysis leans on tail returns and the results underscore the varying nature of correlations based on return percentiles. Such an analysis alludes to the difficulties of estimating tail associations (e.g., Longin and Solnik (2001), Ang and Chen (2002), and Patton (2006)). To strengthen interpretations, we derive standardized option payoff outcomes and investigate the

[2]See Internet Appendix (Table I-1) for the empirical properties of one-day option returns.

consistency of their correlation profiles. These standardized payoffs, namely $\frac{[F^{\mathbf{b}}_{t+\Delta}-K^{\mathbf{b}}]^+}{F^{\mathbf{b}}_t}$ for upside of bond and $\frac{[K^{\mathbf{s}}-S_{t+\Delta}]^+}{S_t}$ for downside of stock, do not require option prices and can be determined over the extended sample of January 5, 1992, to February 23, 2024 (1,781 cycles (as in Table 2)). Although option payoffs normalized by underlying prices are not equal to those normalized by option prices, they inform correlations among the respective state-contingent returns. Table 5 reveals significant evidence of interdependence between bond and stock markets.

A key takeaway is the positive correlations of standardized option payoffs to the upside of bond and downside of stock. Conversely, and as anticipated, we observe weaker correlations between the downside of bond and upside of stock. Emphasizing our justification, Table 4 (Panel B) shows the broader validity of our central findings by scrutinizing the bootstrap-based p-values between correlation pairs. This analysis supports the notion that $\frac{[F^{\mathbf{b}}_{t+\Delta}-K^{\mathbf{b}}]^+}{F^{\mathbf{b}}_t}$ and $\frac{[K^{\mathbf{s}}-S_{t+\Delta}]^+}{S_t}$ display statistically higher correlation in comparison to other combinations.

The analysis conducted in Tables 3, 4, and 5 reveals certain asymmetries in the correlations of small maturity state-contingent payoffs. Specifically, we observe that during significant downward movements in stock prices, bond prices tend to increase (reflecting a flight-to-quality effect). However, in contrast, when stock prices are optimistic, bond prices do not decrease correspondingly, indicating a lack of retreat-from-quality. These findings pose a challenge for models that aim to align the characteristics of state-contingent stock and bond returns across market conditions.

We delve into the link between bond and stock markets, offering insight and support for this relationship. Our fundamental distinction is that we establish an elevated correlation between returns of bond calls and stock puts, indicating a tendency for investors to safeguard against adverse market declines. During such times, both types of protection are revealed to be more costly. These appraisals agree with the evidence from exceedance correlations shown in Table 2.

To enhance our results from a related perspective, we investigate economic relationships and the preference for safer investments during times of stress and high market volatility, using futures returns of stock and bond. In support of our evidence, we utilize synchronized intraday stock and bond returns data at five-minute intervals aligned with the Friday-to-Friday horizon.[3] Our analysis,

[3]Extant empirical understanding is often centered on the equivalence between covariances of five-minute returns and longer-horizon moment constructs (over seven days or 22 days). See the estimation approaches in, among others, Andersen, Bollerslev, Diebold, and Labys (2003), Barndorff-Nielsen and Shephard (2004), Lee and Mykland (2008),

developed in Table 6, yields one central connecting finding: The stock-bond correlation — which correlates with stress variables (shown in column CORR) — is more negative during periods of unfavorable economic conditions.

We uncover this aspect by investigating the environment that motivates flight-to-safety protections over small horizon. The specific evidence is based on the following regression framework:

$$\rho_{t+\Delta} = \overline{\rho}_{\{\mathcal{F}_t \in \mathfrak{s}_{\text{bad}}\}} \times \mathbb{1}_{\{\mathcal{F}_t \in \mathfrak{s}_{\text{bad}}\}} + \overline{\rho}_{\{\mathcal{F}_t \in \mathfrak{s}_{\text{normal}}\}} \times \mathbb{1}_{\{\mathcal{F}_t \in \mathfrak{s}_{\text{normal}}\}} + \overline{\rho}_{\{\mathcal{F}_t \in \mathfrak{s}_{\text{good}}\}} \times \underbrace{\mathbb{1}_{\{\mathcal{F}_t \in \mathfrak{s}_{\text{good}}\}}}_{\text{indicator variable}} + \underbrace{\epsilon_{t+\Delta}}_{\text{error term}}. \quad (3)$$

The stock-bond return correlation — denoted by $\rho_{t+\Delta}$ — is negative for 86.5% of the weeks. We consider nine variables, known at time t, denoted by $\mathcal{F}_t$, as proxies for economic states, such as stress indicators and VIX futures return variances constructed at five-minute intervals. For example, $\overline{\rho}_{\{\mathcal{F}_t \in \mathfrak{s}_{\text{bad}}\}}$ represents the average stock-bond correlation when VIX futures return variance is high. Equation (3) decomposes the correlation into its components in different economic states.

Our analysis is based on the one-sided p-values from the Wald test of $\overline{\rho}_{\{\mathcal{F}_t \in \mathfrak{s}_{\text{bad}}\}} = \overline{\rho}_{\{\mathcal{F}_t \in \mathfrak{s}_{\text{good}}\}}$. The pattern is that the stock-bond correlations are more negative in pessimistic states compared to those in optimistic states. This evidence is in line with our theory that argues that investors are willing to pay a higher premium for protection during periods of heightened economic uncertainty. Additionally, the fluctuations in the seven-day stock-bond correlation are predictable. This is demonstrated by seven significant predictive slope coefficients. Indicative of low levels of predictability over a small horizon, the $\overline{R}^2$ (shown in column $\overline{R}^2_{\text{predictive}}$) range from 0.1% to 14.8%.

In sum, our analysis reveals how combinations of calls on bond and puts on stock serve to neutralize bad uncertainty. Consistent with returns on calls on bond and puts on stock being driven by adverse jumps, our analysis of stock-bond correlation reveals sizable influence of economy-wide variables. We identify the concentration of shocks that markets dislike and that warrant safety.

Our empirical findings arise from the data gathered on small maturity — 7DTE and 1DTE — options on Treasury bond futures and the S&P 500 index. Since monthly stock and bond options have different expiration dates, it is not feasible to use a time-series of paired monthly expiring options to calculate correlations between stock and bond option returns. We next consider a model that aligns with our findings on small maturity phenomena and that can be estimated.

Bollerslev, Tauchen, and Zhou (2009, page 4477), Aït-Sahalia, Fan, and Xiu (2010), Amaya, Christoffersen, Jacobs, and Vasquez (2015, Section 2), and Liu, Patton, and Sheppard (2015, Section 2).

3 A model of small maturity phenomena and price jumps

New to our study, we highlight return phenomena that are entwined across multiple trading venues: stock and bond futures as well as small maturity puts and calls written on stock and bond. In this section, we theoretically address the return properties of stock and bond options over t to $t+\Delta$ and their covariances. Specifically, Δ represents a short holding period. Our contribution is the modeling of simultaneous price jumps in stock and bond markets.

To support our model assumption of simultaneous stock and bond price jumps, we utilize the Barndorff-Nielsen and Shephard (2006) test for jump identification — tailored to detect cojumps — in conjunction with a bootstrap analysis. This test compares realized quadratic variation with bipower variation: A significant and sizable difference indicates a jump.

In implementation, we consider returns at the 15-minute frequency, as this is the frequency at which the percentage of jumps stabilizes in our data (as suggested by Dumitru and Urga (2012)). We define simultaneous jumps as instances where both assets' jump test statistics exceed the 5% critical value (Jacod and Todorov (2009)). Our bootstrap exercise rejects the hypothesis of non-simultaneous price jump movements with a p-value of 0.03. This evidence supports the notion that jumps in the stock and bond markets are interconnected. Equally crucial, these simultaneous price jumps are negatively associated.

Fixing notations, let $(\Omega, \mathcal{F}, (\mathcal{F}_t)_{0\leq t\leq \mathfrak{T}}, \mathbb{P})$ be a filtered probability space, with $\mathfrak{T}$ being a fixed finite time. The filtration $(\mathcal{F}_t)_{0\leq t\leq \mathfrak{T}}$ satisfies the usual conditions. Stochastic processes are assumed to be right-continuous with left limits. Let $\mathbb{P}$ denote the real-world probability measure.

In the presence of price jumps, markets are not complete. Hence, there is neither a unique risk-neutral measure nor a unique pricing kernel. We consider a risk-neutral measure, $\mathbb{Q}$, consistent with the absence of arbitrage. Let $\mathbb{E}_t^{\mathbb{P}}(\bullet) \equiv \mathbb{E}^{\mathbb{P}}(\bullet|\mathcal{F}_t)$ ($\mathbb{E}_t^{\mathbb{Q}}(\bullet) \equiv \mathbb{E}^{\mathbb{Q}}(\bullet|\mathcal{F}_t)$) denote expectation under $\mathbb{P}$ ($\mathbb{Q}$) conditional on $\mathcal{F}_t$. The spot interest-rate, r_t, is assumed to evolve stochastically and the zero-coupon bond price, maturing at $t+\Delta$, is given by $B_t^{t+\Delta} \equiv \mathbb{E}_t^{\mathbb{Q}}(e^{-\int_t^{t+\Delta} r_\ell \, d\ell})$.

For our analysis, let $F_{t-}^{\mathbf{s}}$ ($F_{t-}^{\mathbf{b}}$) denote the pre-jump futures price of the stock (bond). We note that $\max(K^{\mathbf{s}} - F_{t+\Delta}^{\mathbf{s}}, 0) = \max(K^{\mathbf{s}} - S_{t+\Delta}, 0)$ and $\max(F_{t+\Delta}^{\mathbf{s}} - K^{\mathbf{s}}, 0) = \max(S_{t+\Delta} - K^{\mathbf{s}}, 0)$.

We assume that the dynamics of $F_t^{\mathbf{s}}$, under $\mathbb{P}$, are as follows:

$$
\begin{aligned}
\frac{dF_t^{\mathbf{s}}}{F_{t-}^{\mathbf{s}}} &= \mu_t^{\mathbf{s},\mathbb{P}}\,dt \;+\; \overbrace{\sqrt{V_t^{\mathbf{s}}}\,dW_t^{\mathbf{s},\mathbb{P}}}^{\text{diffusive part}} \\
&+ \underbrace{(e^{x^{\mathbf{s}+}}-1)\,d\mathbb{N}_t^{[\text{good}],\mathbb{P}}}_{\text{upside stock jump component}} - \underbrace{\lambda_t^{[\text{good}],\mathbb{P}}}_{\text{stochastic}}\,dt\int_0^\infty (e^{x^{\mathbf{s}+}}-1)\,\underbrace{\mathbb{p}[x^{\mathbf{s}+}]}_{\mathbb{P}\text{ density}}\,dx^{\mathbf{s}+} \\
&+ \underbrace{(e^{-x^{\mathbf{s}-}}-1)\,d\mathbb{N}_t^{[\text{bad}],\mathbb{P}}}_{\text{downside stock jump component}} - \underbrace{\lambda_t^{[\text{bad}],\mathbb{P}}}_{\text{stochastic}}\,dt\int_0^\infty (e^{-x^{\mathbf{s}-}}-1)\,\underbrace{\mathbb{p}[x^{\mathbf{s}-}]}_{\mathbb{P}\text{ density}}\,dx^{\mathbf{s}-}. \qquad (4)
\end{aligned}
$$

In (4), $\mu_t^{\mathbf{s},\mathbb{P}}$ is the time t (instantaneous) stock futures risk premium (allowed to vary stochastically), $\sqrt{V_t^{\mathbf{s}}}$ is the diffusive stock stochastic volatility, and $W_t^{\mathbf{s},\mathbb{P}}$ is a standard Brownian motion under $\mathbb{P}$.

The following description is instructive in our context of small maturity options:

- $\lambda_t^{[\text{good}],\mathbb{P}}$ ($\lambda_t^{[\text{bad}],\mathbb{P}}$) denotes the intensity rate of the Poisson process $\mathbb{N}_t^{[\text{good}],\mathbb{P}}$ producing up jumps ($\mathbb{N}_t^{[\text{bad}],\mathbb{P}}$ producing down jumps) in the stock futures price.
- Up jumps in the stock futures price are denoted by $x^{\mathbf{s}+}$, with $x^{\mathbf{s}+}>0$. Down jumps are given by $-x^{\mathbf{s}-}$, with $x^{\mathbf{s}-}>0$. This treatment implies that down jumps are of magnitude $x^{\mathbf{s}-}$. The marginal density under $\mathbb{P}$ of up jumps is $\mathbb{p}[x^{\mathbf{s}+}]$, and that of down jumps is $\mathbb{p}[x^{\mathbf{s}-}]$.
- $\int_0^\infty (e^{x^{\mathbf{s}+}}-1)\,\mathbb{p}[x^{\mathbf{s}+}]\,dx^{\mathbf{s}+}$ is the expected jump size under $\mathbb{P}$, conditional on an up jump occurring. Furthermore, $\int_0^\infty (e^{-x^{\mathbf{s}-}}-1)\,\mathbb{p}[x^{\mathbf{s}-}]\,dx^{\mathbf{s}-}$ is the expected jump size under $\mathbb{P}$, conditional on a down jump occurring in the stock futures price.

Correspondingly, we assume the following dynamics for $F_t^{\mathbf{b}}$, under $\mathbb{P}$:

$$
\begin{aligned}
\frac{dF_t^{\mathbf{b}}}{F_{t-}^{\mathbf{b}}} &= \mu_t^{\mathbf{b},\mathbb{P}}\,dt \;+\; \overbrace{\sqrt{V_t^{\mathbf{b}}}\,dW_t^{\mathbf{b},\mathbb{P}}}^{\text{diffusive part}} \\
&+ \underbrace{(e^{x^{\mathbf{b}+}}-1)\,d\mathbb{N}_t^{[\text{bad}],\mathbb{P}}}_{\text{upside bond jump component}} - \lambda_t^{[\text{bad}],\mathbb{P}}\,dt\int_0^\infty (e^{x^{\mathbf{b}+}}-1)\,\underbrace{\mathbb{p}[x^{\mathbf{b}+}]}_{\mathbb{P}\text{ density}}\,dx^{\mathbf{b}+} \\
&+ \underbrace{(e^{-x^{\mathbf{b}-}}-1)\,d\mathbb{N}_t^{[\text{good}],\mathbb{P}}}_{\text{downside bond jump component}} - \lambda_t^{[\text{good}],\mathbb{P}}\,dt\int_0^\infty (e^{-x^{\mathbf{b}-}}-1)\,\underbrace{\mathbb{p}[x^{\mathbf{b}-}]}_{\mathbb{P}\text{ density}}\,dx^{\mathbf{b}-}. \qquad (5)
\end{aligned}
$$

In (5), $\mu_t^{\mathbf{b},\mathbb{P}}$ is the time t (instantaneous) bond futures risk premium.

Our distinction from the stock-bond literature is in the nature of the jumps induced by the Poisson processes $\mathbb{N}_t^{[\text{bad}],\mathbb{P}}$ and $\mathbb{N}_t^{[\text{good}],\mathbb{P}}$, explained as follows:

- The process $\mathbb{N}_t^{[\text{bad}],\mathbb{P}}$ drives down jumps in the stock futures prices, but it drives up jumps in the bond futures prices. $\mathbb{N}_t^{[\text{bad}],\mathbb{P}}$ exerts a significant role in modeling economic phenomena.

- Conversely, the process $\mathbb{N}_t^{[\text{good}],\mathbb{P}}$ is responsible for up jumps in the stock futures prices, but it tends to drive down jumps in the bond futures prices.

While, for example, down jumps in the stock futures prices occur simultaneously with up jumps in the bond futures prices, their codependence is captured through the bivariate probability distribution of the jump sizes ($x^{\mathbf{s}-}$, $x^{\mathbf{b}+}$) and that of the jump sizes ($x^{\mathbf{s}+}$, $x^{\mathbf{b}-}$). Analogous to equation (4), $x^{\mathbf{b}+} > 0$ and $x^{\mathbf{b}-} > 0$.

We denote by $\mathbb{p}[x^{\mathbf{s}-}, x^{\mathbf{b}+}]$ the bivariate probability density function, under $\mathbb{P}$, of jumps of size $-x^{\mathbf{s}-} < 0$ and $x^{\mathbf{b}+} > 0$. The parametric forms of the two associated marginal densities are assumed compatible with the parametric form of the bivariate density. For example, the marginal densities satisfy the following relations: $\mathbb{p}[x^{\mathbf{s}-}] = \int_0^\infty \mathbb{p}[x^{\mathbf{s}-}, x^{\mathbf{b}+}]\, dx^{\mathbf{b}+}$ and $\mathbb{p}[x^{\mathbf{b}+}] = \int_0^\infty \mathbb{p}[x^{\mathbf{s}-}, x^{\mathbf{b}+}]\, dx^{\mathbf{s}-}$.

Analogously, we denote by $\mathbb{p}[x^{\mathbf{s}+}, x^{\mathbf{b}-}]$ the bivariate probability density, under $\mathbb{P}$, of jumps of size $x^{\mathbf{s}+} > 0$ and $-x^{\mathbf{b}-} < 0$. The parametric forms of $\mathbb{p}[x^{\mathbf{s}+}]$ and $\mathbb{p}[x^{\mathbf{b}-}]$ align with the underlying bivariate density $\mathbb{p}[x^{\mathbf{s}+}, x^{\mathbf{b}-}]$.

In sum, we model two — not four — Poisson processes. We assume independence of $x^{\mathbf{s}+}$ and $x^{\mathbf{b}+}$ and independence of $x^{\mathbf{s}-}$ and $x^{\mathbf{b}-}$: $\mathbb{p}[x^{\mathbf{s}+}, x^{\mathbf{b}+}] = \mathbb{p}[x^{\mathbf{s}+}] \times \mathbb{p}[x^{\mathbf{b}+}]$ and $\mathbb{p}[x^{\mathbf{s}-}, x^{\mathbf{b}-}] = \mathbb{p}[x^{\mathbf{s}-}] \times \mathbb{p}[x^{\mathbf{b}-}]$.

Each of $\mu_t^{\mathbf{s},\mathbb{P}}$, $\sqrt{V_t^{\mathbf{s}}}$, $\mu_t^{\mathbf{b},\mathbb{P}}$, $\sqrt{V_t^{\mathbf{b}}}$, $\lambda_t^{[\text{good}],\mathbb{P}}$, and $\lambda_t^{[\text{bad}],\mathbb{P}}$ can be stochastic, by, for example, being functions of state variables, but we do not, for notational brevity, make such dependence explicit. We assume that each quantity is predictable with respect to $\mathcal{F}_t$. The standard Brownian motion increments $dW_t^{\mathbf{s},\mathbb{P}}$ and $dW_t^{\mathbf{b},\mathbb{P}}$ can have a flexible correlation structure, as may $\sqrt{V_t^{\mathbf{s}}}$ and $\sqrt{V_t^{\mathbf{b}}}$.

The dynamics of $F_t^{\mathbf{s}}$ and $F_t^{\mathbf{b}}$, under $\mathbb{Q}$, have the same interpretations (and forms) as in (4) and (5), with three adjustments (as is explicit in the context of equation (B3)). First, the risk-neutral marginal densities of down and up jumps in the stock and bond are internally determined from the system of risk-neutral bivariate densities $\mathbb{q}[x^{\mathbf{s}-}, x^{\mathbf{b}+}]$ and $\mathbb{q}[x^{\mathbf{s}+}, x^{\mathbf{b}-}]$. Second, the futures prices are martingales under $\mathbb{Q}$. Finally, the time-varying jump intensities under $\mathbb{P}$ and $\mathbb{Q}$ are distinct, specifically $\lambda_t^{[\text{bad}],\mathbb{P}}$ and $\lambda_t^{[\text{bad}],\mathbb{Q}}$, as well as $\lambda_t^{[\text{good}],\mathbb{P}}$ and $\lambda_t^{[\text{good}],\mathbb{Q}}$. Collectively, these jump intensities drive fluctuations in stock-bond correlations, option prices, and return volatilities.[4]

[4]Our stock and bond modeling offers perspectives distinct from those of Carr and Wu (2007), who acknowledge upward and downward jumps in their modeling of currency movements, using two separate Lévy processes.

3.1 Implications of the model for option prices and state-contingent correlations

For our characterizations pertaining to small option maturity (Δ) and correlations, we define

$$\text{the asymptotic equivalence notation } \ \mathbb{f}(\Delta) \sim \mathbb{g}(\Delta) \ \text{ to mean } \ \lim_{\Delta \to 0} \frac{\mathbb{f}(\Delta)}{\mathbb{g}(\Delta)} = 1. \tag{6}$$

We provide a proof of the following relations in Appendix A.

Result 1 In the limit of small option maturity Δ, the prices of OTM puts ($k < 1$) and OTM calls ($k > 1$), expiring in Δ years from t, have the following forms:

$$\text{OTM call bond: } \text{call}_t[K^{\mathbf{b}}] \ \sim \ F_t^{\mathbf{b}} \, B_t^{t+\Delta} \, \lambda_t^{[\text{bad}],\mathbb{Q}} \, \Delta \int_0^{\infty} \max(e^{x^{\mathbf{b}+}} - k^{\mathbf{b}}, 0) \, \mathbb{q}[x^{\mathbf{b}+}] \, dx^{\mathbf{b}+}, \tag{7}$$

$$\text{OTM put stock: } \text{put}_t[K^{\mathbf{s}}] \ \sim \ F_t^{\mathbf{s}} B_t^{t+\Delta} \, \lambda_t^{[\text{bad}],\mathbb{Q}} \, \Delta \int_0^{\infty} \max(k^{\mathbf{s}} - e^{-x^{\mathbf{s}-}}, 0) \, \mathbb{q}[x^{\mathbf{s}-}] \, dx^{\mathbf{s}-}, \tag{8}$$

$$\text{OTM put bond: } \text{put}_t[K^{\mathbf{b}}] \ \sim \ F_t^{\mathbf{b}} \, B_t^{t+\Delta} \, \lambda_t^{[\text{good}],\mathbb{Q}} \, \Delta \int_0^{\infty} \max(k^{\mathbf{b}} - e^{-x^{\mathbf{b}-}}, 0) \, \mathbb{q}[x^{\mathbf{b}-}] \, dx^{\mathbf{b}-}, \tag{9}$$

$$\text{OTM call stock: } \text{call}_t[K^{\mathbf{s}}] \ \sim \ F_t^{\mathbf{s}} \, B_t^{t+\Delta} \, \lambda_t^{[\text{good}],\mathbb{Q}} \, \Delta \underbrace{\int_0^{\infty} \max(e^{x^{\mathbf{s}+}} - k^{\mathbf{s}}, 0) \, \mathbb{q}[x^{\mathbf{s}+}] \, dx^{\mathbf{s}+}}_{\text{formulated from a parametric density assumption}}. \tag{10}$$

For small Δ, option pricing is dominated by the possibility of jumps and are detached from diffusive volatilities $\sqrt{V_t^{\mathbf{s}}}$ and $\sqrt{V_t^{\mathbf{b}}}$. The pricing equations (7)–(10) hold for a broad class of jump densities.

The task of understanding the combined behaviors of claims on bond, stock, and volatility futures over a small horizon is not possible without applying an appropriate parametric framework. We recognize that various alternative dynamics could conceivably reproduce the state-contingent return associations. With that said, the upshot of Result 1 is that a model solely based on continuous time dynamics as diffusions — without any jumps, simultaneous or otherwise — is inadequate for explaining small maturity OTM option prices and related small maturity phenomena.

Our modeling approach, with downward and upward price jumps, is reasoned by the fact that multi-asset options on stock and bond are not yet traded. That is to say, for a given small maturity, option prices can be used to deduce the *univariate* risk-neutral distributions for bond and stock returns but *not* their *joint* distributions. To answer questions related to the structure of bivariate return moments pertinent to small maturity, we model simultaneous jumps in stock and bond with each jump process having its own stochastic intensity rate. This link has the advantage of joint-modeling the stock and bond returns under both $\mathbb{P}$ and $\mathbb{Q}$ while allowing flexibility in parameterizing the jump size distributions. A notable insight of Result 1 is that $\lambda_t^{[\text{bad}],\mathbb{Q}}$ (respectively, $\lambda_t^{[\text{good}],\mathbb{Q}}$) drives

the variation in both $\frac{\text{call}_t[K^{\mathbf{b}}]}{F_t^{\mathbf{b}}}$ and $\frac{\text{put}_t[K^{\mathbf{s}}]}{F_t^{\mathbf{s}}}$ (respectively, $\frac{\text{put}_t[K^{\mathbf{b}}]}{F_t^{\mathbf{b}}}$ and $\frac{\text{call}_t[K^{\mathbf{s}}]}{F_t^{\mathbf{s}}}$). Viewed from these standpoints, theoretical approaches equipped with simultaneous price jumps and separate jump intensity rates are essential for capturing small maturity phenomena within estimated models.

3.2 Distinctions of our model from the literature and benchmarking

The distinguishing feature of our framework from other models lies in the incorporation of two Poisson processes controlled by stochastic intensity rates (i.e., $\lambda_t^{[\text{bad}],\mathbb{P}}$ and $\lambda_t^{[\text{good}],\mathbb{P}}$). This aspect plays a crucial role in explaining the imperfect and dynamic small maturity state-contingent stock and bond return correlations, as illustrated in Table 3.

To benchmark our new evidence and model framework with down and up price jumps, the analysis in the Internet Appendix (Section I) examines a modified version of the standard Merton (1976) model that includes only one stochastic jump intensity. Specifically (analogously under $\mathbb{Q}$),

$$\frac{dF_t^{\mathbf{i}}}{F_{t-}^{\mathbf{i}}} = \mu_t^{\mathbf{i},\mathbb{P}}\,dt + \sqrt{V_t^{\mathbf{i}}}\,dW_t^{\mathbf{i},\mathbb{P}} + \underbrace{(e^{x^{\mathbf{i}}}-1)\,d\mathbb{N}_t^{\mathbb{P}}}_{\text{jump component}} - \underbrace{\lambda_t^{\mathbb{P}}}_{\text{stochastic}}\,dt \int_{-\infty}^{\infty}(e^{x^{\mathbf{i}}}-1)\,\mathbb{p}[x^{\mathbf{i}}]\,dx^{\mathbf{i}}, \quad \mathbf{i}\in\{\mathbf{s},\mathbf{b}\}. \tag{11}$$

This model of stock and bond futures price dynamics encounters challenges in explaining the imperfect small maturity state-contingent correlations and representing the joint dynamic nature of OTM puts and call prices for stock and bond. In particular, all small maturity OTM option prices are restricted by the single jump intensity rate $\lambda_t^{\mathbb{Q}}$ (as indicated by equations (I-2)–(I-3) of Internet Appendix (Section I)).

Viewed from the perspectives of our model for small maturity options and state-contingent return correlations, Wachter (2013) develops an equilibrium framework influenced by variable rate disasters. This model captures variations in the state-contingent stock and bond correlations that are attributable to purely diffusive drivers (using Wachter (2013, equations (21) and (B3))). Relative to our approach, the derived zero-coupon bond price dynamics in this model are absent of price jump risks, which is a consideration when analyzing data on small maturity options.

Other approaches conduct their analysis at a quarterly frequency and employ general equilibrium models fitted to consumption data. For example, David and Veronesi (2013) present a model that takes into account the learning process of agents regarding the growth rates of consumption and inflation. This model shapes stock returns and bond returns whose volatilities transition, according to the state of a Markov chain. However, this model does not incorporate price discontinuities.

Campbell, Sunderam, and Viceira (2017) produce a squared Gaussian model for studying stock and bond return relationships. Their assumption of constant volatility without discontinuous price jump components presents a limitation when analyzing options. Thus, the scope of existing papers promotes different inquiries, utilizes alternative samples, and operates at longer-spaced frequencies.

Adopting a New Keynesian framework to characterize stock and bond returns, Campbell, Pflueger, and Viceira (2020) model the real pricing kernel, real and nominal interest-rates, expected cash flows, and inflation. Their formulations are absent of consumption disasters, which are pertinent in the context of pricing state-contingent claims with small maturity. As a result, their model with Gaussian shocks — while aligned with quarterly economic data — is not suitable for addressing our evidence on small maturity phenomena and the relevance of bad news and good news price jump intensities.

4 Bond and stock state-contingent returns in an estimated model

We examine the empirical consistency of model constructions with returns obtained from options on bond and stock with a seven-day expiry. To do so, we introduce bivariate jump distributions and assess whether our estimated model is compatible with the data from state-contingent returns and option prices. Reconciling small maturity empirical phenomena over seven days (Friday to Friday), we extract the time-series of bad and good jump intensities under $\mathbb{P}$ using Kalman filtering.

4.1 Bivariate distributions for jumps in bond and stock

To investigate the empirical implications of our model, we consider bivariate exponential densities specific to down (up) jumps in stock and up (down) jumps in bond. For estimation, we suppose that the bivariate density — see Balakrishnan and Lai (2009, Chapter 10) — of $x^{\mathbf{s}-}$ and $x^{\mathbf{b}+}$ is

$$\underbrace{\mathbb{p}[x^{\mathbf{s}-}, x^{\mathbf{b}+}]}_{\text{bivariate density}} = \frac{1}{(1-\rho^{\text{bad}})\mu^{\mathbf{s}-}\mu^{\mathbf{b}+}} \exp\left(-\frac{x^{\mathbf{s}-}}{\mu^{\mathbf{s}-}(1-\rho^{\text{bad}})} - \frac{x^{\mathbf{b}+}}{\mu^{\mathbf{b}+}(1-\rho^{\text{bad}})}\right) I_0[\frac{2\,(\rho^{\text{bad}}\,\mathbf{x}^{s-}x^{\mathbf{b}+})^{\frac{1}{2}}}{(1-\rho^{\text{bad}})(\mu^{\mathbf{s}-}\mu^{\mathbf{b}+})^{\frac{1}{2}}}], \quad (12)$$

where $I_0[\bullet]$ is the modified Bessel function of the first kind of order zero. The correlation coefficient between $x^{\mathbf{s}-}$ and $x^{\mathbf{b}+}$ is ρ^{bad}, and the mean jump size for stock (bond) is $\mu^{\mathbf{s}-}$ ($\mu^{\mathbf{b}+}$).

Additionally, the bivariate density for up price jumps in stock (i.e., $x^{\mathbf{s}+}$) and down price jumps in bond (i.e., $x^{\mathbf{b}-}$), namely, $\mathbb{p}[x^{\mathbf{s}+}, x^{\mathbf{b}-}]$, is assumed to be of the same parametric form as in equation (12). This bivariate density is distinguished by mean jump parameters ($\mu^{\mathbf{s}+}$, $\mu^{\mathbf{b}-}$) and correlation coefficient ρ^{good}.

Two features guide our choice of the bivariate exponential densities under $\mathbb{P}$ and $\mathbb{Q}$. First, the joint moment-generating function has a closed-form representation (Balakrishnan and Lai (2009, page 436)), as follows (for parameters $\phi \in \mathbb{R}$ and $\varphi \in \mathbb{R}$):

$$\int_0^\infty \int_0^\infty e^{\phi\, x^{\mathbf{s}-} + \varphi\, x^{\mathbf{b}+}}\, \mathbb{p}[x^{\mathbf{s}-}, x^{\mathbf{b}+}]\, dx^{\mathbf{s}-} dx^{\mathbf{b}+} = \frac{1}{\{1-(\mu^{\mathbf{s}-})\phi\}\{1-(\mu^{\mathbf{b}+})\varphi\} \;-\; \rho^{\text{bad}}\, \mu^{\mathbf{s}-}\, \mu^{\mathbf{b}+} \phi\, \varphi}. \tag{13}$$

The superscripts $\mathbb{P}$ and $\mathbb{Q}$ on the parameters are suppressed in (12) and (13). The parameters ρ^{bad} and ρ^{good} are unaltered under $\mathbb{P}$ and $\mathbb{Q}$ (i.e., no Girsanov change of measure transformation).

Second, pertinent to the measurement equations in the Kalman filtering procedure, the univariate distributions of $x^{\mathbf{b}-}$ ($x^{\mathbf{b}+}$) and $x^{\mathbf{s}-}$ ($x^{\mathbf{s}+}$) inherit exponential marginals. Specifically,

$$\begin{cases} \mathbb{p}[x^{\mathbf{b}-}] \;=\; \overbrace{\frac{1}{\mu^{\mathbf{b}-,\mathbb{P}}}\, e^{-\frac{1}{\mu^{\mathbf{b}-,\mathbb{P}}}\, x^{\mathbf{b}-}}}^{\text{bond jump density, } \mathbb{P}}, \\ \mathbb{p}[x^{\mathbf{b}+}] \;=\; \frac{1}{\mu^{\mathbf{b}+,\mathbb{P}}}\, e^{-\frac{1}{\mu^{\mathbf{b}+,\mathbb{P}}}\, x^{\mathbf{b}+}}, \end{cases} \quad \text{and} \quad \begin{cases} \mathbb{q}[x^{\mathbf{b}-}] \;=\; \overbrace{\frac{1}{\mu^{\mathbf{b}-,\mathbb{Q}}}\, e^{-\frac{1}{\mu^{\mathbf{b}-,\mathbb{Q}}}\, x^{\mathbf{b}-}}}^{\text{bond jump density, } \mathbb{Q}}, \\ \mathbb{q}[x^{\mathbf{b}+}] \;=\; \frac{1}{\mu^{\mathbf{b}+,\mathbb{Q}}}\, e^{-\frac{1}{\mu^{\mathbf{b}+,\mathbb{Q}}}\, x^{\mathbf{b}+}}. \end{cases} \tag{14}$$

Accordingly, the mean jump sizes of positive price jumps in bond are $0 < \mu^{\mathbf{b}+,\mathbb{P}} < 1$ and $0 < \mu^{\mathbf{b}+,\mathbb{Q}} < 1$ under $\mathbb{P}$ and $\mathbb{Q}$, respectively. Likewise, the mean (absolute) jump size of negative price jumps in bond are $0 < \mu^{\mathbf{b}-,\mathbb{P}} < \infty$ and $0 < \mu^{\mathbf{b}-,\mathbb{Q}} < \infty$.

The marginal price jump distributions of stock are analogously characterized — as in the stock model of Kou (2002) — indicated by the form in equation (14), complying with aforementioned parametric constraints on $(\mu^{\mathbf{s}-,\mathbb{P}}, \mu^{\mathbf{s}-,\mathbb{Q}})$ and $(\mu^{\mathbf{s}+,\mathbb{P}}, \mu^{\mathbf{s}+,\mathbb{Q}})$.

4.2 Measurement equations based on covariances, variances, and options

Simultaneous stock and bond movements are represented using two Poisson processes, both with stochastic intensity rates. The magnitude of these jumps follows a bivariate distribution. The movements categorized as bad jumps play a pivotal role in interpreting the observed market dynamics. These jumps represent the flight-to-quality phenomenon, a situation often seen during market turmoil, where bonds experience an upward movement and stocks a downward movement. In our model, bad jumps are those in which stock prices decrease while bond prices increase. Conversely, good jumps align with an increase in stock prices while bond prices decrease.

To establish our results and empirically assess model implications, we extract the time-series of

$$\underset{(4\times 1)}{\mathbf{z}_t} \;\equiv\; [\lambda_t^{[\text{good}],\mathbb{P}}, \lambda_t^{[\text{bad}],\mathbb{P}}, V_t^{\mathbf{b}}, V_t^{\mathbf{s}}]', \qquad \text{for } t = 1, \ldots, 630, \tag{15}$$

through Kalman filtering and quasi-maximum likelihood. We scrutinize the distinguishing features of good and bad jump intensities and how they impact stock and bond markets. Furthermore, we examine the evolution of diffusive volatilities in the presence of price jumps and jump intensities.

For the estimation procedure, we utilize information from return covariances and variances. The following relations are derived (proof available from authors):

$$\frac{1}{\Delta}\text{cov}_t^{\mathbb{P}}(\log(\frac{F^{\mathbf{s}}_{t+\Delta}}{F^{\mathbf{s}}_t}),\log(\frac{F^{\mathbf{b}}_{t+\Delta}}{F^{\mathbf{b}}_t})) \quad\sim\quad \mathrm{a}_{\text{good}}^{\{r^{\mathbf{s}}\},\{r^{\mathbf{b}}\}}\times\lambda_t^{[\text{good}],\mathbb{P}}+\mathrm{a}_{\text{bad}}^{\{r^{\mathbf{s}}\},\{r^{\mathbf{b}}\}}\times\lambda_t^{[\text{bad}],\mathbb{P}}, \tag{16}$$

$$\frac{1}{\Delta}\text{cov}_t^{\mathbb{P}}(\{\log(\frac{F^{\mathbf{s}}_{t+\Delta}}{F^{\mathbf{s}}_t})\}^2,\{\log(\frac{F^{\mathbf{b}}_{t+\Delta}}{F^{\mathbf{b}}_t})\}^2) \quad\sim\quad \mathrm{a}_{\text{good}}^{\{r^{\mathbf{s}}\}^2,\{r^{\mathbf{b}}\}^2}\times\lambda_t^{[\text{good}],\mathbb{P}}+\mathrm{a}_{\text{bad}}^{\{r^{\mathbf{s}}\}^2,\{r^{\mathbf{b}}\}^2}\times\lambda_t^{[\text{bad}],\mathbb{P}}. \tag{17}$$

These covariances illustrate that the impact of diffusion-related factors is minimal in the small time limit of $\Delta\to 0$. It holds that

$$\mathrm{a}_{\text{good}}^{\{r^{\mathbf{s}}\},\{r^{\mathbf{b}}\}} \equiv -(\mu^{\mathbf{s}+,\mathbb{P}})(\mu^{\mathbf{b}-,\mathbb{P}})(1+\rho^{\text{good}}) \quad\text{and}\quad \mathrm{a}_{\text{bad}}^{\{r^{\mathbf{s}}\},\{r^{\mathbf{b}}\}}\equiv -(\mu^{\mathbf{s}-,\mathbb{P}})(\mu^{\mathbf{b}+,\mathbb{P}})(1+\rho^{\text{bad}}), \tag{18}$$

$$\mathrm{a}_{\text{good}}^{\{r^{\mathbf{s}}\}^2,\{r^{\mathbf{b}}\}^2} \equiv 4(\mu^{\mathbf{s}+,\mathbb{P}})^2(\mu^{\mathbf{b}-,\mathbb{P}})^2\left\{(\rho^{\text{good}})^2+4\,\rho^{\text{good}}+1\right\},\ \text{and} \tag{19}$$

$$\mathrm{a}_{\text{bad}}^{\{r^{\mathbf{s}}\}^2,\{r^{\mathbf{b}}\}^2} \equiv 4(\mu^{\mathbf{s}-,\mathbb{P}})^2(\mu^{\mathbf{b}+,\mathbb{P}})^2\left\{(\rho^{\text{bad}})^2+4\,\rho^{\text{bad}}+1\right\}. \tag{20}$$

Aligning measurements with the model, we employ returns sampled at five-minute synchronized observations. That is, for $r^{\mathbf{s}}_{t,\ell}=\log(F^{\mathbf{s}}_{t,\frac{\ell}{N}})-\log(F^{\mathbf{s}}_{t,\frac{\ell-1}{N}})$ and $r^{\mathbf{b}}_{t,\ell}=\log(F^{\mathbf{b}}_{t,\frac{\ell}{N}})-\log(F^{\mathbf{b}}_{t,\frac{\ell-1}{N}})$,

$$\text{covar}_{\{t\to t+\Delta\}}^{\{r^{\mathbf{s}}\}^i,\{r^{\mathbf{b}}\}^i,\mathbb{P}}\equiv 52\times\sum_{\ell=1}^{\mathcal{I}}\{r^{\mathbf{s}}_{t,\ell}\times r^{\mathbf{b}}_{t,\ell}\}^i,\quad\text{for}\ \ i=1,2, \tag{21}$$

where $\mathcal{I}$ is the number of observations in a trading week (i.e., $\mathcal{I}=12\times 6.5\times 5$). In so doing, we are guided by the theory on building seven-day moments from high-frequency returns (e.g., Amaya, Christoffersen, Jacobs, and Vasquez (2015, Section 2) and Liu, Patton, and Sheppard (2015)). We additionally incorporate realized variances in our measurements, as follows:

$$\{\text{rv}^{\mathbf{b},\mathbb{P}}_{\{t\to t+\Delta\}}\}^2\equiv\text{realized variance from five-minute return intervals (Friday to Friday).} \tag{22}$$

Analogously, we construct $\{\text{rv}^{\mathbf{s},\mathbb{P}}_{\{t\to t+\Delta\}}\}^2$ (expressed as annualized decimals). We stack these realized covariances and return variances in the 4×1 vector, as follows:

$$\mathbf{y}_t^{\text{covar/var}}=[\text{covar}_{\{t\to t+\Delta\}}^{\{r^{\mathbf{s}}\},\{r^{\mathbf{b}}\},\mathbb{P}},\text{covar}_{\{t\to t+\Delta\}}^{\{r^{\mathbf{s}}\}^2,\{r^{\mathbf{b}}\}^2,\mathbb{P}},\{\text{rv}^{\mathbf{b},\mathbb{P}}_{\{t\to t+\Delta\}}\}^2,\{\text{rv}^{\mathbf{s},\mathbb{P}}_{\{t\to t+\Delta\}}\}^2]'. \tag{23}$$

Our measurements also combine information from options markets, as follows:

$$\underbrace{\mathbf{y}_t^{\text{options}}}_{10\times 1}=[\underbrace{\frac{\text{put}[K^{\mathbf{b}}]}{F^{\mathbf{b}}_tB^{t+\Delta}_t\Delta},\frac{\text{call}[K^{\mathbf{b}}]}{F^{\mathbf{b}}_tB^{t+\Delta}_t\Delta},\frac{\text{put}[K^{\mathbf{s}}]}{F^{\mathbf{s}}_tB^{t+\Delta}_t\Delta},\frac{\text{call}[K^{\mathbf{s}}]}{F^{\mathbf{s}}_tB^{t+\Delta}_t\Delta}}_{\text{scaled 7DTE bond and stock option prices (}\pm\text{ 7 and }\pm\text{ 20 delta)}},\underbrace{\{\text{VIX}^{\mathbf{b}}_t\}^2,\{\text{VIX}^{\mathbf{s}}_t\}^2}_{\text{seven-day VIX}}]'. \tag{24}$$

Specifically, we utilize scaled 7DTE OTM option prices. As evidenced by equations (9)–(10), these prices reflect the expected size of jumps, taking into account whether they are up or down.

Next, the seven-day VIX is created using $\{\text{VIX}_t^{\mathbf{b}}\}^2 = \mathbb{E}_t^{\mathbb{Q}}(\{\frac{-2}{\Delta}\}\,\frac{e^{-\int_t^{t+\Delta} r_\ell\, d\ell}}{B_t^{t+\Delta}}\log(\frac{F_{t+\Delta}^{\mathbf{b}}}{F_t^{\mathbf{b}}}))$ from 7DTE option prices (analogously for seven-day $\{\text{VIX}_t^{\mathbf{s}}\}^2$):

$$\underbrace{\{\text{VIX}_t^{\mathbf{b}}\}^2}_{\text{annualized decimals}} \;=\; \frac{2}{B_t^{t+\Delta}\Delta}\int_0^{F_t^{\mathbf{b}}}\frac{1}{K^2}\,\text{put}_t[K]\,dK \;+\; \frac{2}{B_t^{t+\Delta}\Delta}\int_{F_t^{\mathbf{b}}}^{\infty}\frac{1}{K^2}\,\text{call}_t[K]\,dK. \tag{25}$$

We assume that the stock and bond diffusive variances evolve as follows (with $\mathbf{i}\in\{\mathbf{s},\mathbf{b}\}$):

$$dV_t^{\mathbf{i}} = \begin{cases} (\theta_{\mathbf{i}}^{\mathbb{P}} - \kappa_{\mathbf{i}}^{\mathbb{P}}\,V_t^{\mathbf{i}})\,dt + \sigma_{\mathbf{i}}\sqrt{V_t^{\mathbf{i}}}\big\{\rho_{\mathbf{i}}\,dW_t^{\mathbf{i},\mathbb{P}} + \sqrt{1-\rho_{\mathbf{i}}^2}\,dW_t^{\mathbf{i}\bullet,\mathbb{P}}\big\}, & \text{(under }\mathbb{P}\text{)} \\ (\theta_{\mathbf{i}}^{\mathbb{Q}} - \kappa_{\mathbf{i}}^{\mathbb{Q}}V_t^{\mathbf{i}})\,dt + \sigma_{\mathbf{i}}\sqrt{V_t^{\mathbf{i}}}\big\{\rho_{\mathbf{i}}\,dW_t^{\mathbf{i},\mathbb{Q}} + \sqrt{1-\rho_{\mathbf{i}}^2}\,dW_t^{\mathbf{i}\bullet,\mathbb{Q}}\big\}, & \text{(under }\mathbb{Q}\text{)} \end{cases} \tag{26}$$

for independent standard Brownian motions $(W_t^{\mathbf{i},\mathbb{P}}, W_t^{\mathbf{i}\bullet,\mathbb{P}})$ and $(W_t^{\mathbf{i},\mathbb{Q}}, W_t^{\mathbf{i}\bullet,\mathbb{Q}})$. Furthermore, we assume that both the good and bad jump intensities follow mean-reverting processes:

$$d\lambda_t^{[\text{h}],\mathbb{P}} = (\theta_{\text{h}}^{\mathbb{P}} - \kappa_{\text{h}}^{\mathbb{P}}\,\lambda_t^{[\text{h}],\mathbb{P}})\,dt \;+\; \sigma_{\text{h}}\sqrt{\lambda_t^{[\text{h}],\mathbb{P}}}dW_t^{\text{h},\mathbb{P}}, \qquad \text{for h}\in\{\text{good},\text{bad}\}. \tag{27}$$

All standard Brownian motions are mutually independent. We favor tractable estimation and map the risk premiums for jump intensities as follows:

$$\underbrace{\log(\frac{\lambda_t^{[\text{good}],\mathbb{P}}}{\lambda_t^{[\text{good}],\mathbb{Q}}})}_{\text{risk premium}} \;=\; -\chi^{\text{good}} < 0 \qquad \text{and} \qquad \underbrace{\log(\frac{\lambda_t^{[\text{bad}],\mathbb{P}}}{\lambda_t^{[\text{bad}],\mathbb{Q}}})}_{\text{risk premium}} \;=\; -\chi^{\text{bad}} < 0, \tag{28}$$

where χ^{good} and χ^{bad} are constants. Thus, $\lambda_t^{[\text{good}],\mathbb{Q}} = e^{\chi^{\text{good}}}\,\lambda_t^{[\text{good}],\mathbb{P}}$ and $\lambda_t^{[\text{bad}],\mathbb{Q}} = e^{\chi^{\text{bad}}}\,\lambda_t^{[\text{bad}],\mathbb{P}}$. The essence of model specification (28) is to inflate the jump intensities under $\mathbb{Q}$ in relation to $\mathbb{P}$.[5]

Our approach is guided by the amenability of measurement equations, given our formulation of option prices, volatilities, and stock and bond return covariances over small maturity. Compared to models with constant jump intensity, models with two stochastic jump intensities offer a more favorable alignment with the actual behavior of short maturity options and return volatilities.

4.3 Kalman filtering estimation

The model in state-space form for the vector $\mathbf{y}_t \equiv [(\mathbf{y}_t^{\text{covar/var}})', (\mathbf{y}_t^{\text{options}})']'$ is

[5]We recognize that there is no unique pricing kernel (when markets are not complete) and that other risk premium specifications for jump intensities are possible (e.g., Shreve (2003, Chapter 11.6) and Bollerslev and Todorov (2023)).

$$\underset{(14\times 1)}{\mathbf{y}_t} = \boldsymbol{\alpha} \; + \; \boldsymbol{\beta}\, \mathbf{z}_t + \tilde{\boldsymbol{\epsilon}}_t, \qquad \text{where} \qquad \tilde{\boldsymbol{\epsilon}}_t \text{ is distributed Normal}(0, \boldsymbol{\mho}). \tag{29}$$

The representation in equation (29) allows for deviations due to the asymptotic equivalence approach (in (7)–(10)) for determining OTM option prices. Equations (7)–(10), in conjunction with equation (14), establish the form of the 7DTE $\frac{\text{put}[K^{\mathbf{b}}]}{F_t^{\mathbf{b}} B_t^{t+\Delta}\Delta}$, $\frac{\text{call}[K^{\mathbf{b}}]}{F_t^{\mathbf{b}} B_t^{t+\Delta}\Delta}$, $\frac{\text{put}[K^{\mathbf{s}}]}{F_t^{\mathbf{s}} B_t^{t+\Delta}\Delta}$, and $\frac{\text{call}[K^{\mathbf{s}}]}{F_t^{\mathbf{s}} B_t^{t+\Delta}\Delta}$ (each for ± 7 and ± 20 delta).

Our estimation approach accounts for interdependencies between bond and stock option returns and volatilities through variations in $\lambda_t^{[\text{good}],\mathbb{P}}$ and $\lambda_t^{[\text{bad}],\mathbb{P}}$. Incorporating $\text{covar}_{\{t\to t+\Delta\}}^{\{r^{\mathbf{s}}\},\{r^{\mathbf{b}}\},\mathbb{P}}$ and $\text{covar}_{\{t\to t+\Delta\}}^{\{r^{\mathbf{s}}\}^2,\{r^{\mathbf{b}}\}^2,\mathbb{P}}$ in measurements is essential to the estimation of ρ^{good} and ρ^{bad}.

In equation (29), $\widetilde{\boldsymbol{\epsilon}}_t$ is a vector of i.i.d. Gaussian errors with a constant diagonal matrix represented by $\boldsymbol{\mho}$. We assume that the measurement errors are cross-sectionally uncorrelated. Moreover, the variance of the measurement errors is captured by one free parameter for the two small maturity covariances, one for the two realized return variances, one each for the 7 delta bond and stock option prices, one each for the 20 delta bond and stock option prices, and one each for the bond and stock VIX. This specification entails eight elements in $\boldsymbol{\mho}$.

The model-based quantities $\boldsymbol{\alpha}$ and $\boldsymbol{\beta}$ in equation (29) are determined from (26)–(28), as follows:

$$\underset{(14\times 1)}{\boldsymbol{\alpha}} = \begin{bmatrix} 0 \\ 0 \\ 0 \\ 0 \\ 0 \\ 0 \\ 0 \\ 0 \\ 0 \\ 0 \\ 0 \\ 0 \\ 0 \\ 0 \end{bmatrix}, \quad \underset{(14\times 4)}{\boldsymbol{\beta}} = \begin{bmatrix} \mathrm{a}_{\text{good}}^{\{r^{\mathbf{s}}\},\{r^{\mathbf{b}}\}} & \mathrm{a}_{\text{bad}}^{\{r^{\mathbf{s}}\},\{r^{\mathbf{b}}\}} & 0 & 0 \\ \mathrm{a}_{\text{good}}^{\{r^{\mathbf{s}}\}^2,\{r^{\mathbf{b}}\}^2} & \mathrm{a}_{\text{bad}}^{\{r^{\mathbf{s}}\}^2,\{r^{\mathbf{b}}\}^2} & 0 & 0 \\ \{\mu^{\mathbf{b}-,\mathbb{P}}\}^2 & \{\mu^{\mathbf{b}+,\mathbb{P}}\}^2 & 1 & 0 \\ \{\mu^{\mathbf{s}+,\mathbb{P}}\}^2 & \{\mu^{\mathbf{s}-,\mathbb{P}}\}^2 & 0 & 1 \\ e^{\chi^{\text{good}}} \frac{\{e^{(\frac{1}{\mu^{\mathbf{b}-,\mathbb{Q}}}+1)\log(k^{\mathbf{b}})}\}}{\frac{1}{\mu^{\mathbf{b}-,\mathbb{Q}}}+1} & 0 & 0 & 0 \\ \cdots & 0 & 0 & 0 \\ 0 & e^{\chi^{\text{bad}}} \frac{\{e^{-(\frac{1}{\mu^{\mathbf{b}+,\mathbb{Q}}}-1)\log(k^{\mathbf{b}})}\}}{\frac{1}{\mu^{\mathbf{b}+,\mathbb{Q}}}-1} & 0 & 0 \\ 0 & \cdots & 0 & 0 \\ 0 & e^{\chi^{\text{bad}}} \frac{\{e^{(\frac{1}{\mu^{\mathbf{s}-,\mathbb{Q}}}+1)\log(k^{\mathbf{s}})}\}}{\frac{1}{\mu^{\mathbf{s}-,\mathbb{Q}}}+1} & 0 & 0 \\ 0 & \cdots & 0 & 0 \\ e^{\chi^{\text{good}}} \frac{\{e^{-(\frac{1}{\mu^{\mathbf{s}+,\mathbb{Q}}}-1)\log(k^{\mathbf{s}})}\}}{\frac{1}{\mu^{\mathbf{s}+,\mathbb{Q}}}-1} & 0 & 0 & 0 \\ \cdots & 0 & 0 & 0 \\ 2\, e^{\chi^{\text{good}}} \{\frac{1}{1+\mu^{\mathbf{b}-,\mathbb{Q}}} - 1 + \mu^{\mathbf{b}-,\mathbb{Q}}\} & 2\, e^{\chi^{\text{bad}}} \{\frac{1}{1-\mu^{\mathbf{b}+,\mathbb{Q}}} - 1 - \mu^{\mathbf{b}+,\mathbb{Q}}\} & 1 & 0 \\ 2\, e^{\chi^{\text{good}}} \{\frac{1}{1-\mu^{\mathbf{s}+,\mathbb{Q}}} - 1 - \mu^{\mathbf{s}+,\mathbb{Q}}\} & 2\, e^{\chi^{\text{bad}}} \{\frac{1}{1+\mu^{\mathbf{s}-,\mathbb{Q}}} - 1 + \mu^{\mathbf{s}-,\mathbb{Q}}\} & 0 & 1 \end{bmatrix}. \tag{30}$$

The model expressions for $\{\mathrm{rv}^{\mathbf{b},\mathbb{P}}_{\{t\to t+\Delta\}}\}^2 = \frac{1}{\Delta}\mathbb{E}^{\mathbb{P}}_t(\int_t^{t+\Delta}\{\frac{1}{d\ell}\mathrm{var}^{\mathbb{P}}_t[d\log(F^{\mathbf{b}}_\ell)]\}d\ell$ and $\{\mathrm{VIX}^{\mathbf{b}}_t\}^2$ appearing in rows 3 and 13 of equation (30) are standard, likewise for $\{\mathrm{rv}^{\mathbf{s},\mathbb{P}}_{\{t\to t+\Delta\}}\}^2$.

The 7DTE horizon — as opposed to 1DTE — is unique due to the fact that we maintain a seven day expiration without the possibility of irregular time-series gaps in the estimation procedure.

Each measurement is linear in the 4×1 vector $\mathbf{z}_t = [\lambda^{[\mathrm{good}],\mathbb{P}}_t, \lambda^{[\mathrm{bad}],\mathbb{P}}_t, V^{\mathbf{b}}_t, V^{\mathbf{s}}_t]'$, and we apply the Kalman filter. The transition equations link the discrete-time evolution of $\mathbf{z}_t$, as follows:

$$\mathbf{z}_{t+\Delta} \;=\; \mathbf{C} \;+\; \mathbf{D}\,\mathbf{z}_t \;+\; \widetilde{\mathbf{e}}_{t+\Delta} \qquad \text{and} \qquad \widetilde{\mathbf{e}}_{t+\Delta} \text{ is distributed Normal}(0, \mathbf{\Lambda}_{t+\Delta}). \tag{31}$$

Although the exact transition density of $\mathbf{z}_t$ under $\mathbb{P}$ is not known, we can determine its mean and variance. We approximate the transition density as a Gaussian density with the same mean and variance. The structure of $\mathbf{C}$, $\mathbf{D}$, and $\mathbf{\Lambda}_t$ for the estimation is specified in (B4)–(B5) of Appendix B.

Using the Kalman filter, we can generate one-step-ahead forecasts for $\mathbf{y}_t$, denoted by $\widehat{\mathbf{y}}_{t|t-1}$, along with their corresponding error covariance matrices, $\mathbf{\Sigma}_{t|t-1}$. The log-likelihood function is

$$\mathcal{L}[\Theta] \;=\; -\frac{1}{2}\sum_{t=1}^{630}\Big\{14\times\log(2\pi) \;+\; \log(\mathbf{\Sigma}_{t|t-1}) \;+\; (\mathbf{y}_t - \widehat{\mathbf{y}}_{t|t-1})'\,\mathbf{\Sigma}^{-1}_{t|t-1}\,(\mathbf{y}_t - \widehat{\mathbf{y}}_{t|t-1})\Big\}, \tag{32}$$

where Θ is the 32×1 vector of unknown parameters with the quasi-maximum-likelihood estimator, $\widehat{\Theta} = \arg\ \max_\Theta\ \mathcal{L}[\Theta]$.[6]

5 Replicating interrelated small maturity phenomena in markets

Our investigation reveals that the small maturity stock and bond markets exhibit unequal state-contingent returns correlation: a strong relationship between state-contingent returns on the downside of stock and upside of bond, whereas the upside of stock and downside of bond have negligible correlation. Despite ongoing discussions about the forces driving these markets, there are few estimated models of small maturity pricing that analyze the economic implications that are consistent with empirical results across bond and stock options markets. What is new is that we appraise whether the estimated model captures essential characteristics of small maturity bond and stock markets, such as realized volatilities, VIX, option prices, and stock-bond return association.

[6] Our inferences about correlations are under the $\mathbb{P}$ measure, and jump sizes are under both $\mathbb{P}$ and $\mathbb{Q}$. Andersen, Fusari, and Todorov (2017, equation (6)) design a different objective function for their estimation compared to ours. They utilize the squared differences between the Black-Scholes-implied volatility and include a penalty term to account for estimation error in diffusive variance. They break down the estimation process into two steps: first optimizing over the state vector on each day t, and then optimizing over the model parameters using the overarching objective function. Andersen, Fusari, and Todorov do not estimate jump sizes under $\mathbb{P}$.

Additionally, 7DTE VIX futures — denoted by F_t^{vix} — and VIX of VIX — denoted by CBOE as VVIX_t — can be integrated into small maturity S&P 500 index claims pricing. Guided by this reasoning, we include Friday-to-Friday data from F_t^{vix} and synthesized 11-day VVIX_t in our analysis. The 11-day VVIX_t arises as 7DTE options on VIX futures expire on Tuesday close (settle Wednesday AM). This approach enables us to distinguish between data that was used to create the model and new data on VIX options and 7DTE VIX futures that the model has not yet encountered.

5.1 Properties of $[\lambda_t^{[\mathbf{good}],\mathbb{P}}, \lambda_t^{[\mathbf{bad}],\mathbb{P}}, V_t^{\mathbf{b}}, V_t^{\mathbf{s}}]'$ anchored to small maturity phenomena

Although there are studies that consider the relationship between stock and bond returns within macrofinance models and consumption growth dynamics, we expand and improve beyond this connection. We aim to understand the mechanisms that drive the variation in small maturity state-contingent returns of stock and bond, as well as small maturity stock and bond VIX. To this end, using the Kalman filtering approach based on small maturity data as captured in equation (29), we extract the time-series of $[\lambda_t^{[\text{good}],\mathbb{P}}, \lambda_t^{[\text{bad}],\mathbb{P}}, V_t^{\mathbf{b}}, V_t^{\mathbf{s}}]'$ to describe the time-series and cross-sectional properties of the 7DTE options data. Our methodology quantifies the properties of diffusive variances, good and bad jump intensities, and estimated jump sizes under $\mathbb{P}$ and $\mathbb{Q}$.

Table 7 presents the descriptive statistics for the small maturity data moments for extant models to match. One notable feature is the essentially symmetric pricing for OTM puts and calls for bond (i.e., $\frac{\text{put}_t[K^{\mathbf{b}}]}{F_t^{\mathbf{b}} B_t^{t+\Delta}\Delta}$ versus $\frac{\text{call}_t[K^{\mathbf{b}}]}{F_t^{\mathbf{b}} B_t^{t+\Delta}\Delta}$). There is also a significant difference between the actual average $\text{VIX}_t^{\mathbf{s}}$ (16.2%) and $\text{VIX}_t^{\mathbf{b}}$ (4.6%), which highlights the considerable asymmetry in the cost of protection in stock and bond markets. Additionally, there is a significant difference between realized stock returns variability at 11.3% and bond futures returns variability at 3.4%.

Reported parameter estimates in Table 8 reflect the distinction between stock and bond markets. Figure 1 emphasizes this contrast, showing time-series estimates of the filtered diffusive variances. The bond market consistently maintains a low diffusive variance, whereas the stock market experiences spikes during periods of market turmoil, such as Black Monday in August 2011, the coronavirus outbreak in March 2020, and the 41-year high-inflation realization in June 2022. On average, the annualized $\sqrt{V_t^{\mathbf{b}}} \times 100$ and $\sqrt{V_t^{\mathbf{s}}} \times 100$ are 0.04% and 10.64%, respectively.

Figure 1 also shows the time-series estimates of the good and bad jump intensity rates, which seem to peak during market stress events. It is evident that the taper tantrum in June 2013,

while leading to increased jump intensities, did not have a significant impact on diffusive variances, indicating that jump risks and diffusive risks evolve distinctly. The mean values for $\lambda_t^{[\text{good}],\mathbb{P}}$ and $\lambda_t^{[\text{bad}],\mathbb{P}}$ are 0.72 and 0.08, respectively.

Table 8 also displays the parameters affecting the bivariate densities $\mathbb{p}[x^{\mathbf{s}-}, x^{\mathbf{b}+}]$ and $\mathbb{p}[x^{\mathbf{s}+}, x^{\mathbf{b}-}]$ together with those of $\mathbb{q}[x^{\mathbf{s}-}, x^{\mathbf{b}+}]$ and $\mathbb{q}[x^{\mathbf{s}+}, x^{\mathbf{b}-}]$. They show that the mean jump size to the downside of stock under $\mathbb{Q}$ is higher in comparison to that of the upside under $\mathbb{Q}$, whereas the size of down and up bond jumps appears symmetric under $\mathbb{Q}$.

Jump intensity rates are characterized by positive Girsanov jump parameters, with $\chi^{\text{good}} = 3.01$ and $\chi^{\text{bad}} = 5.23$, indicating a higher perceived probability of jumps under the $\mathbb{Q}$-measure compared to the $\mathbb{P}$-measure, particularly for bad jumps. In economic terms, news about good and bad events drive risk premiums that introduce a wedge between total variances of stock and bond returns under $\mathbb{P}$ and $\mathbb{Q}$. Taken all together, the good and bad jump components play an outsized role in determining the volatility of stock and bond returns and option prices, as well as small maturity $\text{VIX}_t^{\mathbf{s}}$ and $\text{VIX}_t^{\mathbf{b}}$, as seen from their relatively higher values compared to diffusive variances.

Our framework offers conditional jump size formulations, such as $\mathbb{E}^{\mathbb{P}}(x^{\mathbf{b}+}\big|x^{\mathbf{s}-}) = (1-\rho^{\text{bad}})\mu^{\mathbf{b}+} + \rho^{\text{bad}}\{\frac{\mu^{\mathbf{b}+}}{\mu^{\mathbf{s}-}}\}\, x^{\mathbf{s}-}$ and $\mathbb{E}^{\mathbb{P}}(x^{\mathbf{b}-}\big|x^{\mathbf{s}+}) = (1-\rho^{\text{good}})\,\mu^{\mathbf{b}-} + \rho^{\text{good}}\{\frac{\mu^{\mathbf{b}-}}{\mu^{\mathbf{s}+}}\}x^{\mathbf{s}+}$. In our estimation, we obtain near-zero estimates of ρ^{good} and ρ^{bad}, which has twofold implications. First, when stock jumps down (up), the size of the corresponding up (down) bond jump is determined by the estimated unconditional mean jump size. Second, the stock and bond return covariations can then be plausibly attributed to variations in good and bad stochastic jump intensity rates.

As a robust theoretical structure, the four variable model presents a viable approach, utilizing the concept of good and bad jump intensities to capture the patterns in stock and bond return distributions. The estimated values of the model parameters and $[\lambda_t^{[\text{good}],\mathbb{P}}, \lambda_t^{[\text{bad}],\mathbb{P}}, V_t^{\mathbf{b}}, V_t^{\mathbf{s}}]'$ reflect the characteristics of volatilities and option prices. In particular, the stochastic jump intensities mirror the frequency of price jumps observed in stock and bond markets, and this estimated model provides a baseline understanding of the behavior and traits of small maturity option prices.

5.2 Assessing empirical consistency with small maturity bond and stock options

Extant research has not yet examined the effectiveness of models for weekly option prices for both bond futures and stock, nor the empirical characteristics of state-contingent bond and stock returns.

To address this gap, we investigate the relevance of our model by analyzing its ability to match quantitative features of volatilities, VIX indices, and option prices for both bond and stock markets.

Table 9 (for volatility and VIX) and Table 10 (for options implied-volatility) present model and actual descriptive statistics for these variables. To assess the dynamic performance of the model, we conduct regressions with actual (log) values against model-predicted values. For realized volatility and VIX, the $\overline{R}^2_{\text{model}}$ values range from 65% to 100%, with slope coefficients between 0.84 and 1.08, indicating the model's ability to explain a significant portion of their variations (Table 9).

Bond option-implied volatility variations — inferred from option prices — are also well-captured, with $\overline{R}^2_{\text{model}}$ ranging from 86% to 92% (Table 10). These results indicate that the model effectively captures time-series variation across a multitude of data dimensions. However, the model appears less valuable in tracking actual stock option prices, with $\overline{R}^2_{\text{model}}$ values between 28% and 47%.

These results are consistent with the errors computed using the log percentage fitting method, calculated as $\log(\frac{\text{model}_t}{\text{actual}_t})$. We observe that the mean absolute percentage errors (MAEs) for return volatilities and VIX indices are within the range of 0% and 32% for both bond and stock. Furthermore, bond options show MAEs between 7% and 11%.

While this model effectively captures the dynamic nature of volatilities and 7DTE OTM options for bonds, it also reveals some tension in pricing 7DTE deep OTM options for stocks. Stock put options have MAEs between 20% and 23%, and stock call options have MAEs between 31% to 33%. This indicates the model's difficulties in pricing such small maturity stock options and replicating fluctuations during tail episodes such as COVID-19 weekly cycles. A comparison with the closest small maturity stock option model, Andersen, Fusari, and Todorov (2017), is limited, as they do not benchmark to absolute error fit statistics.

Although this is not a formal hypothesis test, we demonstrate that 11 out of 12 model-implied means bracket the 95% stationary bootstrap confidence intervals of the actual means in Tables 9 and 10, indicating a close correspondence. By incorporating good and bad jump intensities, the model offers a theoretical basis to explain several observed small maturity phenomena. Its strength lies in its ability to establish the economic fundamentals behind the empirical observations. The estimated model recognizes the impact of positive and negative news on both mitigating and exacerbating risk and uncertainty in financial markets.

5.3 Characterizing consistency with small maturity phenomena in markets

We now examine whether our model can account for the small maturity characteristics of the market for traded stock volatility and small maturity correlations that are at the center of stock and bond markets. This analysis, pursued in Tables 11 and 12, is new to the literature.

5.3.1 Small maturity phenomena and model estimated VVIX to stock VIX ratio

To further assess the effectiveness of the model, we evaluate its performance using data that was not included during the estimation and development process. This evaluation examines the ability of the model to adjust to fluctuations in volatility and stock fundamentals during periods of market turmoil, as characterized by a decrease in the small maturity $\frac{\text{VVIX}_t}{\text{VIX}_t^{\mathbf{s}}}$ ratio. Such a measure reflects the changing cost relationship between small maturity VIX futures options and S&P 500 index options, with a lower ratio typically coinciding with an increase in VIX futures prices.

We first generate the 7DTE VIX futures prices, $F_t^{\text{vix}} \equiv \mathbb{E}_t^{\mathbb{Q}}\left(\sqrt{\{\text{VIX}_{t+\Delta}^{\mathbf{s}}\}^2}\right)$ — a forward-looking measure of traded stock volatility, capturing small maturity volatility expectations. The model-based F_t^{vix} is derived from the integral representation of the square root function (e.g., Schürger (2002)) with integration parameter ν, as follows:

$$F_t^{\text{vix}} = \frac{1}{2\sqrt{\pi}} \int_0^\infty \frac{1 - \mathbb{E}_t^{\mathbb{Q}}(e^{-\nu\,\{\text{VIX}_{t+\Delta}^{\mathbf{s}}\}^2})}{\nu^{\frac{3}{2}}} d\nu, \tag{33}$$

$$\text{with } \{\text{VIX}_t^{\mathbf{s}}\}^2 = \mathsf{w}^{\text{constant}} + \mathsf{w}^{\text{v}} \times V_t^{\mathbf{s}} + \mathsf{w}^{\text{good}} \times \lambda_t^{[\text{good}],\mathbb{Q}} + \mathsf{w}^{\text{bad}} \times \lambda_t^{[\text{bad}],\mathbb{Q}}, \tag{34}$$

where the constants $\mathsf{w}^{\text{constant}}$, w^{v}, w^{good}, and w^{bad} are shown in equations (C7)–(C10) of Appendix C. The expression for $\mathbb{E}_t^{\mathbb{Q}}(e^{-\nu\,\{\text{VIX}_{t+\Delta}^{\mathbf{s}}\}^2})$ is shown in (C11) of Appendix C. We construct the actual 7DTE F_t^{vix} by interpolating VIX futures contract prices of different maturities at Friday close.

Each Friday, we also construct the actual 11-day VVIX_t, as the 7DTE VIX options expiration cycle spans Tuesday to Tuesday. The first (last) weekly cycle for options on VIX futures is October 16, 2015 (February 17, 2023), for a total of 384 observations. The 11-day VVIX_t is

$$\underbrace{\{\text{VVIX}_t\}^2}_{\text{annualized decimals}} = \frac{2}{B_t^{t+\Delta}\Delta} \int_0^{F_t^{\text{vix}}} \frac{1}{K^2} \underbrace{\text{put}_t^{\text{vix}}[K]}_{\text{VIX put}}\, dK + \frac{2}{B_t^{t+\Delta}\Delta} \int_{F_t^{\text{vix}}}^\infty \frac{1}{K^2} \underbrace{\text{call}_t^{\text{vix}}[K]}_{\text{VIX call}}\, dK, \qquad \Delta = \frac{11}{365}. \tag{35}$$

Appendix C shows that the model-based $\{\text{VVIX}_t\}^2 \equiv \mathbb{E}_t^{\mathbb{Q}}(\{\frac{-2}{\Delta}\}\log(\frac{F_{t+\Delta}^{\text{vix}}}{F_t^{\text{vix}}}))$ is of the form

$$\{\text{VVIX}_t\}^2 = \frac{1}{\pi} \int_0^\infty \text{Re}\left[\left(\mathbb{C}_t[\phi] \times \frac{2\log(F_t^{\text{vix}}) + \log(i\,\phi) + \gamma^{\text{euler}}}{\Delta\, i\, \phi}\right)\Big|_{\phi=\mathsf{a}+i\,\mathsf{b}}\right] d\mathsf{a}. \tag{36}$$

The characteristic function $\mathbb{C}_t[\phi] \equiv \mathbb{E}_t^{\mathbb{Q}}(e^{i\,\phi\,\{\mathrm{VIX}^{\mathbf{s}}_{t+\Delta}\}^2})$ is presented in equation (C12). Equation (36) enforces $\mathrm{Re}[i\,\phi] > 0$, and γ^{euler} is Euler's constant with a numerical value ≈ 0.577216.

The consideration of the $\frac{\mathrm{VVIX}_t}{\mathrm{VIX}^{\mathbf{s}}_t}$ ratio and 7DTE F_t^{vix} enables us to examine the impact of stochastic intensity rates and diffusive volatility on traded stock volatility and VIX option prices. Furthermore, this analysis helps determine the robustness and out-of-sample applicability of our model to a traded stock volatility benchmark and VIX option prices, featuring two Poisson processes, each governed by independent jump intensity rates.

Table 11 shows the comparison between model and actual $\frac{\mathrm{VVIX}_t}{\mathrm{VIX}^{\mathbf{s}}_t}$ and 7DTE F_t^{vix}. We evaluate the dynamic performance via the regression $\log(\text{actual}_t) = \mathbb{a} + \mathbb{b}\log(\text{model}_t) + \widetilde{e}_t$. The estimated $\mathbb{b}$ is 0.32 for $\frac{\mathrm{VVIX}_t}{\mathrm{VIX}^{\mathbf{s}}_t}$ and 0.66 for F_t^{vix}, both with a NW$[p]$ of 0.00. The regressions support an $\overline{R}^2_{\text{model}}$ of 49% and 56%, respectively. The 95% confidence interval on the actual mean $\log(\frac{\mathrm{VVIX}_t}{\mathrm{VIX}^{\mathbf{s}}_t})$ is [1.6 1.9] whereas the model mean is 1.7, with an MAE of 46% for $\frac{\mathrm{VVIX}_t}{\mathrm{VIX}^{\mathbf{s}}_t}$. Furthermore, the 95% confidence interval on actual mean F_t^{vix} is [16.2 22.7] and the model mean is 16.1, yielding an MAE of 26%.[7] Thus, being developed independently of information on VIX futures options, the model shows its quantitative correspondence through external validation.

Figure 3 indicates that the model captures the behavior of traded stock volatility and the $\frac{\mathrm{VVIX}_t}{\mathrm{VIX}^{\mathbf{s}}_t}$ ratio, with the exception of some periods of extreme market movements. These discrepancies are likely caused by limitations in the model's ability to forecast spikes in volatility and VIX call option prices during times of adverse market-wide events. Crucial to our themes, the model consistently reflects a decline in $\frac{\mathrm{VVIX}_t}{\mathrm{VIX}^{\mathbf{s}}_t}$ during periods of market stress, as seen, for example, during the four weekly cycles of the COVID-19 pandemic in March 2020.

Table 11 additionally conducts a regression analysis analogous to Table 6, followed by the predictability regressions using model-implied and actual $\log(\frac{\mathrm{VVIX}_t}{\mathrm{VIX}^{\mathbf{s}}_t})$, respectively, as dependent variables. We investigate whether our model can replicate small maturity phenomena founded in safety in that $\frac{\mathrm{VVIX}_t}{\mathrm{VIX}^{\mathbf{s}}_t}$ tends to go down during periods of heightened uncertainty. Our results are consistent with the notion that the model-generated $\log(\frac{\mathrm{VVIX}_t}{\mathrm{VIX}^{\mathbf{s}}_t})$ aligns with the data pattern by being lower in pessimistic states and higher in optimistic states. Furthermore, variations in

[7] The formula for VVIX_t in equation (36) is new to the literature. Additionally, our small maturity approach and dynamic consistency exercises differ from, among others, Zhu and Lian (2012) and Bardgett, Gourier, and Leippold (2019), who model constant jump intensity rate, and Eraker and Yang (2022), who rely on equilibrium model calibrations. Bacon, Bégin, and Gauthier (2024) employ jump intensities that depend on the return variances.

the model-based $\log(\frac{\text{VVIX}_t}{\text{VIX}_t^{\mathbf{s}}})$ can be forecasted by a group of variables that also anticipate a negative stock-bond correlation. A key finding is the adherence in the model's and actual predictive slope coefficients' signs. Notably, this analysis corroborates the relevance of understanding market reactions to negative events and their impact on investor behavior.

In closing, our model characterizations examine the observed attributes of $\frac{\text{VVIX}_t}{\text{VIX}_t^{\mathbf{s}}}$ in relation to estimated jump intensities and diffusive stock volatility. Previous research has analyzed volatility-of-volatility expectations using monthly VVIX_t, but the quantitative implications of small maturity VVIX_t have remained unexplored. We reconcile by quantifying the $\frac{\text{VVIX}_t}{\text{VIX}_t^{\mathbf{s}}}$ ratio, which reflects the manner in which the cost of volatility protection differs from the cost of downside stock risk protection. This new empirical and modeling angle helps us understand the interconnected dynamics of small maturity volatility protection and safety phenomena evident in stock and bond markets.

5.3.2 Model-implied predictions of small maturity stock-bond association

Can the model predict subsequent interdependencies between the bond and stock markets? Connecting to flight-to-quality effects, this exercise focuses on the small maturity correlation between stock returns and bond returns. Our objective is to analyze and contrast the model forecast with the empirical data, taking into account the predictive capabilities of variables in Tables 6 and 11.

The following model-based forecasts are generated over t and $t+\Delta$, computed at time-t:

$$\rho_t^{r^{\mathbf{s}},r^{\mathbf{b}}} = \text{cov}_t^{\mathbb{P}}(\log(\frac{F_{t+\Delta}^{\mathbf{s}}}{F_t^{\mathbf{s}}}), \log(\frac{F_{t+\Delta}^{\mathbf{b}}}{F_t^{\mathbf{b}}}))/\sqrt{\text{var}_t^{\mathbb{P}}(\log(\frac{F_{t+\Delta}^{\mathbf{s}}}{F_t^{\mathbf{s}}})) \times \text{var}_t^{\mathbb{P}}(\log(\frac{F_{t+\Delta}^{\mathbf{b}}}{F_t^{\mathbf{b}}}))}. \tag{37}$$

The manner in which $\rho_t^{r^{\mathbf{s}},r^{\mathbf{b}}}$ is linked to $[\lambda_t^{[\text{good}],\mathbb{P}}, \lambda_t^{[\text{bad}],\mathbb{P}}, V_t^{\mathbf{b}}, V_t^{\mathbf{s}}]'$ is

$$\underbrace{\frac{1}{\Delta}\text{cov}_t^{\mathbb{P}}(\log(\frac{F_{t+\Delta}^{\mathbf{s}}}{F_t^{\mathbf{s}}}), \log(\frac{F_{t+\Delta}^{\mathbf{b}}}{F_t^{\mathbf{b}}}))}_{\text{in equation (16)}}, \quad \text{where} \tag{38}$$

$$\frac{1}{\Delta}\text{var}_t^{\mathbb{P}}(\log(\frac{F_{t+\Delta}^{\mathbf{s}}}{F_t^{\mathbf{s}}})) \sim V_t^{\mathbf{s}} + 2\left\{\mu^{\mathbf{s}+,\mathbb{P}}\right\}^2 \lambda_t^{[\text{good}],\mathbb{P}} + 2\left\{\mu^{\mathbf{s}-,\mathbb{P}}\right\}^2 \lambda_t^{[\text{bad}],\mathbb{P}} \quad \text{and} \tag{39}$$

$$\frac{1}{\Delta}\text{var}_t^{\mathbb{P}}(\log(\frac{F_{t+\Delta}^{\mathbf{b}}}{F_t^{\mathbf{b}}})) \sim V_t^{\mathbf{b}} + 2\left\{\mu^{\mathbf{b}-,\mathbb{P}}\right\}^2 \lambda_t^{[\text{good}],\mathbb{P}} + 2\left\{\mu^{\mathbf{b}+,\mathbb{P}}\right\}^2 \lambda_t^{[\text{bad}],\mathbb{P}}. \tag{40}$$

We benchmark model estimates to actual magnitudes of small maturity stock-bond association, thereby posing a challenge for models. The gist of our investigation in this section is that the estimated model captures a crucial data property observed in stock and bond markets.

In this regard, Table 12 shows a comparison between the model-based forecasts and the actual correlations calculated from intraday stock and bond return observations sampled at synchronized five-minute intervals during t and $t + \Delta$ (in line with the methods of, among others, Barndorff-Nielsen and Shephard (2004) and Aït-Sahalia, Fan, and Xiu (2010)). The model produces an average negative stock-bond correlation of -0.20, while the data shows a cross-correlation of -0.28 (95% bootstrap confidence interval of $[-0.35 \ -0.21]$), indicating a close anchoring. Furthermore, the model correctly predicts the sign of the stock-bond correlation 86% of the time.

Despite the model identifying the general pattern, the reported $\overline{R}^2$ of 5.3% from the predictive regression, as shown in the $\overline{R}^2_{\text{model}}$ column, indicates a limitation in producing precise point-to-point forecasts. To benchmark the model's performance, we contrast this $\overline{R}^2_{\text{model}}$ to alternative regression-based $\overline{R}^2$ values. Specifically, we perform predictability regressions equivalent to those in Table 6, using the actual $\rho_t^{r^{\mathbf{s}},r^{\mathbf{b}}}$ as the dependent variable, and gauge the $\overline{R}^2$ values based on the 11 variables. This evaluation produces a highest $\overline{R}^2$ of 14.8% (displayed under the $\overline{R}^2_{\text{highest}}$ column), which suggests that predicting small maturity stock-bond correlations is not confined to the model-based forecasts, but rather a difficulty with forecasting the data series itself.

6 Conclusion

Unifying patterns emerge pertinent to the modeling of small maturity phenomena. A key finding is the asymmetry in correlations of small maturity option returns. Returns of OTM calls on bond are positively correlated with returns of OTM puts on stock. In contrast, returns of OTM puts on bond show little correlation with returns of OTM calls on stock. Our inferences are backed by statistical assurances using the bootstrap method. Moreover, these effects align with a decrease in the small maturity VVIX to the stock VIX ratio during market stress, indicating a higher cost for downside stock risk protection compared to upside volatility risk protection. Reproducing these small maturity data features may prove challenging for extant models.

Our study reveals the consequences of de-risking, a strategy employed by investors after significant stock market declines to shift their funds from risky stocks to safer bonds. This shift coincides with a rise in the demand for small maturity bond futures calls, which act as a safeguard against underperforming stocks. Additionally, this heightened uncertainty coincides with an

increased demand for small maturity stock puts and VIX calls, highlighting the reasons behind investors' inclination toward purchasing bond futures calls.

In our investigation, we explore the role of small maturity options in asset pricing within a framework that focuses on jump risks and safety considerations. This framework stands apart from extant theories and considers simultaneous jumps in stock and bond dynamics, utilizing bivariate jump distributions and two stochastic intensities. Critically, these model attributes distinguish between good and bad jump intensity rates, which has implications for the joint dynamics of stock and bond prices and the pricing of small maturity options.

Respecting our empirical findings, our framework suggests that downward stock price jumps occur simultaneously with upward bond price jumps, and vice versa, each governed by distinct jump size distributions. This theoretical structure enables us to capture salient empirical outcomes. Furthermore, our framework incorporates bad and good stochastic jump intensity rates, along with stochastic volatility and interest rates in the dynamics of both stock and bond prices, allowing us to explore their role in capturing empirical phenomena in financial markets.

We employ the Kalman filter and quasi-maximum-likelihood estimation to estimate the model. Our empirical evaluation shows progress in reproducing various aspects of financial markets. This includes fitting stock and bond volatilities and small maturity bond futures VIX and stock VIX, reflecting risk-neutral volatilities. The model performs well to the range of bond options while tracking fluctuations in the ratio of small maturity VVIX to stock VIX. Our analysis highlights the promises and difficulties of simultaneously fitting the cross-section of small maturity bond and stock option prices.

The proposed model takes into account the connection between stock and bond returns, evidenced by the correlation between them. Our estimated model mimics the observed data by showing data-consistent negative values for the stock-bond correlation, capturing critical aspects of the stock-bond relationship.

References

Y. Aït-Sahalia. Disentangling diffusion from jumps. *Journal of Financial Economics*, 74(3):487–528, 2004.

Y. Aït-Sahalia and J. Jacod. Analyzing the spectrum of asset returns: Jump and volatility components in high frequency data. *Journal of Econometrics*, 50(4):1007–1050, 2012.

Y. Aït-Sahalia, J. Fan, and D. Xiu. High-frequency covariance estimates with noisy and asynchronous financial data. *Journal of the American Statistical Association*, 105:15014–1517, 2010.

D. Amaya, P. Christoffersen, K. Jacobs, and A. Vasquez. Does realized skewness predict the cross-section of equity returns? *Journal of Financial Economics*, 118:135–167, 2015.

T. Andersen, T. Bollerslev, F. Diebold, and P. Labys. Modeling and forecasting realized volatility. *Econometrica*, 71(2):529–626, 2003.

T. Andersen, T. Bollerslev, F. Diebold, and C. Vega. Real-time price discovery in global stock, bond and foreign exchange markets. *Journal of International Economics*, 73:251–277, 2007.

T. Andersen, N. Fusari, and V. Todorov. Short-term market risks implied by weekly options. *Journal of Finance*, 72(3):1336–1386, 2017.

A. Ang and J. Chen. Asymmetric correlations of equity portfolios. *Journal of Financial Economics*, 63:443–494, 2002.

E. Bacon, J. Bégin, and G. Gauthier. On general semi-closed-form solutions for VIX derivative pricing. *Quantitative Finance*, 24(12):1875–1882, 2024.

L. Baele, G. Bekaert, and K. Inghelbrecht. The determinants of stock and bond return comovements. *Review of Financial Studies*, 23:2374–2428, 2010.

L. Baele, G. Bekaert, K. Inghelbrecht, and M. Wei. Flights to safety. *Review of Financial Studies*, 33:689–746, 2020.

G. Bakshi, J. Crosby, and X. Gao. Dark matter in (volatility and) equity option risk premiums. *Operations Research*, 70(6):3108–3124, 2022.

G. Bakshi, J. Crosby, X. Gao, and J. Hansen. Treasury option returns and models with unspanned risks. *Journal of Financial Economics*, 150(3):82–110, 2023.

N. Balakrishnan and C. Lai. *Continuous Bivariate Distributions*. Springer, New York, NY, 2009.

C. Bardgett, E. Gourier, and M. Leippold. Inferring volatility dynamics and risk premia from the S&P 500 and VIX markets. *Journal of Financial Economics*, 131:593–618, 2019.

O. Barndorff-Nielsen and N. Shephard. Econometric analysis of realized covariation: High frequency based covariance, regression, and correlation in financial economics. *Econometrica*, 72:885–925, 2004.

O. Barndorff-Nielsen and N. Shephard. Econometrics of testing for jumps in financial economics using bipower variation. *Journal of Financial Econometrics*, 4(1):1–30, 2006.

T. Bollerslev and V. Todorov. Tails, fears and risk premia. *Journal of Finance*, 66:2165–2211, 2011.

T. Bollerslev and V. Todorov. The jump leverage risk premium? *Journal of Financial Economics*, 150(3):103723, 2023.

T. Bollerslev, G. Tauchen, and H. Zhou. Expected stock returns and variance risk premia. *Review of Financial Studies*, 22:4463–4493, 2009.

J. Campbell, A. Sunderam, and L. Viceira. Inflation bets or deflation hedges? The changing risks of nominal bonds. *Critical Finance Review*, 6(2):263–301, 2017.

J. Campbell, C. Pflueger, and L. Viceira. Macroeconomic drivers of bond and equity risks. *Journal of Political Economy*, 128(8):3148–3185, 2020.

P. Carr and L. Wu. What type of process underlies options? A simple robust test. *Journal of Finance*, 58(6):2581–2610, 2003.

P. Carr and L. Wu. Stochastic skew in currency options. *Journal of Financial Economics*, 86: 213–247, 2007.

A. Cieslak and H. Pang. Common shocks in stocks and bonds. *Journal of Financial Economics*, 142(2):880–904, 2021.

R. Connolly, L. Sun, and C. Stivers. Stock market uncertainty and the stock-bond return relation. *Journal of Financial and Quantitative Analysis*, 40:161–194, 2005.

A. David and P. Veronesi. What ties return volatilities to price valuations and fundamentals? *Journal of Political Economy*, 121:682–746, 2013.

A.-M. Dumitru and G. Urga. Identifying jumps in financial assets: A comparison between nonparametric jump tests. *Journal of Business & Economic Statistics*, 30(2):242–255, 2012.

B. Eraker and A. Yang. The price of higher order catastrophe insurance: The case of VIX options. *Journal of Finance*, 77:3289–3337, 2022.

A. Ermolov. Time-varying risk of nominal bonds: How important are macroeconomic shocks? *Journal of Financial Economics*, 145(1):1–28, 2022.

Y. Hong, J. Tu, and G. Zhou. Asymmetries in stock returns: Statistical tests and economic evaluation. *Review of Financial Studies*, 20(5):1547–1581, 2006.

J. Jacod and V. Todorov. Testing for common arrivals of jumps for discretely observed multidimensional processes. *Annals of Statistics*, 37(4):1792–1838, 2009.

S. Kou. A jump-diffusion model for option pricing. *Management Science*, 48:1086–1101, 2002.

S. Kozak. Dynamics of bond and stock returns. *Journal of Monetary Economics*, 126:188–209, 2022.

S. Lee and P. Mykland. Jumps in financial markets: A new nonparametric test and jump dynamics. *Review of Financial Studies*, 21:2535–2563, 2008.

L. Liu, A. Patton, and K. Sheppard. Does anything beat 5-minute RV? A comparison of realized measures across multiple asset classes. *Journal of Econometrics*, 187:293–311, 2015.

F. Longin and B. Solnik. Extreme correlation of international equity markets. *Journal of Finance*, 56:649–676, 2001.

R. Merton. Option pricing when underlying stock returns are discontinuous. *Journal of Financial Economics*, 3(1):125–144, 1976.

A. Patton. Modelling asymettric exchange rate dependence. *International Economic Review*, 47: 527–556, 2006.

P. Protter. *Stochastic Integration and Differential Equations*. Springer, Berlin, 2013.

K. Schürger. Laplace transforms and suprema of stochastic processes. Working paper, University of Bonn, 2002.

S. Shreve. *Stochastic Calculus for Finance*. Springer, New York, NY, USA, 2003.

J. Wachter. Can time-varying risk of rare disasters explain aggregate stock market volatility? *Journal of Finance*, 68:987–1035, 2013.

S. Zhu and G. Lian. An analytical formula for VIX futures and its applications. *Journal of Futures Markets*, 32(2):166–190, 2012.

Appendix

A Proof of (9)–(10) when option maturity Δ is small

In what follows, we make the assumption that $\mu_\ell^{\mathbf{s},\mathbb{P}}$, $V_\ell^{\mathbf{s}}$, $\mu_\ell^{\mathbf{b},\mathbb{P}}$, $V_\ell^{\mathbf{b}}$, $\lambda_\ell^{[\text{good}],\mathbb{P}}$, $\lambda_\ell^{[\text{bad}],\mathbb{P}}$, $\lambda_\ell^{[\text{good}],\mathbb{Q}}$, and $\lambda_\ell^{[\text{bad}],\mathbb{Q}}$ (defined, for example, in (4) and (5)), are predictable with respect to the filtration $\mathcal{F}_\ell$. Importantly, we assume that they are bounded in some neighborhood of $\ell = t$, and they are such that the futures prices are always nonnegative.

Define the gross futures returns, for $\ell \geq t$, as follows:

$$G_\ell^{\mathbf{s}} \equiv \underbrace{\frac{F_\ell^{\mathbf{s}}}{F_t^{\mathbf{s}}}}_{\text{gross stock futures return}} \quad \text{and} \quad G_\ell^{\mathbf{b}} \equiv \underbrace{\frac{F_\ell^{\mathbf{b}}}{F_t^{\mathbf{b}}}}_{\text{gross bond futures return}}, \quad \text{for } \ell \geq t. \tag{A1}$$

By construction, $G_t^{\mathbf{s}} = 1$ and $G_t^{\mathbf{b}} = 1$. It holds that $\frac{dF_\ell^{\mathbf{s}}}{F_{\ell-}^{\mathbf{s}}} = \frac{dG_\ell^{\mathbf{s}}}{G_{\ell-}^{\mathbf{s}}}$.

Tanaka's formula for OTM call option payoffs implies that

$$\begin{aligned}
\overbrace{\max(G_{t+\Delta}^{\mathbf{s}} - k^{\mathbf{s}}, 0)}^{\text{option payoff}} &= \overbrace{[G_t^{\mathbf{s}} - k^{\mathbf{s}}]^+}^{\text{intrinsic value}} + \overbrace{\int_{t+}^{t+\Delta} \mathbb{1}_{\{G_{\ell-}^{\mathbf{s}} > k^{\mathbf{s}}\}} dG_\ell^{\mathbf{s}}}^{\text{trading strategy in futures}} + \overbrace{\mathbb{L}_t^{t+\Delta}[k^{\mathbf{s}}]}^{\text{local time}} \\
&+ \underbrace{\sum_{t<\ell\leq t+\Delta} \mathbb{1}_{\{G_{\ell-}^{\mathbf{s}} \leq k^{\mathbf{s}}\}} \max(G_\ell^{\mathbf{s}} - k^{\mathbf{s}}, 0)}_{\text{jumps crossing the strike from below}} \\
&+ \underbrace{\sum_{t<\ell\leq t+\Delta} \mathbb{1}_{\{G_{\ell-}^{\mathbf{s}} > k^{\mathbf{s}}\}} \max(k^{\mathbf{s}} - G_\ell^{\mathbf{s}}, 0)}_{\text{jumps crossing the strike from above}},
\end{aligned} \tag{A2}$$

where $\mathbb{1}_{\{a\}}$ is an indicator function. Denote by $[G^{\mathbf{s}}, G^{\mathbf{s}}]_\ell^{\text{c}}$ the path-by-path continuous part of the quadratic variation (see Protter (2013, page 70)) and $\boldsymbol{\delta}_{\{\bullet\}}$ as the Dirac delta function. Recognize that $d[G^{\mathbf{s}}, G^{\mathbf{s}}]_\ell^{\text{c}} = (\sqrt{V_\ell^{\mathbf{s}}}\, G_{\ell-}^{\mathbf{s}})^2\, d\ell$. In equation (A2), the term

$$\mathbb{L}_t^{t+\Delta}[k^{\mathbf{s}}] \;=\; \frac{1}{2}\int_t^{t+\Delta} \boldsymbol{\delta}_{\{G_\ell^{\mathbf{s}} \,-\, k^{\mathbf{s}}\}}\, d[G^{\mathbf{s}}, G^{\mathbf{s}}]_\ell^{\text{c}} \;=\; \frac{1}{2}\int_t^{t+\Delta} \boldsymbol{\delta}_{\{G_\ell^{\mathbf{s}} \,-\, k^{\mathbf{s}}\}}\, (\sqrt{V_\ell^{\mathbf{s}}}\, G_{\ell-}^{\mathbf{s}})^2\, d\ell \tag{A3}$$

is the *local time* (Protter (2013, Theorem 71, page 221)). Intuitively, $\mathbb{L}_t^{t+\Delta}[k^{\mathbf{s}}]$ captures the variance uncertainty associated with the times when $G_\ell^{\mathbf{s}}$ is exactly equal to the level $k^{\mathbf{s}}$.

Since $(G_\ell^{\mathbf{s}})$ is a martingale under $\mathbb{Q}$, it follows that $\mathbb{E}_t^{\mathbb{Q}}(\int_{t+}^{t+\Delta} \mathbb{1}_{\{G_{\ell-}^{\mathbf{s}} > k^{\mathbf{s}}\}} dG_\ell^{\mathbf{s}}) = 0$. Taking expectations under $\mathbb{Q}$ of equation (A2) implies the following:

$$\begin{aligned}\mathbb{E}_t^{\mathbb{Q}}([G^{\mathbf{s}}_{t+\Delta}-k^{\mathbf{s}}]^+) &= [G^{\mathbf{s}}_t-k^{\mathbf{s}}]^+ + \frac{1}{2}\int_t^{t+\Delta}\mathbb{E}_t^{\mathbb{Q}}(\boldsymbol{\delta}_{\{G^{\mathbf{s}}_\ell - k^{\mathbf{s}}\}}(\sqrt{V^{\mathbf{s}}_\ell}\,G^{\mathbf{s}}_{\ell-})^2)\,d\ell \\ &+ \int_t^{t+\Delta}\mathbb{E}_t^{\mathbb{Q}}(\lambda_\ell^{[\text{good}],\mathbb{Q}}\int_0^\infty \mathbb{1}_{\{G^{\mathbf{s}}_{\ell-}\le k^{\mathbf{s}}\}}\max(G^{\mathbf{s}}_{\ell-}e^{x^{\mathbf{s}+}}-k^{\mathbf{s}},0)\,\mathbb{q}[x^{\mathbf{s}+}]\,dx^{\mathbf{s}+})\,d\ell \\ &+ \int_t^{t+\Delta}\mathbb{E}_t^{\mathbb{Q}}(\lambda_\ell^{[\text{bad}],\mathbb{Q}}\int_0^\infty \mathbb{1}_{\{G^{\mathbf{s}}_{\ell-}>k^{\mathbf{s}}\}}\max(k^{\mathbf{s}}-G^{\mathbf{s}}_{\ell-}e^{-x^{\mathbf{s}-}},0)\,\mathbb{q}[x^{\mathbf{s}-}]\,dx^{\mathbf{s}-})\,d\ell. \end{aligned} \tag{A4}$$

In the second and third lines, we have substituted $G^{\mathbf{s}}_\ell = G^{\mathbf{s}}_{\ell-}e^{x^{\mathbf{s}+}}$ (for up price jumps) and $G^{\mathbf{s}}_\ell = G^{\mathbf{s}}_{\ell-}e^{-x^{\mathbf{s}-}}$ (for down price jumps). Additionally, in the first line, we have used the definition of the Dirac delta function and the sifting property, to write

$$\mathbb{E}_t^{\mathbb{Q}}(\boldsymbol{\delta}_{\{G^{\mathbf{s}}_\ell - k^{\mathbf{s}}\}}(\sqrt{V^{\mathbf{s}}_\ell}\,G^{\mathbf{s}}_{\ell-})^2) = \mathbb{E}_t^{\mathbb{Q}}(\{\sqrt{V^{\mathbf{s}}_\ell}\}^2\,|\,G^{\mathbf{s}}_{\ell-}=k^{\mathbf{s}})\times(k^{\mathbf{s}})^2\times q^{\mathbb{Q}}_{t,\ell}[k^{\mathbf{s}}]. \tag{A5}$$

$$\text{Hence, } \mathbb{E}_t^{\mathbb{Q}}(\mathbb{L}_t^{t+\Delta}[k^{\mathbf{s}}]) = \frac{\Delta}{2}\{\mathbb{E}_t^{\mathbb{Q}}(\{\sqrt{V^{\mathbf{s}}_\ell}\}^2\,|\,G^{\mathbf{s}}_{\ell-}=k^{\mathbf{s}})\}\times(k^{\mathbf{s}})^2\times q^{\mathbb{Q}}_{t,\ell}[k^{\mathbf{s}}], \tag{A6}$$

where $q^{\mathbb{Q}}_{t,\ell}[k^{\mathbf{s}}]$ is the probability density function for the futures price to move from $G^{\mathbf{s}}_t$ at time t to $k^{\mathbf{s}}$ at time ℓ.

In the right side of equation (A4), we have that $[G^{\mathbf{s}}_t - k^{\mathbf{s}}]^+ = 0$ (since we consider OTM call options). Now, we consider the limit of equation (A4) as $\Delta \to 0$.

- In the limit, we can replace $G^{\mathbf{s}}_{\ell-}$ by $G^{\mathbf{s}}_t \equiv 1$ in the second and third lines.
- Thus, in the third line, $\mathbb{1}_{\{G^{\mathbf{s}}_{\ell-}>k^{\mathbf{s}}\}}$ is replaced by $\mathbb{1}_{\{1>k^{\mathbf{s}}\}}$, but this is zero since we consider only OTM call options and, hence, the third line vanishes.
- Similarly, $\mathbb{1}_{\{G^{\mathbf{s}}_{\ell-}\le k^{\mathbf{s}}\}}$ is replaced by $\mathbb{1}_{\{1\le k^{\mathbf{s}}\}}$, which is one.
- The term $\lambda_\ell^{[\text{good}],\mathbb{Q}}$ is replaced by $\lambda_t^{[\text{good}],\mathbb{Q}}$ since $\lambda_\ell^{[\text{good}],\mathbb{Q}}$ is predictable with respect to the filtration $\mathcal{F}_\ell$.

Regarding the probability density function $q^{\mathbb{Q}}_{t,\ell}[k^{\mathbf{s}}]$, we set

$$c_t^{\mathbb{Q}} \equiv \frac{(G^{\mathbf{s}}_t - k^{\mathbf{s}})^2}{2\,\mathbb{E}_t^{\mathbb{Q}}(\{\sqrt{V^{\mathbf{s}}_\ell}\}^2\,|\,G^{\mathbf{s}}_{\ell-}=k^{\mathbf{s}})}. \tag{A7}$$

Following Carr and Wu (2003, page 2589), and references therein, in the small Δ limit, $q^{\mathbb{Q}}_{t,\ell}[k^{\mathbf{s}}]$ becomes the Gaussian density function, expressed as follows:

$$q^{\mathbb{Q}}_{t,\ell}[k^{\mathbf{s}}] = \frac{1}{\sqrt{2\,\pi\,\Delta}\,\sqrt{\mathbb{E}_t^{\mathbb{Q}}(\{\sqrt{V^{\mathbf{s}}_\ell}\}^2\,|\,G^{\mathbf{s}}_{\ell-}=k^{\mathbf{s}})}}\,\exp(-c_t^{\mathbb{Q}}/\Delta), \quad \text{for } c_t^{\mathbb{Q}} \text{ in equation (A7).} \tag{A8}$$

Thus, considering the small Δ limit, equation (A4) becomes

$$\mathbb{E}_t^{\mathbb{Q}}(\max(G^{\mathbf{s}}_{t+\Delta} - k^{\mathbf{s}}, 0)) \;\sim\; \frac{1}{2}\,(k^{\mathbf{s}})^2\,\{\mathbb{E}_t^{\mathbb{Q}}(\{\sqrt{V^{\mathbf{s}}_\ell}\}^2 \,|\, G^{\mathbf{s}}_{\ell-} = k^{\mathbf{s}})\}\,\frac{\sqrt{\Delta}\,\exp(-c_t^{\mathbb{Q}}/\Delta)}{\sqrt{2\pi}\sqrt{\mathbb{E}_t^{\mathbb{Q}}(\{\sqrt{V^{\mathbf{s}}_\ell}\}^2 \,|\, G^{\mathbf{s}}_{\ell-} = k^{\mathbf{s}})}}$$
$$+ \quad \Delta\,\lambda_t^{[\text{good}],\mathbb{Q}} \int_0^\infty \max(e^{x^{\mathbf{s}+}} - k^{\mathbf{s}}, 0)\,\mathbb{q}[x^{\mathbf{s}+}]\,dx^{\mathbf{s}+}. \tag{A9}$$

Since, for small Δ, $\sqrt{\Delta}\,\exp(-c_t^{\mathbb{Q}}/\Delta) \ll \Delta$, we obtain the following (provided $\lambda_t^{[\text{good}],\mathbb{Q}} \neq 0$):

$$\mathbb{E}_t^{\mathbb{Q}}(\max(G^{\mathbf{s}}_{t+\Delta} - k^{\mathbf{s}}, 0)) \;\sim\; \lambda_t^{[\text{good}],\mathbb{Q}}\,\Delta \int_0^\infty \max(e^{x^{\mathbf{s}+}} - k^{\mathbf{s}}, 0)\,\mathbb{q}[x^{\mathbf{s}+}]\,dx^{\mathbf{s}+}. \tag{A10}$$

Thus, the expectation under $\mathbb{Q}$ of $\max(G^{\mathbf{s}}_{t+\Delta} - k^{\mathbf{s}}, 0)$ is linear in Δ and in $\lambda_t^{[\text{good}],\mathbb{Q}}$.

Finally, using the definition of covariance, we can write

$$\begin{aligned}
\frac{\text{call}[k^{\mathbf{s}}]}{F_t^{\mathbf{s}}} = \mathbb{E}_t^{\mathbb{Q}}(e^{-\int_t^{t+\Delta} r_\ell\,d\ell}\max(G^{\mathbf{s}}_{t+\Delta} - k^{\mathbf{s}}, 0)) \;&=\; B_t^{t+\Delta}\,\mathbb{E}_t^{\mathbb{Q}}(\max(G^{\mathbf{s}}_{t+\Delta} - k^{\mathbf{s}}, 0)) \\
&+\; \underbrace{B_t^{t+\Delta}\,\text{Cov}_t^{\mathbb{Q}}(\frac{e^{-\int_t^{t+\Delta} r_\ell d\ell}}{B_t^{t+\Delta}}, \max(G^{\mathbf{s}}_{t+\Delta} - k^{\mathbf{s}}, 0))}_{\approx\ 0 \text{ for small horizon } \Delta} \\
&=\; B_t^{t+\Delta}\,\mathbb{E}_t^{\mathbb{Q}}(\max(G^{\mathbf{s}}_{t+\Delta} - k^{\mathbf{s}}, 0)).
\end{aligned} \tag{A11}$$

In the second line, we recognize that, in the small Δ limit, $\frac{e^{-\int_t^{t+\Delta} r_\ell d\ell}}{B_t^{t+\Delta}}$ tends to a constant, and, thus, the covariance vanishes. The proof of puts on stock and bond options (e.g., $\mathbb{E}_t^{\mathbb{Q}}(e^{-\int_t^{t+\Delta} r_\ell\,d\ell}\max(G^{\mathbf{b}}_{t+\Delta} - k^{\mathbf{b}}, 0))$) is almost identical and, therefore, omitted (but available from authors). ■

B Proof of measurement expressions used in the Kalman filter

With the form of the exponential density in equation (14) and $\log(k) > 0$, an integration step yields

$$\int_0^\infty \max(e^x - k, 0)\,\mathbb{q}[x]\,dx = \int_{\log(k)}^\infty (e^x - k)\,\underbrace{\mu^{-1}\,e^{-x/\mu}}_{\substack{\text{exponential}\\ \text{density}}}\,dx \;=\; \frac{1}{\frac{1}{\mu} - 1}\{e^{-(\frac{1}{\mu}-1)\log(k)}\}. \tag{B1}$$

Noting that $\log(k) < 0$ for OTM put on stock, we have

$$\int_0^\infty \max(k - e^{-x}, 0)\,\mathbb{q}[x]\,dx = \int_{-\log(k)}^\infty (k - e^{-x})\,\frac{1}{\mu}\,e^{-x/\mu}\,dx \;=\; \frac{1}{1 + \frac{1}{\mu}}\{e^{(1+\frac{1}{\mu})\log(k)}\}. \tag{B2}$$

We obtain the forms of the OTM option price expressions in the measurement equation (29). ■

Aligning with the form of the dynamics of $F_t^{\mathbf{s}}$ under $\mathbb{P}$ in equation (4), we postulate the corresponding $\mathbb{Q}$ dynamics — with zero drift — as follows:

$$\frac{dF_t^{\mathbf{s}}}{F_{t-}^{\mathbf{s}}} = \sqrt{V_t^{\mathbf{s}}}\, dW_t^{\mathbf{s},\mathbb{Q}} + (e^{x^{\mathbf{s}+}}-1)\, d\mathbb{N}_t^{[\text{good}],\mathbb{Q}} - \lambda_t^{[\text{good}],\mathbb{Q}}\, dt \int_0^\infty (e^{x^{\mathbf{s}+}}-1)\, \mathfrak{q}[x^{\mathbf{s}+}] dx^{\mathbf{s}+}$$
$$+ \underbrace{(e^{-x^{\mathbf{s}-}}-1)\, d\mathbb{N}_t^{[\text{bad}],\mathbb{Q}}}_{\text{downside stock jump component, } \mathbb{Q}} - \underbrace{\lambda_t^{[\text{bad}],\mathbb{Q}}}_{\text{stochastic}}\, dt \int_0^\infty (e^{-x^{\mathbf{s}-}}-1)\, \underbrace{\mathfrak{q}[x^{\mathbf{s}-}]}_{\mathbb{Q}\text{ density}}\, dx^{\mathbf{s}-}. \quad \text{(B3)}$$

We then obtain the form of $\{\text{VIX}_t\}^2 = \mathbb{E}_t^{\mathbb{Q}}(\{\frac{-2}{\Delta}\}\log(\frac{F_{t+\Delta}}{F_t}))$ using the moment-generating function of the exponential density and the standard formulation of $\frac{1}{\Delta}\int_t^{t+\Delta}\mathbb{E}_t^{\mathbb{Q}}(V_\ell)d\ell$. See Appendix C. ■

The expected integrated variance of futures return under $\mathbb{P}$ has two steps. First,

$$\mathbb{v}_t^{\mathbf{s}} = \frac{1}{dt}\text{var}_t^{\mathbb{P}}[d\log(F_t^{\mathbf{s}})] = \{\mu^{\mathbf{s}+}\}^2\lambda_t^{[\text{good}],\mathbb{P}} + \{\mu^{\mathbf{s}-}\}^2\lambda_t^{[\text{bad}],\mathbb{P}} + V_t^{\mathbf{s}}.$$

We then have the expression in the limit of small Δ for $\frac{1}{\Delta}\mathbb{E}_t^{\mathbb{P}}\int_t^{t+\Delta}\mathbb{v}_\ell d\ell$. ■

By a calculation for the transition equations, it follows that

$$\mathbf{C} = \begin{bmatrix} \frac{\theta_{\text{good}}}{\kappa_{\text{good}}}(1-e^{-\kappa_{\text{good}}\Delta}) \\ \frac{\theta_{\text{bad}}}{\kappa_{\text{bad}}}(1-e^{-\kappa_{\text{bad}}\Delta}) \\ \frac{\theta_{\mathbf{b}}^{\mathbb{P}}}{\kappa_{\mathbf{b}}^{\mathbb{P}}}(1-e^{-\kappa_{\mathbf{b}}^{\mathbb{P}}\Delta}) \\ \frac{\theta_{\mathbf{s}}^{\mathbb{P}}}{\kappa_{\mathbf{s}}^{\mathbb{P}}}(1-e^{-\kappa_{\mathbf{s}}^{\mathbb{P}}\Delta}) \end{bmatrix}, \quad \mathbf{D} = \begin{bmatrix} e^{-\kappa_{\text{good}}\Delta} & 0 & 0 & 0 \\ 0 & e^{-\kappa_{\text{bad}}\Delta} & 0 & 0 \\ 0 & 0 & e^{-\kappa_{\mathbf{b}}^{\mathbb{P}}\Delta} & 0 \\ 0 & 0 & 0 & e^{-\kappa_{\mathbf{s}}^{\mathbb{P}}\Delta} \end{bmatrix}, \text{ and} \quad \text{(B4)}$$

$$\mathbf{\Lambda}_{t+\Delta} = \begin{bmatrix} \Lambda_{t+\Delta}^{\mathbf{good},\mathbf{good}} & 0 & 0 & 0 \\ 0 & \Lambda_{t+\Delta}^{\mathbf{bad},\mathbf{bad}} & 0 & 0 \\ 0 & 0 & \Lambda_{t+\Delta}^{\mathbf{b},\mathbf{b}} & 0 \\ 0 & 0 & 0 & \Lambda_{t+\Delta}^{\mathbf{s},\mathbf{s}}, \end{bmatrix}, \text{ where} \quad \text{(B5)}$$

$$\left(\Lambda_{t+\Delta}^{\mathbf{good},\mathbf{good}}\right)^2 = \frac{\sigma_{\text{good}}^2}{\kappa_{\text{good}}}(1-e^{-\kappa_{\text{good}}\Delta})\left(\frac{\theta_{\text{good}}}{2\kappa_{\text{good}}}(1-e^{-\kappa_{\text{good}}\Delta}) + e^{-\kappa_{\text{good}}\Delta}\times\lambda_t^{[\text{good}],\mathbb{P}}\right), \quad \text{(B6)}$$

$$\left(\Lambda_{t+\Delta}^{\mathbf{bad},\mathbf{bad}}\right)^2 = \frac{\sigma_{\text{bad}}^2}{\kappa_{\text{bad}}}(1-e^{-\kappa_{\text{bad}}\Delta})\left(\frac{\theta_{\text{bad}}}{2\kappa_{\text{bad}}}(1-e^{-\kappa_{\text{bad}}\Delta}) + e^{-\kappa_{\text{bad}}\Delta}\times\lambda_t^{[\text{bad}],\mathbb{P}}\right), \quad \text{(B7)}$$

$$\left(\Lambda_{t+\Delta}^{\mathbf{b},\mathbf{b}}\right)^2 = \frac{\sigma_{\mathbf{b}}^2}{\kappa_{\mathbf{b}}^{\mathbb{P}}}(1-e^{-\kappa_{\mathbf{b}}^{\mathbb{P}}\Delta})\left(\frac{\theta_{\mathbf{b}}^{\mathbb{P}}}{2\kappa_{\mathbf{b}}^{\mathbb{P}}}(1-e^{-\kappa_{\mathbf{b}}^{\mathbb{P}}\Delta}) + e^{-\kappa_{\mathbf{b}}^{\mathbb{P}}\Delta}\times V_t^{\mathbf{b}}\right), \quad \text{and} \quad \text{(B8)}$$

$$\left(\Lambda_{t+\Delta}^{\mathbf{s},\mathbf{s}}\right)^2 = \frac{\sigma_{\mathbf{s}}^2}{\kappa_{\mathbf{s}}^{\mathbb{P}}}(1-e^{-\kappa_{\mathbf{s}}^{\mathbb{P}}\Delta})\left(\frac{\theta_{\mathbf{s}}^{\mathbb{P}}}{2\kappa_{\mathbf{s}}^{\mathbb{P}}}(1-e^{-\kappa_{\mathbf{s}}^{\mathbb{P}}\Delta}) + e^{-\kappa_{\mathbf{s}}^{\mathbb{P}}\Delta}\times V_t^{\mathbf{s}}\right). \quad \blacksquare \quad \text{(B9)}$$

C Formulation of VVIX_t

For integration parameter ν, $\sqrt{\{\text{VIX}_{t+\Delta}^{\mathbf{s}}\}^2} = \frac{1}{2\sqrt{\pi}}\int_0^\infty \frac{1-e^{-\nu\{\text{VIX}_{t+\Delta}^{\mathbf{s}}\}^2}}{\nu^{\frac{3}{2}}}d\nu$. This leads to the form of $F_t^{\text{vix}} \equiv \mathbb{E}_t^{\mathbb{Q}}\left(\sqrt{\{\text{VIX}_{t+\Delta}^{\mathbf{s}}\}^2}\right) = \frac{1}{2\sqrt{\pi}}\int_0^\infty \frac{1-\mathbb{E}_t^{\mathbb{Q}}(e^{-\nu\{\text{VIX}_{t+\Delta}^{\mathbf{s}}\}^2})}{\nu^{\frac{3}{2}}}d\nu$.

The VIX futures contracts are tied to the 30-day VIX index. We first fix notations, as follows:

$$\Delta^* = \frac{30}{365}. \tag{C1}$$

Next, observe that

$$\log(\frac{S^{\mathbf{s}}_{t+\Delta^*}}{F^{\mathbf{s}}_t}) = \log(\frac{F^{\mathbf{s}}_{t+\Delta^*}}{F^{\mathbf{s}}_t}). \tag{C2}$$

Using equation (B3), it then follows that

$$\begin{aligned}
\mathrm{VIX}_t^2 &= \mathbb{E}^{\mathbb{Q}}_t(\{\frac{-2}{\Delta^*}\}\log(\frac{S_{t+\Delta^*}}{F^{\mathbf{s}}_t})) = \mathbb{E}^{\mathbb{Q}}_t(\{\frac{-2}{\Delta^*}\}\log(\frac{F^{\mathbf{s}}_{t+\Delta^*}}{F^{\mathbf{s}}_t})) \qquad \text{(C3)}\\
&= \frac{1}{\Delta^*}\int_t^{t+\Delta^*} \mathbb{E}^{\mathbb{Q}}_t(V^{\mathbf{s}}_\ell)d\ell \\
&\quad - \{\frac{-2}{\Delta^*}\}\,\mathbb{E}^{\mathbb{Q}}_t(\int_t^{t+\Delta^*} \lambda_\ell^{[\mathrm{good}],\mathbb{Q}}\, d\ell \int_0^\infty (e^{x^{\mathbf{s}+}}-1)\,\mathfrak{q}[x^{\mathbf{s}+}]\,dx^{\mathbf{s}+}) \quad + \{\frac{-2}{\Delta^*}\}\,\mathbb{E}^{\mathbb{Q}}_t(\sum_{i=\mathbb{N}_t^{[\mathrm{good}],\mathbb{Q}}}^{\mathbb{N}_{t+\Delta^*}^{[\mathrm{good}],\mathbb{Q}}} x_i^{\mathbf{s}+}) \\
&\quad - \{\frac{-2}{\Delta^*}\}\,\mathbb{E}^{\mathbb{Q}}_t(\int_t^{t+\Delta^*} \lambda_\ell^{[\mathrm{bad}],\mathbb{Q}}\, d\ell \int_0^\infty (e^{-x^{\mathbf{s}-}}-1)\,\mathfrak{q}[x^{\mathbf{s}-}]\,dx^{\mathbf{s}-}) + \{\frac{-2}{\Delta^*}\}\,\mathbb{E}^{\mathbb{Q}}_t(\sum_{i=\mathbb{N}_t^{[\mathrm{bad}],\mathbb{Q}}}^{\mathbb{N}_{t+\Delta^*}^{[\mathrm{bad}],\mathbb{Q}}} \{-x_i^{\mathbf{s}-}\}).
\end{aligned}$$

It holds that

$$\mathbb{E}^{\mathbb{Q}}_t(e^{x^{\mathbf{s}+}}-1-x^{\mathbf{s}+}) = \frac{1}{1-\mu^{\mathbf{s}+,\mathbb{Q}}} - 1 - \mu^{\mathbf{s}+,\mathbb{Q}} \text{ and} \tag{C4}$$

$$\mathbb{E}^{\mathbb{Q}}_t(e^{-x^{\mathbf{s}-}}-1+x^{\mathbf{s}-}) = \frac{1}{1+\mu^{\mathbf{s}-,\mathbb{Q}}} - 1 + \mu^{\mathbf{s}-,\mathbb{Q}}. \tag{C5}$$

Then the 30-day VIX formula, when there are both down and up price jumps, satisfies

$$\mathrm{VIX}_t^2 = \mathsf{w}^{\mathrm{constant}} + \mathsf{w}^{\mathrm{v}} \times V_t^{\mathbf{s}} + \mathsf{w}^{\mathrm{good}} \times \lambda_t^{[\mathrm{good}],\mathbb{Q}} + \mathsf{w}^{\mathrm{bad}} \times \lambda_t^{[\mathrm{bad}],\mathbb{Q}}, \tag{C6}$$

where

$$\begin{aligned}
\mathsf{w}^{\mathrm{constant}} \equiv\ & \frac{1}{\Delta^*}\left(\frac{\Delta^*\theta^{\mathbb{Q}}_{\mathbf{s}}}{\kappa^{\mathbb{Q}}_{\mathbf{s}}} + \frac{(1-e^{-\kappa^{\mathbb{Q}}_{\mathbf{s}}\Delta^*})}{\kappa^{\mathbb{Q}}_{\mathbf{s}}}\{-\frac{\theta^{\mathbb{Q}}_{\mathbf{s}}}{\kappa^{\mathbb{Q}}_{\mathbf{s}}}\}\right) \\
&+ 2\left(\frac{\theta^{\mathbb{Q}}_{\mathrm{good}}}{\kappa^{\mathbb{Q}}_{\mathrm{good}}} + \frac{(1-e^{-\kappa^{\mathbb{Q}}_{\mathrm{good}}\Delta^*})}{\Delta^*\,\kappa^{\mathbb{Q}}_{\mathrm{good}}}\{-\frac{\theta^{\mathbb{Q}}_{\mathrm{good}}}{\kappa^{\mathbb{Q}}_{\mathrm{good}}}\}\right)\{\mathbb{E}^{\mathbb{Q}}_t(e^{x^{\mathbf{s}+}}-1-x^{\mathbf{s}+})\} \\
&+ 2\left(\frac{\theta^{\mathbb{Q}}_{\mathrm{bad}}}{\kappa^{\mathbb{Q}}_{\mathrm{bad}}} + \frac{(1-e^{-\kappa^{\mathbb{Q}}_{\mathrm{bad}}\Delta^*})}{\Delta^*\,\kappa^{\mathbb{Q}}_{\mathrm{bad}}}\{-\frac{\theta^{\mathbb{Q}}_{\mathrm{bad}}}{\kappa^{\mathbb{Q}}_{\mathrm{bad}}}\}\right)\{\mathbb{E}^{\mathbb{Q}}_t(e^{-x^{\mathbf{s}-}}-1+x^{\mathbf{s}-})\},
\end{aligned} \tag{C7}$$

and

$$\mathsf{w}^{\mathrm{v}} \equiv \frac{(1-e^{-\kappa^{\mathbb{Q}}_{\mathbf{s}}\,\Delta^*})}{\Delta^*\,\kappa^{\mathbb{Q}}_{\mathbf{s}}}, \tag{C8}$$

$$\mathsf{w}^{\mathrm{good}} \equiv 2\left(\frac{(1-e^{-\kappa^{\mathbb{Q}}_{\mathrm{good}}\Delta^*})}{\Delta^*\,\kappa^{\mathbb{Q}}_{\mathrm{good}}}\right)\{\mathbb{E}^{\mathbb{Q}}_t(e^{x^{\mathbf{s}+}}-1-x^{\mathbf{s}+})\} \quad \text{and} \tag{C9}$$

$$\mathsf{w}^{\mathrm{bad}} \equiv 2\left(\frac{(1-e^{-\kappa^{\mathbb{Q}}_{\mathrm{bad}}\Delta^*})}{\Delta^*\,\kappa^{\mathbb{Q}}_{\mathrm{bad}}}\right)\{\mathbb{E}^{\mathbb{Q}}_t(e^{-x^{\mathbf{s}-}}-1+x^{\mathbf{s}-})\}. \tag{C10}$$

Define the moment-generating functions $\mathrm{mgf}^{\mathrm{v}}_t[\mathbb{u}] \equiv \mathbb{E}^{\mathbb{Q}}_t(e^{\mathbb{u}V^{\mathbf{s}}_{t+\Delta}})$, $\mathrm{mgf}^{\mathrm{good}}_t[\mathbb{u}] \equiv \mathbb{E}^{\mathbb{Q}}_t(e^{\mathbb{u}\lambda^{[\mathrm{good}],\mathbb{Q}}_{t+\Delta}})$, and $\mathrm{mgf}^{\mathrm{bad}}_t[\mathbb{u}] \equiv \mathbb{E}^{\mathbb{Q}}_t(e^{\mathbb{u}\lambda^{[\mathrm{bad}],\mathbb{Q}}_{t+\Delta}})$. Then,

$$\begin{aligned}
\log(\mathrm{mgf}^{\mathrm{good}}_t[\mathbb{u}]) &= \frac{2\theta^{\mathbb{Q}}_{\mathrm{good}}}{\sigma^2_{\mathrm{good}}}\{\log(\frac{2\kappa^{\mathbb{Q}}_{\mathrm{good}}}{e^{\Delta\kappa^{\mathbb{Q}}_{\mathrm{good}}}(2\kappa^{\mathbb{Q}}_{\mathrm{good}}-\mathbb{u}\sigma^2_{\mathrm{good}})+\mathbb{u}\sigma^2_{\mathrm{good}}})+\Delta\,\kappa^{\mathbb{Q}}_{\mathrm{good}}\} \\
&+ \frac{2\mathbb{u}\kappa^{\mathbb{Q}}_{\mathrm{good}}}{e^{\Delta\kappa^{\mathbb{Q}}_{\mathrm{good}}}(2\kappa^{\mathbb{Q}}_{\mathrm{good}}-\mathbb{u}\sigma^2_{\mathrm{good}})+\mathbb{u}\sigma^2_{\mathrm{good}}}\lambda^{[\mathrm{good}],\mathbb{Q}}_t, \\
\log(\mathrm{mgf}^{\mathrm{bad}}_t[\mathbb{u}]) &= \frac{2\theta^{\mathbb{Q}}_{\mathrm{bad}}}{\sigma^2_{\mathrm{bad}}}\{\log(\frac{2\kappa^{\mathbb{Q}}_{\mathrm{bad}}}{e^{\Delta\kappa^{\mathbb{Q}}_{\mathrm{bad}}}(2\kappa^{\mathbb{Q}}_{\mathrm{bad}}-\mathbb{u}\sigma^2_{\mathrm{bad}})+\mathbb{u}\sigma^2_{\mathrm{bad}}})+\Delta\,\kappa^{\mathbb{Q}}_{\mathrm{bad}}\} \\
&+ \frac{2\mathbb{u}\kappa^{\mathbb{Q}}_{\mathrm{bad}}}{e^{\Delta\kappa^{\mathbb{Q}}_{\mathrm{bad}}}(2\kappa^{\mathbb{Q}}_{\mathrm{bad}}-\mathbb{u}\sigma^2_{\mathrm{bad}})+\mathbb{u}\sigma^2_{\mathrm{bad}}}\lambda^{[\mathrm{bad}],\mathbb{Q}}_t \quad \text{and} \\
\log(\mathrm{mgf}^{\mathrm{v}}_t[\mathbb{u}]) &= \frac{2\theta^{\mathbb{Q}}_{\mathbf{s}}}{\sigma^2_{\mathbf{s}}}\{\log(\frac{2\kappa^{\mathbb{Q}}_{\mathbf{s}}}{e^{\Delta\kappa^{\mathbb{Q}}_{\mathbf{s}}}(2\kappa^{\mathbb{Q}}_{\mathbf{s}}-\mathbb{u}\sigma^2_{\mathbf{s}})+\mathbb{u}\sigma^2_{\mathbf{s}}})+\Delta\kappa^{\mathbb{Q}}_{\mathbf{s}}\}+\frac{2\mathbb{u}\kappa^{\mathbb{Q}}_{\mathbf{s}}}{e^{\Delta\kappa^{\mathbb{Q}}_{\mathbf{s}}}(2\kappa^{\mathbb{Q}}_{\mathbf{s}}-\mathbb{u}\sigma^2_{\mathbf{s}})+\mathbb{u}\sigma^2_{\mathbf{s}}}V^{\mathbf{s}}_t.
\end{aligned}$$

In the context of our model framework and seven-day VIX futures, we derive

$$\begin{aligned}
F^{\mathrm{vix}}_t &= \frac{1}{2\sqrt{\pi}}\int_0^\infty \frac{1-\mathbb{E}^{\mathbb{Q}}_t(e^{-\nu\{\mathrm{VIX}^{\mathbf{s}}_{t+\Delta}\}^2})}{\nu^{\frac{3}{2}}}d\nu \\
&= \frac{1}{2\sqrt{\pi}}\int_0^\infty \frac{1-\mathbb{E}^{\mathbb{Q}}_t(e^{-\nu\{\mathsf{w}^{\mathrm{constant}}+\mathsf{w}^{\mathrm{v}}\times V^{\mathbf{s}}_{t+\Delta}+\mathsf{w}^{\mathrm{good}}\times\lambda^{[\mathrm{good}],\mathbb{Q}}_{t+\Delta}+\mathsf{w}^{\mathrm{bad}}\times\lambda^{[\mathrm{bad}],\mathbb{Q}}_{t+\Delta}\}})}{\nu^{\frac{3}{2}}}d\nu \qquad \text{(C11)} \\
&= \frac{1}{2\sqrt{\pi}}\int_0^\infty \frac{1-e^{-\nu\{\mathsf{w}^{\mathrm{constant}}\}}\times\mathrm{mgf}^{\mathrm{v}}_t[\mathbb{u}]\big|_{\mathbb{u}=-\nu\,\mathsf{w}^{\mathrm{v}}}\times\mathrm{mgf}^{\mathrm{good}}_t[\mathbb{u}]\big|_{\mathbb{u}=-\nu\,\mathsf{w}^{\mathrm{good}}}\times\mathrm{mgf}^{\mathrm{bad}}_t[\mathbb{u}]\big|_{\mathbb{u}=-\nu\,\mathsf{w}^{\mathrm{bad}}}}{\nu^{\frac{3}{2}}}d\nu.
\end{aligned}$$

Consequently, the characteristic function of $\{\mathrm{VIX}^{\mathbf{s}}_{t+\Delta}\}^2$ equates to the following:

$$\begin{aligned}
\mathbb{C}_t[\phi] &\equiv \mathbb{E}^{\mathbb{Q}}_t(e^{i\phi\{\mathrm{VIX}^{\mathbf{s}}_{t+\Delta}\}^2}) = \mathbb{E}^{\mathbb{Q}}_t(e^{i\phi\{\mathsf{w}^{\mathrm{constant}}\,+\,\mathsf{w}^{\mathrm{v}}\times V^{\mathbf{s}}_t\,+\,\mathsf{w}^{\mathrm{good}}\times\lambda^{[\mathrm{good}],\mathbb{Q}}_t\,+\,\mathsf{w}^{\mathrm{bad}}\times\lambda^{[\mathrm{bad}],\mathbb{Q}}_t\}}) \\
&= e^{i\phi\,\mathsf{w}^{\mathrm{constant}}}\times\mathrm{mgf}^{\mathrm{v}}_t[\mathbb{u}]\big|_{\mathbb{u}=i\,\phi\,\mathsf{w}^{\mathrm{v}}}\times\mathrm{mgf}^{\mathrm{good}}_t[\mathbb{u}]\big|_{\mathbb{u}=i\,\phi\,\mathsf{w}^{\mathrm{good}}}\times\mathrm{mgf}^{\mathrm{bad}}_t[\mathbb{u}]\big|_{\mathbb{u}=i\,\phi\,\mathsf{w}^{\mathrm{bad}}}. \qquad \text{(C12)}
\end{aligned}$$

Next we formulate $\{\mathrm{VVIX}_t\}^2$. Using the Fourier inversion, the density of $\mathsf{h}_{t+\Delta} \equiv \{\mathrm{VIX}^{\mathbf{s}}_{t+\Delta}\}^2$ is $\mathsf{q}^{\mathrm{vix}}[\mathsf{h}_{t+\Delta}] = \frac{1}{\pi}\int_0^\infty \mathrm{Re}\left[e^{-i\,\phi\,\mathsf{h}_{t+\Delta}}\,\mathbb{C}_t[\phi]\right]\,d\phi$, noting $F^{\mathrm{vix}}_{t+\Delta} = \sqrt{\{\mathrm{VIX}^{\mathbf{s}}_{t+\Delta}\}^2} = \sqrt{\mathsf{h}_{t+\Delta}}$ and $\Delta = \frac{11}{365}$.

Hence, we show, for $\{\text{VVIX}_t\}^2 \equiv \mathbb{E}_t^{\mathbb{Q}}(\{\frac{-2}{\Delta}\}\log(\frac{F^{\text{vix}}_{t+\Delta}}{F^{\text{vix}}_t}))$, that

$$\begin{aligned}
\{\text{VVIX}_t\}^2 &\equiv \int_0^\infty \mathsf{q}^{\text{vix}}[\mathsf{h}_{t+\Delta}]\,\{\frac{-2}{\Delta}\}\log(\frac{\sqrt{\mathsf{h}_{t+\Delta}}}{F^{\text{vix}}_t})\,d\mathsf{h}_{t+\Delta} \\
&= \int_0^\infty \frac{1}{\pi}\int_0^\infty \text{Re}\left[e^{-i\,\phi\,\mathsf{h}_{t+\Delta}}\,\mathbb{C}_t[\phi]\right]\,d\phi\,\{\frac{-2}{\Delta}\}\log(\frac{\sqrt{\mathsf{h}_{t+\Delta}}}{F^{\text{vix}}_t})\,d\mathsf{h}_{t+\Delta} \\
&= \frac{1}{\pi}\int_0^\infty \text{Re}\left[\mathbb{C}_t[\phi]\int_0^\infty e^{-i\,\phi\,\mathsf{h}_{t+\Delta}}\,\{\frac{-2}{\Delta}\}\log(\frac{\sqrt{\mathsf{h}_{t+\Delta}}}{F^{\text{vix}}_t})\,d\mathsf{h}_{t+\Delta}\right]\,d\phi \quad \text{(Fubini)} \\
&= \frac{1}{\pi}\int_0^\infty \text{Re}\left[\mathbb{C}_t[\phi]\int_0^\infty e^{-\xi\,u}\,\{\frac{-2}{\Delta}\}\log(\frac{\sqrt{u}}{F^{\text{vix}}_t})\,du\right]\,d\phi \qquad (\text{Re}[\xi]>0) \\
&= \frac{1}{\pi}\int_0^\infty \text{Re}\left[\left(\mathbb{C}_t[\phi]\times\frac{2\log\left(F^{\text{vix}}_t\right)+\log(i\,\phi)+\gamma^{\text{euler}}}{\Delta\,i\,\phi}\right)\Big|_{\phi=\mathsf{a}+i\,\mathsf{b}}\right]d\mathsf{a}. \qquad \text{(C13)}
\end{aligned}$$

We embed the constraint $\text{Re}[\xi]>0$ for complex-valued ξ, and γ^{euler} is the Euler's constant. ■

Table 1: **Properties of weekly excess returns of buying options on the 10-year Treasury bond futures and the S&P 500 index**

This table is based on matched weekly options (Friday PM initiation to Friday PM expiration) on futures on the 10-year Treasury bond and the S&P 500 index. The sample period is January 28, 2011, to February 24, 2023, comprising 630 expiration cycles. Excess returns for buying options on the S&P 500 index (and bond futures) are calculated according to equations (1)–(2). Option returns are based on non-overlapping weekly holding periods. Reported 95% stationary bootstrap confidence intervals rely on 10,000 bootstrap draws. The unit of the reported average option excess return is a weekly percentage. We compute the excess returns of buying OTM options on bond (stock) with fixed-option delta, denoted $\delta^{\mathbf{b}}$ ($\delta^{\mathbf{s}}$). For the standard normal cumulative distribution function, $\mathcal{N}[.]$, we compute

$$\text{put (call) delta for S\&P 500 as } -\mathcal{N}[-d_1] \ (\mathcal{N}[d_1]), \text{ where } d_1 = \tfrac{1}{\sigma\sqrt{\Delta}}\{-\log(k) + \{R_t^{\text{rf}} - 1\}\,\Delta + \tfrac{1}{2}\sigma^2\Delta\},$$

$$\text{put (call) delta for bond futures as } -e^{-\{R_t^{\text{rf}}-1\}\Delta}\mathcal{N}[-d_1] \ (e^{-\{R_t^{\text{rf}}-1\}\Delta}\mathcal{N}[d_1]), \text{ where } d_1 = \tfrac{1}{\sigma\sqrt{\Delta}}\{-\log(k) + \tfrac{1}{2}\sigma^2\Delta\}.$$

Reported $\mathbb{1}_{\{\mathrm{r}>0\}}$ refers to the number of weekly expiration cycles in which the excess return of the option is positive. σ is the average option-implied volatility computed at the beginning of the expiration cycle. The reported dollar open interest (respectively, volume) is the number of contracts outstanding (respectively, traded) multiplied by the underlier on Friday of each expiration cycle, averaged across the 630 expiration cycles. Stationary bootstrap confidence intervals that do not bracket zero are indicated by "*."

Panel A: Buying options on the 10-year Treasury bond futures

	Puts on bond		Bond	Calls on bond		Futures
Bond option delta: $\delta^{\mathbf{b}}$ (%)	-7	-20	straddle	20	7	return:
OTM moneyness (%)	1	0.5		0.5	1	10-year bond
Average options excess return (weekly, %)	-30*	-17*	-6*	-18*	-68*	0.036*
Bootstrap CI: [Lower Upper]	[-57 -14]	[-24 -12]	[-9 -3]	[-29 -6]	[-82 -66]	[0.01 0.07]
$\mathbb{1}_{\{\mathrm{r}>0\}}$ (out of 630)	42	103	258	124	37	351
Average option price	\$61.2	\$147.1		\$144.3	\$58.4	
Dollar open interest (Friday, millions)	\$2095	\$2070		\$1870	\$1701	
Dollar volume (Friday, millions)	\$795	\$1097		\$953	\$602	

Panel B: Buying options on the S&P 500 index

	Puts on stock		Stock	Calls on stock		Index
Stock option delta: $\delta^{\mathbf{s}}$ (%)	-7	-20	straddle	20	7	return:
OTM moneyness (%)	3	1.5		1.5	3	S&P 500
Average options excess return (weekly, %)	-54*	-32*	-6*	-6	-61*	0.228*
Bootstrap CI: [Lower Upper]	[-78 -32]	[-46 -24]	[-13 -0]	[-22 9]	[-85 -55]	[0.20 0.32]
$\mathbb{1}_{\{\mathrm{r}>0\}}$ (out of 630)	35	88	259	120	37	370
Average option price	\$6.0	\$10.9		\$7.0	\$2.5	
Dollar open interest (Friday, millions)	\$1284	\$1265		\$1353	\$958	
Dollar volume (Friday, millions)	\$499	\$490		\$591	\$286	

Panel C: Differences between option returns of the 10-year bond and the S&P 500 index

Difference in options excess return (weekly, %)	23.2*	15.6*		-12.3	-7.2
Bootstrap CI: [Lower Upper]	[0 30]	[6 27]		[-37 11]	[-16 7]

Table 2: **Small maturity exceedance correlation statistics**

Data used in the table comprise seven-day returns of S&P 500 E-mini futures and those of 10-year Treasury bond futures, spanning the sample period of January 5, 1990, to February 23, 2023 (1,781 return observations (Friday to Friday)). For reference, the unconditional stock-bond correlation in this extended sample is -0.11, with a stationary bootstrap confidence interval of $[-0.34 \ -0.07]$.

In the context of the exceedance correlation of Ang and Chen (2002, page 464), we cover two outcomes of return strategies for the variables $\log(F^{\mathbf{s}}_{t+\Delta}/F^{\mathbf{s}}_t)$ and $\{-\log(F^{\mathbf{b}}_{t+\Delta}/F^{\mathbf{b}}_t)\}$ and report the following associated H^- and H^+ statistics:

- Correlation for negative sigma events (H^-) in row (a): The exceedance correlation in this case corresponds to the pairing of simultaneous downward movements in the stock and gains on the Treasury bond futures position (as reflected in the losses on the short position).
- Correlation for positive sigma events (H^+) in row (b): The exceedance correlation in this case captures the pairing of upward movements in the stock and losses on the Treasury bond futures position (as reflected in the gains on the short position).

These H^- and H^+ statistics represent the distinction between the data-implied correlations versus those implied by a bivariate normal distribution. The downside (upside) exceedance correlation is the correlation when both series are below (above) a threshold.

We show the stationary bootstrap test for the hypothesis of $\mathrm{H}^- < \mathrm{H}^+$, with low p-value implying test rejection. Additionally, we report the Hong, Tu, and Zhou (2006, equation (8)) p-value for the hypothesis of equal extreme correlation $\boldsymbol{\rho}^- = \boldsymbol{\rho}^+$ (vector-valued), with p-value lower than 0.1, implying test rejection.

	Correlation between return strategies	Sigma event threshold	Ang-Chen asymmetric correlation statistic
row (a)	$\log(F^{\mathbf{s}}_{t+\Delta}/F^{\mathbf{s}}_t)$ and $\{-\log(F^{\mathbf{b}}_{t+\Delta}/F^{\mathbf{b}}_t)\}$	Negative	$\mathrm{H}^- = 23\%$
row (b)	$\log(F^{\mathbf{s}}_{t+\Delta}/F^{\mathbf{s}}_t)$ and $\{-\log(F^{\mathbf{b}}_{t+\Delta}/F^{\mathbf{b}}_t)\}$	Positive	$\mathrm{H}^+ = 18\%$
	• Bootstrap p-value for $\mathrm{H}^- < \mathrm{H}^+$ is $\boxed{0.02}$		
	• Hong, Tu, and Zhou (2006, equation (8)) two-sided p-value for $\boldsymbol{\rho}^- = \boldsymbol{\rho}^+$ is $\boxed{0.07}$		

Table 3: **Correlations between returns of options on bond and options on stock**

This table shows the 7DTE and 1DTE correlations between (i) the excess returns of calls on bond and excess returns of puts on stock, (ii) the excess returns of puts on bond and excess returns of calls on stock, (iii) the excess returns of puts on bond and excess returns of puts on stock, and (iv) the excess returns of calls on bond and excess returns of calls on stock. Presented are the full sample correlations and 52-week rolling window correlations, updated weekly. Reported 95% bootstrap confidence intervals rely on 10,000 stationary bootstrap draws. Bootstrap confidence intervals that do not bracket zero are indicated by "*." The fixed-option deltas of bond and stock are denoted by $\delta^{\mathbf{b}}$ and $\delta^{\mathbf{s}}$, respectively.

		I: Option maturity is seven-day January 28, 2011, to February 24, 2023 630 weekly cycles (Friday PM initiation to Friday PM expiration)				**II: Option maturity is one-day** January 28, 2011, to February 24, 2023 630 daily cycles (Thursday PM initiation to Friday PM expiration)			
		Full sample correlation	**52-week rolling correlation**			**Full sample correlation**	**52-week rolling correlation**		
Option delta $\delta^{\mathbf{b}}$	$\delta^{\mathbf{s}}$	Mean [95% CI]	Mean	5^{th}	95^{th}	Mean [95% CI]	Mean	5^{th}	95^{th}
Panel A: Correlation between returns of *buying* calls on bond and puts on stock									
20	-20	**0.34*** [0.13 0.52]	0.25	-0.11	0.65	**0.24*** [0.05 0.47]	0.22	-0.09	0.74
20	-7	**0.28*** [0.02 0.48]	0.26	-0.12	0.63	**0.20*** [0.00 0.44]	0.25	-0.06	0.70
7	-20	**0.45*** [0.12 0.68]	0.34	-0.08	0.92	**0.25*** [0.02 0.49]	0.20	-0.08	0.79
7	-7	**0.47*** [0.05 0.73]	0.43	-0.06	1.00	**0.21** [−0.02 0.46]	0.23	-0.07	0.78
Panel B: Correlation between returns of *buying* puts on bond and calls on stock									
-20	20	**0.04** [−0.02 0.14]	0.08	-0.12	0.61	**0.03** [−0.04 0.13]	0.04	-0.11	0.32
-20	7	**0.13** [−0.01 0.28]	0.13	-0.07	0.61	**0.06** [−0.04 0.23]	0.04	-0.09	0.41
-7	20	**0.02** [−0.02 0.11]	0.07	-0.11	0.54	**0.06** [−0.05 0.20]	0.04	-0.11	0.45
-7	7	**0.07** [−0.02 0.26]	0.11	-0.08	0.67	**0.18** [−0.03 0.48]	0.05	-0.09	0.65
Panel C: Correlation between returns of *buying* puts on bond and puts on stock									
-20	-20	**-0.02** [−0.07 0.07]	-0.04	-0.15	0.19	**-0.04*** [−0.06 −0.03]	-0.06	-0.10	-0.02
-20	-7	**0.00** [−0.05 0.09]	-0.03	-0.10	0.21	**-0.03*** [−0.04 −0.02]	-0.05	-0.08	-0.02
-7	-20	**-0.02** [−0.03 0.02]	0.01	-0.10	0.19	**-0.03*** [−0.04 −0.02]	-0.04	-0.08	0.00
-7	-7	**-0.01** [−0.03 0.01]	-0.01	-0.07	0.14	**-0.02*** [−0.03 −0.01]	-0.04	-0.07	-0.02
Panel D: Correlation between returns of *buying* calls on bond and calls on stock									
20	20	**-0.08*** [−0.12 −0.05]	-0.08	-0.23	0.16	**-0.11*** [−0.14 −0.07]	-0.12	-0.23	0.00
20	7	**-0.05*** [−0.08 −0.02]	-0.06	-0.14	0.13	**-0.06*** [−0.09 −0.03]	-0.09	-0.16	-0.01
7	20	**-0.04** [−0.06 0.00]	-0.02	-0.14	0.47	**-0.10*** [−0.13 −0.07]	-0.12	-0.19	-0.06
7	7	**-0.01** [−0.04 0.04]	-0.02	-0.09	0.28	**-0.06*** [−0.08 −0.03]	-0.09	-0.15	-0.04

Table 4: **Bootstrap-based comparison of correlation magnitudes across (i) returns of bond and stock option pairs and (ii) standardized option payoff pairs**

This table evaluates the correlation magnitudes computed in Table 3 or Table 5, against those in Panels B, C, and D of the same table. The underlying hypothesis presumes a lower correlation between seven-day (or one-day) returns of bond calls and stock puts compared to (i) returns of bond puts and stock calls, (ii) returns of bond puts and stock puts, and (iii) returns of bond calls and stock calls. Reported p-value, presented, represents the occurrences of stationary bootstraps where the correlation in the first pair is lower in comparison to other pairs. A low p-value suggests a rejection of the test. The fixed-option deltas of bond and stock are denoted by $\delta^{\mathbf{b}}$ and $\delta^{\mathbf{s}}$, respectively.

Hypothesis	Panel A: Based on Table 3		Panel B: Based on Table 5	
	Seven-day expiration	One-day expiration	Seven-day expiration	One-day expiration
	Bootstrap p-value	Bootstrap p-value	Bootstrap p-value	Bootstrap p-value
$\rho[\delta^{\mathbf{b}}=20,\ \delta^{\mathbf{s}}=-20] < \rho[\delta^{\mathbf{b}}=-20,\ \delta^{\mathbf{s}}=20]$	0.00	0.15	0.00	0.00
$\rho[\delta^{\mathbf{b}}=20,\ \delta^{\mathbf{s}}=-20] < \rho[\delta^{\mathbf{b}}=-20,\ \delta^{\mathbf{s}}=-20]$	0.00	0.00	0.00	0.00
$\rho[\delta^{\mathbf{b}}=20,\ \delta^{\mathbf{s}}=-20] < \rho[\delta^{\mathbf{b}}=20,\ \delta^{\mathbf{s}}=20]$	0.00	0.00	0.00	0.00
$\rho[\delta^{\mathbf{b}}=20,\ \delta^{\mathbf{s}}=-7] < \rho[\delta^{\mathbf{b}}=-20,\ \delta^{\mathbf{s}}=7]$	0.00	0.32	0.00	0.02
$\rho[\delta^{\mathbf{b}}=20,\ \delta^{\mathbf{s}}=-7] < \rho[\delta^{\mathbf{b}}=-20,\ \delta^{\mathbf{s}}=-7]$	0.00	0.00	0.00	0.00
$\rho[\delta^{\mathbf{b}}=20,\ \delta^{\mathbf{s}}=-7] < \rho[\delta^{\mathbf{b}}=20,\ \delta^{\mathbf{s}}=7]$	0.00	0.00	0.00	0.00
$\rho[\delta^{\mathbf{b}}=7,\ \delta^{\mathbf{s}}=-20] < \rho[\delta^{\mathbf{b}}=-7,\ \delta^{\mathbf{s}}=20]$	0.00	0.13	0.00	0.00
$\rho[\delta^{\mathbf{b}}=7,\ \delta^{\mathbf{s}}=-20] < \rho[\delta^{\mathbf{b}}=-7,\ \delta^{\mathbf{s}}=-20]$	0.00	0.00	0.01	0.01
$\rho[\delta^{\mathbf{b}}=7,\ \delta^{\mathbf{s}}=-20] < \rho[\delta^{\mathbf{b}}=7,\ \delta^{\mathbf{s}}=20]$	0.00	0.00	0.00	0.00
$\rho[\delta^{\mathbf{b}}=7,\ \delta^{\mathbf{s}}=-7] < \rho[\delta^{\mathbf{b}}=-7,\ \delta^{\mathbf{s}}=7]$	0.00	0.40	0.00	0.00
$\rho[\delta^{\mathbf{b}}=7,\ \delta^{\mathbf{s}}=-7] < \rho[\delta^{\mathbf{b}}=-7,\ \delta^{\mathbf{s}}=-7]$	0.00	0.00	0.00	0.00
$\rho[\delta^{\mathbf{b}}=7,\ \delta^{\mathbf{s}}=-7] < \rho[\delta^{\mathbf{b}}=7,\ \delta^{\mathbf{s}}=7]$	0.00	0.00	0.00	0.00

Table 5: **Correlations between standardized option payoff outcomes for bond and stock**

This table shows the 7DTE and 1DTE correlations between (i) the standardized payoffs of upside of bond and standardized payoffs of downside of stock, (ii) the standardized payoffs of downside of bond and standardized payoffs of upside of stock, (iii) the standardized payoffs of downside of bond and standardized payoffs of downside of stock, (iv) the standardized payoffs of upside of bond and standardized payoffs of upside of stock. Presented are the full sample correlations and 52-week rolling window correlations, updated weekly. Reported 95% stationary bootstrap confidence intervals rely on 10,000 bootstrap draws. Bootstrap confidence intervals that do not bracket zero are indicated by "*." The fixed-option deltas of bond and stock are denoted by $\delta^{\mathbf{b}}$ and $\delta^{\mathbf{s}}$, respectively.

		I: Option maturity is seven-day January 5, 1992, to February 23, 2024 1,781 weekly cycles (Friday PM initiation to Friday PM expiration)				**II: Option maturity is one-day** January 5, 1992, to February 23, 2024 1,781 daily cycles (Thursday PM initiation to Friday PM expiration)			
		Full sample correlation	**52-week rolling correlation**			**Full sample correlation**	**52-week rolling correlation**		
Option delta $\delta^{\mathbf{b}}$	Option delta $\delta^{\mathbf{s}}$	Mean [95% CI]	Mean	5^{th}	95^{th}	Mean [95% CI]	Mean	5^{th}	95^{th}
Panel A: Correlation between standardized payoffs $\frac{[F^{\mathbf{b}}_{t+\Delta}-K^{\mathbf{b}}]^+}{F^{\mathbf{b}}_t}$ and $\frac{[K^{\mathbf{s}}-S_{t+\Delta}]^+}{S_t}$									
20	-20	**0.14*** [0.09 0.19]	0.12	-0.19	0.46	**0.12*** [0.07 0.17]	0.10	-0.31	0.50
20	-7	**0.16*** [0.11 0.21]	0.18	-0.13	0.43	**0.12*** [0.08 0.16]	0.10	-0.21	0.37
7	-20	**0.14*** [0.09 0.19]	0.14	-0.15	0.43	**0.15*** [0.10 0.21]	0.15	-0.16	0.48
7	-7	**0.18*** [0.11 0.25]	0.23	-0.13	0.70	**0.17*** [0.10 0.24]	0.19	-0.10	0.57
Panel B: Correlation between standardized payoffs $\frac{[K^{\mathbf{b}}-F^{\mathbf{b}}_{t+\Delta}]^+}{F^{\mathbf{b}}_t}$ and $\frac{[S_{t+\Delta}-K^{\mathbf{s}}]^+}{S_t}$									
-20	20	**0.05*** [0.00 0.10]	0.06	-0.27	0.48	**0.08*** [0.03 0.13]	0.08	-0.32	0.42
-20	7	**0.07*** [0.02 0.12]	0.07	-0.18	0.39	**0.08*** [0.04 0.13]	0.09	-0.19	0.39
-7	20	**0.04** [−0.01 0.09]	0.05	-0.18	0.38	**0.07*** [0.02 0.12]	0.06	-0.19	0.38
-7	7	**0.07*** [0.01 0.13]	0.06	-0.16	0.38	**0.09*** [0.04 0.16]	0.11	-0.13	0.49
Panel C: Correlation between standardized payoffs $\frac{[K^{\mathbf{b}}-F^{\mathbf{b}}_{t+\Delta}]^+}{F^{\mathbf{b}}_t}$ and $\frac{[K^{\mathbf{s}}-S_{t+\Delta}]^+}{S_t}$									
-20	-20	**0.00** [−0.04 0.05]	-0.01	-0.29	0.38	**-0.03** [−0.07 0.02]	-0.03	-0.32	0.40
-20	-7	**-0.05*** [−0.09 −0.01]	-0.07	-0.22	0.25	**-0.05*** [−0.09 −0.01]	-0.05	-0.26	0.27
-7	-20	**0.09*** [0.04 0.14]	0.09	-0.17	0.51	**0.03** [−0.02 0.08]	0.03	-0.21	0.48
-7	-7	**0.01** [−0.04 0.06]	0.01	-0.14	0.51	**0.00** [−0.04 0.05]	0.02	-0.18	0.47
Panel D: Correlation between standardized payoffs $\frac{[F^{\mathbf{b}}_{t+\Delta}-K^{\mathbf{b}}]^+}{F^{\mathbf{b}}_t}$ and $\frac{[S_{t+\Delta}-K^{\mathbf{s}}]^+}{S_t}$									
20	20	**-0.05** [−0.09 0.00]	-0.06	-0.40	0.36	**-0.03** [−0.08 0.01]	-0.03	-0.40	0.37
20	7	**-0.01** [−0.06 0.03]	-0.03	-0.29	0.36	**-0.05** [−0.09 0.00]	-0.06	-0.34	0.27
7	20	**0.01** [−0.04 0.06]	-0.01	-0.27	0.38	**0.00** [−0.04 0.05]	-0.01	-0.24	0.48
7	7	**0.05** [−0.00 0.11]	0.01	-0.17	0.43	**0.02** [−0.03 0.06]	0.01	-0.17	0.36

Table 6: **Stock-bond correlations and links to unfavorable economic uncertainty**

This table reports estimates of the correlation (denoted $\rho_{t+\Delta}$) between stock and bond returns over weekly intervals, ranging from Friday to Friday. The data used includes five-minute synchronized return observations of E-mini S&P 500 index futures and 10-year Treasury bond futures. For the two return series, $\mathbb{r}^{\mathbf{s}}_{t,\ell} = \log(F^{\mathbf{s}}_{t,\frac{\ell}{N}}) - \log(F^{\mathbf{s}}_{t,\frac{\ell-1}{N}})$ and $\mathbb{r}^{\mathbf{b}}_{t,\ell} = \log(F^{\mathbf{b}}_{t,\frac{\ell}{N}}) - \log(F^{\mathbf{b}}_{t,\frac{\ell-1}{N}})$, the covariances and variances are computed as follows:

$$\text{covar}^{\{r^{\mathbf{s}}\},\{r^{\mathbf{b}}\},\mathbb{P}}_{\{t\to t+\Delta\}} = 52\times\sum_{\ell=1}^{\mathcal{I}}\{\mathbb{r}^{\mathbf{s}}_{t,\ell}\}\times\{\mathbb{r}^{\mathbf{b}}_{t,\ell}\},\quad \text{var}^{\{r^{\mathbf{s}}\},\mathbb{P}}_{\{t\to t+\Delta\}} = 52\times\sum_{\ell=1}^{\mathcal{I}}\{\mathbb{r}^{\mathbf{s}}_{t,\ell}\}^2 \quad\text{and}\quad \text{var}^{\{r^{\mathbf{b}}\},\mathbb{P}}_{\{t\to t+\Delta\}} = 52\times\sum_{\ell=1}^{\mathcal{I}}\{\mathbb{r}^{\mathbf{b}}_{t,\ell}\}^2,$$

where $\mathcal{I}$ is the number of return observations in a trading week (i.e., $\mathcal{I} = 12\times 6.5\times 5$). The data is from Barchart. The indicator function $\mathbb{1}_{\{\text{positive}\}}$ shows the fraction of positive weekly stock-bond correlations. The reported 95% bootstrap confidence interval, shown in square bracket, relies on 10,000 bootstrap draws.

Reported is the correlation between stress variable $\mathcal{F}_t$ and $\rho_{t+\Delta}$ (these magnitudes are shown in the column CORR) and results based on the regression in equation (3). The Office of Financial Research stress indices are taken from https://www.financialresearch.gov/financial-stress-index/, using values to account for the two-day reporting lag:

- $\text{OFR}^{\text{safe asset}}_t$: Times of stress coincide with higher valuations of safe assets. Investors are migrating from risky assets into safer holdings.
- $\text{CDX}^{\text{high yield}}_t$: Markit's North American High Yield CDX Index. Composed of 100 liquid North American entities with high yield credit ratings that trade in the CDS market. This index is low during financial stress.
- $\text{CDX}^{\text{investment grade}}_t$: Markit's North American Investment Grade Index. Composed of 125 liquid North American entities.
- Inflation swap_t: One-year inflation swap rates (source: Bloomberg).
- $\text{OFR}^{\text{equity valuation}}_t$: Reflects investor confidence and risk appetite, with lower values indicating times of stress.
- $\text{Volatility}^{\text{vix futures}}_{\{t-\Delta\to t\}}$: This volatility measure is constructed by analyzing the five-minute returns of VIX futures during the previous weekly expiration cycle.
- $\text{OFR}^{\text{credit}}_t$: Higher values (pessimistic state) indicate that credit market functioning is disrupted.
- $\log(\text{Stock VIX}_t)$: CBOE VIX index (30-day). Reflects the cost of S&P 500 put protection.

The "Wald" column refers to the one-sided p-value from the test of the hypothesis $\overline{\rho}_{\{\mathcal{F}_t\in \mathbb{s}_{\text{bad}}\}} = \overline{\rho}_{\{\mathcal{F}_t\in \mathbb{s}_{\text{good}}\}}$ versus $\overline{\rho}_{\{\mathcal{F}_t\in \mathbb{s}_{\text{bad}}\}} > \overline{\rho}_{\{\mathcal{F}_t\in \mathbb{s}_{\text{good}}\}}$. There are a total of 630 expiration cycles from January 28, 2011, to February 24, 2023. Bootstrap confidence intervals that do not bracket zero are indicated by "*" and statistical significance of predictive coefficients are indicated by "•."

	Mean	$\mathbb{1}_{\{\text{positive}\}}$ (%)	Min.	Max.
Stock-bond correlation ($\rho_{t+\Delta}$)	$\underset{[-0.35\quad -0.21]}{\mathbf{-0.28}^*}$	13.5	-0.78	0.57

		Regression specification in equation (3)				Predictive regressions $\rho_{t+\Delta} = \mathsf{c}_0 + \mathsf{c}\times\mathcal{F}_t + e_{t+\Delta}$		
$\mathcal{F}_t$ variable	CORR	$\overline{\rho}_{\{\mathcal{F}_t\in \mathbb{s}_{\text{bad}}\}}$	$\overline{\rho}_{\{\mathcal{F}_t\in \mathbb{s}_{\text{normal}}\}}$	$\overline{\rho}_{\{\mathcal{F}_t\in \mathbb{s}_{\text{good}}\}}$	Wald p-val.	c	NW[p]	$\overline{R}^2_{\text{predictive}}$ (%)
$\text{OFR}^{\text{safe asset}}_t$	-0.39	-0.38	-0.33	-0.14	(0.00)	-0.45•	(0.00)	14.8
$\log(1/\text{CDX}^{\text{high yield}}_t)$	-0.38	-0.43	-0.32	-0.24	(0.00)	-1.81•	(0.00)	14.7
$\log(\text{CDX}^{\text{investment grade}}_t)$	-0.37	-0.43	-0.29	-0.27	(0.00)	-0.31•	(0.00)	13.6
Minus of inflation swap_t	-0.27	-0.38	-0.31	-0.27	(0.00)	-0.07•	(0.00)	7.0
$\log(\text{VIX futures}_t)$	-0.21	-0.37	-0.34	-0.26	(0.00)	-0.15•	(0.00)	4.0
$\text{OFR}^{\text{equity valuation}}_t$	-0.20	-0.31	-0.31	-0.23	(0.09)	-0.13•	(0.01)	4.0
$\text{Volatility}^{\text{vix futures}}_{\{t-\Delta\to t\}}$	-0.19	-0.36	-0.27	-0.22	(0.00)	-0.21•	(0.00)	3.4
$\text{OFR}^{\text{credit}}_t$	-0.14	-0.32	-0.28	-0.25	(0.10)	-0.06	(0.12)	1.7
$\log(\text{Stock VIX}_t)$	-0.05	-0.30	-0.29	-0.26	(0.18)	-0.03	(0.53)	0.1

Table 7: **Small maturity data moments for extant models to match**

This table displays the summary statistics of the data used in the Kalman filtering estimation. All reported summary statistics are based on matched weekly expiring options (Friday PM initiation to subsequent Friday PM expiration) on futures on the 10-year Treasury bond and the S&P 500 index. For absolute delta fixed to 7 and 20, we compute $\frac{\text{put}_t[K^{\mathbf{b}}]}{F_t^{\mathbf{b}} B_t^{t+\Delta}\Delta}$, $\frac{\text{call}_t[K^{\mathbf{b}}]}{F_t^{\mathbf{b}} B_t^{t+\Delta}\Delta}$, $\frac{\text{put}_t[K^{\mathbf{s}}]}{F_t^{\mathbf{s}} B_t^{t+\Delta}\Delta}$, and $\frac{\text{call}_t[K^{\mathbf{s}}]}{F_t^{\mathbf{s}} B_t^{t+\Delta}\Delta}$. Additionally, we construct seven-day VIX as in equation (25). The realized volatilities (annualized, %) are based on high-frequency futures return data as in equation (22). The sample period is January 28, 2011, to February 24, 2023, comprising 630 expiration cycles.

Panel A: Descriptive statistics of data

	δ	Mean	SD	Min.	Percentiles 5^{th}	50^{th}	95^{th}	Max.
$\frac{\text{put}_t[K^{\mathbf{b}}]}{F_t^{\mathbf{b}} B_t^{t+\Delta}\Delta}$	-7	0.025	0.026	0.006	0.006	0.013	0.081	0.152
$\frac{\text{put}_t[K^{\mathbf{b}}]}{F_t^{\mathbf{b}} B_t^{t+\Delta}\Delta}$	-20	0.061	0.042	0.006	0.013	0.049	0.149	0.277
$\frac{\text{call}_t[K^{\mathbf{b}}]}{F_t^{\mathbf{b}} B_t^{t+\Delta}\Delta}$	20	0.060	0.043	0.006	0.013	0.047	0.142	0.348
$\frac{\text{call}_t[K^{\mathbf{b}}]}{F_t^{\mathbf{b}} B_t^{t+\Delta}\Delta}$	7	0.024	0.026	0.003	0.006	0.013	0.074	0.271
$\frac{\text{put}_t[K^{\mathbf{s}}]}{F_t^{\mathbf{s}} B_t^{t+\Delta}\Delta}$	-7	0.123	0.173	0.009	0.015	0.067	0.384	1.839
$\frac{\text{put}_t[K^{\mathbf{s}}]}{F_t^{\mathbf{s}} B_t^{t+\Delta}\Delta}$	-20	0.221	0.218	0.024	0.044	0.155	0.586	2.092
$\frac{\text{call}_t[K^{\mathbf{s}}]}{F_t^{\mathbf{s}} B_t^{t+\Delta}\Delta}$	20	0.139	0.193	0.003	0.009	0.071	0.483	2.070
$\frac{\text{call}_t[K^{\mathbf{s}}]}{F_t^{\mathbf{s}} B_t^{t+\Delta}\Delta}$	7	0.050	0.122	0.002	0.002	0.010	0.228	1.681
$\text{VIX}_t^{\mathbf{b}}$ (%)		4.6	1.8	1.8	2.6	4.2	8.0	14.2
$\text{VIX}_t^{\mathbf{s}}$ (%)		16.2	9.4	5.7	7.6	13.7	32.1	115.6
$\text{rv}^{\mathbf{b},\mathbb{P}}_{\{t\to t+\Delta\}}$ (%)		3.4	1.3	1.4	2.0	3.0	5.7	12.3
$\text{rv}^{\mathbf{s},\mathbb{P}}_{\{t\to t+\Delta\}}$ (%)		11.3	7.4	2.9	4.8	9.4	22.3	85.9

Panel B: Correlation matrix

	δ	$\frac{\text{put}[K^{\mathbf{b}}]}{F_t^{\mathbf{b}} B_t^{t+\Delta}\Delta}$ -7	$\frac{\text{put}_t[K^{\mathbf{b}}]}{F_t^{\mathbf{b}} B_t^{t+\Delta}\Delta}$ -20	$\frac{\text{call}_t[K^{\mathbf{b}}]}{F_t^{\mathbf{b}} B_t^{t+\Delta}\Delta}$ 20	$\frac{\text{call}_t[K^{\mathbf{b}}]}{F_t^{\mathbf{b}} B_t^{t+\Delta}\Delta}$ 7	$\frac{\text{put}_t[K^{\mathbf{s}}]}{F_t^{\mathbf{s}} B_t^{t+\Delta}\Delta}$ -7	$\frac{\text{put}_t[K^{\mathbf{s}}]}{F_t^{\mathbf{s}} B_t^{t+\Delta}\Delta}$ -20	$\frac{\text{call}_t[K^{\mathbf{s}}]}{F_t^{\mathbf{s}} B_t^{t+\Delta}\Delta}$ 20	$\frac{\text{call}_t[K^{\mathbf{s}}]}{F_t^{\mathbf{s}} B_t^{t+\Delta}\Delta}$ 7	$\text{VIX}_t^{\mathbf{b}}$	$\text{VIX}_t^{\mathbf{s}}$	$\text{rv}^{\mathbf{b},\mathbb{P}}_{\{t\to t+\Delta\}}$
$\frac{\text{put}_t[K^{\mathbf{b}}]}{F_t^{\mathbf{b}} B_t^{t+\Delta}\Delta}$	-20	0.92										
$\frac{\text{call}_t[K^{\mathbf{b}}]}{F_t^{\mathbf{b}} B_t^{t+\Delta}\Delta}$	20	0.88	0.91									
$\frac{\text{call}_t[K^{\mathbf{b}}]}{F_t^{\mathbf{b}} B_t^{t+\Delta}\Delta}$	7	0.85	0.84	0.90								
$\frac{\text{put}_t[K^{\mathbf{s}}]}{F_t^{\mathbf{s}} B_t^{t+\Delta}\Delta}$	-7	0.42	0.41	0.47	0.53							
$\frac{\text{put}_t[K^{\mathbf{s}}]}{F_t^{\mathbf{s}} B_t^{t+\Delta}\Delta}$	-20	0.46	0.45	0.52	0.56	0.98						
$\frac{\text{call}_t[K^{\mathbf{s}}]}{F_t^{\mathbf{s}} B_t^{t+\Delta}\Delta}$	20	0.48	0.46	0.52	0.57	0.96	0.97					
$\frac{\text{call}_t[K^{\mathbf{s}}]}{F_t^{\mathbf{s}} B_t^{t+\Delta}\Delta}$	7	0.41	0.39	0.45	0.50	0.94	0.91	0.95				
$\text{VIX}_t^{\mathbf{b}}$		0.92	0.94	0.94	0.90	0.48	0.52	0.53	0.46			
$\text{VIX}_t^{\mathbf{s}}$		0.49	0.48	0.53	0.58	0.95	0.97	0.97	0.91	0.55		
$\text{rv}^{\mathbf{b},\mathbb{P}}_{\{t\to t+\Delta\}}$		0.74	0.73	0.75	0.72	0.45	0.49	0.48	0.43	0.77	0.51	
$\text{rv}^{\mathbf{s},\mathbb{P}}_{\{t\to t+\Delta\}}$		0.45	0.44	0.50	0.56	0.81	0.82	0.80	0.75	0.49	0.82	0.63

Table 8: **Estimation results by Kalman filtering and quasi-maximum likelihood**

This table presents the results obtained from estimating the model using the quasi-maximum likelihood and Kalman filter methods. Each estimate is accompanied by its corresponding asymptotic t-statistic, which is calculated based on a central finite difference approach. The model is described by equation (30), which includes 14 measurement equations. There are eight standard deviations that account for the measurement errors. The data used for estimation consists of weekly option prices, ranging from Friday to Friday, for the 10-year Treasury bond and the S&P 500 index. The sample period spans 630 expiration cycles, starting on January 28, 2011, and ending on February 24, 2023.

Panel A: Estimated time-series of $[\lambda_t^{[\text{good}],\mathbb{P}}, \lambda_t^{[\text{bad}],\mathbb{P}}, V_t^{\mathbf{b}}, V_t^{\mathbf{s}}]'$

			Percentiles			
	Mean	Min.	25^{th}	50^{th}	75^{th}	Max.
$\lambda_t^{[\text{good}],\mathbb{P}}$	0.72	0.12	0.32	0.53	0.93	3.58
$\lambda_t^{[\text{bad}],\mathbb{P}}$	0.08	0.02	0.04	0.06	0.10	0.62
$\sqrt{V_t^{\mathbf{b}}} \times 100$	0.04	0.00	0.00	0.00	0.00	3.37
$\sqrt{V_t^{\mathbf{s}}} \times 100$	10.64	1.33	6.29	8.78	12.84	85.49

Panel B: Model parameters

	$\mu^{\mathbf{b}-,\mathbb{Q}}$	$\mu^{\mathbf{b}+,\mathbb{Q}}$		$\mu^{\mathbf{s}-,\mathbb{Q}}$	$\mu^{\mathbf{s}+,\mathbb{Q}}$			
Estimate	0.0072	0.0069		0.0260	0.0180			
t-statistic	[2.16]	[9.59]		[7.49]	[1.95]			
	$\mu^{\mathbf{b}-,\mathbb{P}}$	$\mu^{\mathbf{b}+,\mathbb{P}}$		$\mu^{\mathbf{s}-,\mathbb{P}}$	$\mu^{\mathbf{s}+,\mathbb{P}}$			
Estimate	0.0207	0.1241		0.1257	0.0000			
t-statistic	[3.99]	[7.10]		[25.07]	[6.96]			
	$\theta^{\mathbb{P}}_{\text{good}}$	$\kappa^{\mathbb{P}}_{\text{good}}$	σ_{good}		$\theta^{\mathbb{P}}_{\text{bad}}$	$\kappa^{\mathbb{P}}_{\text{bad}}$	σ_{bad}	
Estimate	2.03	0.03	1.06		1.17	12.83	1.06	
t-statistic	[3.07]	[7.15]	[2.38]		[16.08]	[11.21]	[30.81]	
	$\theta^{\mathbb{P}}_{\mathbf{b}}$	$\kappa^{\mathbb{P}}_{\mathbf{b}}$	$\sigma_{\mathbf{b}}$		$\theta^{\mathbb{P}}_{\mathbf{s}}$	$\kappa^{\mathbb{P}}_{\mathbf{s}}$	$\sigma_{\mathbf{s}}$	
Estimate	0.000	80.0	0.43		0.000	80.0	0.43	
t-statistic	[0.12]	[3.92]	[3.02]		[1.56]	[5.26]	[2.37]	
	χ^{good}	χ^{bad}		ρ^{good}	ρ^{bad}			
Estimate	3.01	5.23		2.5E-06	1.5E-06		$\mathcal{L}[\Theta]$	
t-statistic	[1.60]	[4.08]		[0.00]	[0.00]		23,034	
	Ω_1^{cov}	Ω_2^{rv}	Ω_3^{7bond}	Ω_4^{7stock}	Ω_5^{20bond}	$\Omega_6^{\text{20stock}}$	$\Omega_7^{\text{bondvix}}$	$\Omega_8^{\text{stockvix}}$
Estimate	0.0018	0.0010	0.0099	0.1216	0.0184	0.1631	0.0005	0.0517
t-statistic	[82.19]	[71.77]	[35.66]	[35.18]	[69.01]	[32.43]	[18.24]	[71.64]

Table 9: **Dynamic model performance for stock and bond volatilities**

This table shows properties of the actual and model-implied variables. Dynamic model performance is measured by the regression $\log(\text{actual}_t) = \mathbb{a} + \mathbb{b}\log(\text{model}_t) + \widetilde{e}_t$, with the inclusion of a constant term (not reported in table). Reported statistics are based on matched weekly expiring options (Friday initiation to subsequent Friday expiration). We compute the 95% confidence intervals on the mean of the variable, displayed in square brackets, using the stationary bootstrap procedure. The sample period is January 28, 2011, to February 24, 2023, comprising 630 expiration cycles. The units of volatility and VIX are annualized percentages.

			Percentiles			MAE	Regression in logs		
		Mean	25^{th}	50^{th}	75^{th}	$\lvert\log(\frac{\text{model}_t}{\text{actual}_t})\rvert \times 100$	$\mathbb{b}$	NW[p]	$\overline{R}^2_{\text{model}}$ (%)
Bond futures volatility	actual	3.4 [3.0 3.7]	2.5	3.0	3.9				
	model	3.7	2.7	3.4	4.4	18	0.84	(0.00)	65
Stock volatility	actual	11.3 [9.6 13.1]	6.9	9.4	13.5				
	model	11.3	6.9	9.4	13.5	0	1.00	(0.00)	100
Bond futures VIX	actual	4.6 [4.1 5.2]	3.3	4.2	5.5				
	model	5.1	3.8	4.7	6.1	12	1.07	(0.00)	95
Stock VIX	actual	16.2 [13.8 18.8]	10.3	13.7	18.8				
	model	19.9	14.6	17.8	22.8	32	1.08	(0.00)	66

Table 10: **Dynamic model performance and absolute pricing errors ($|\log(\frac{\mathbf{model}_t}{\mathbf{actual}_t})|$)**

This table displays results based on the actual and model-implied volatilities derived from the weekly options prices. Dynamic model performance is measured by the regression $\log(\text{actual}_t) = \mathbb{a} + \mathbb{b}\log(\text{model}_t) + \widetilde{e}_t$, with the inclusion of a constant term (not reported in table). Reported statistics are based on matched weekly expiring options (Friday PM initiation to subsequent Friday PM expiration) on futures on the 10-year Treasury bond and the S&P 500 index. The sample period is January 28, 2011, to February 24, 2023, comprising 630 expiration cycles.

		Mean	Percentiles			MAE	Regression in logs		
			25th	50th	75th	$\lvert\log(\frac{\text{model}_t}{\text{actual}_t})\rvert \times 100$	$\mathbb{b}$	NW[p]	$\overline{R}^2_{\text{model}}$ (%)
Panel A: Options on the 10-year Treasury bond futures									
-7 delta put: implied volatility	actual	5.7 [5.1 6.4]	4.5	5.3	6.4				
	model	5.8	4.8	5.7	6.6	7	1.09	(0.00)	92
-20 delta put: implied volatility	actual	5.4 [4.7 6.0]	4.0	5.0	6.3				
	model	5.0	3.7	4.4	5.8	10	0.91	(0.00)	92
20 delta call: implied volatility	actual	5.3 [4.7 5.8]	4.0	4.9	6.2				
	model	4.9	3.8	4.4	5.6	11	0.99	(0.00)	86
7 delta call: implied volatility	actual	5.6 [5.2 6.1]	4.5	5.3	6.4				
	model	5.8	5.0	5.6	6.5	8	1.16	(0.00)	90
Panel B: Options on the S&P 500 index									
-7 delta put: implied volatility	actual	20.1 [17.8 22.3]	14.9	17.8	22.8				
	model	20.2	16.8	18.9	22.2	20	1.03	(0.00)	45
-20 delta put: implied volatility	actual	17.6 [15.2 20.1]	12.2	15.3	20.7				
	model	17.3	12.8	15.3	19.4	23	0.85	(0.00)	47
20 delta call: implied volatility	actual	13.6 [11.2 16.1]	8.4	11.2	16.0				
	model	13.3	10.1	12.0	15.1	33	0.85	(0.00)	28
7 delta call: implied volatility	actual	14.0 [12.2 15.8]	10.2	11.6	15.1				
	model	15.9	13.5	15.2	17.6	31	0.99	(0.00)	30

Table 11: **Small maturity phenomena and model versus actual** $\log(\frac{\text{VVIX}_t}{\text{VIX}^{\mathfrak{s}}_t})$ **and 7DTE VIX futures**

The sample period covers 384 VIX option expiration cycles, from October 16, 2015, to February 17, 2023, with calculations performed from Friday close to Friday close. Each Friday, we construct the 11-day VVIX_t, according to (35), as the weekly VIX options expiration cycle is Tuesday to Tuesday. The model-based F_t^{vix} and VVIX_t are computed using (33) and (36), with input values obtained from the Kalman filtering estimation. Dynamic model performance is measured by the regression $\log(\text{actual}_t) = \mathbb{a} + \mathbb{b}\log(\text{model}_t) + \widetilde{e}_t$, with the inclusion of a constant term (not reported in table). The following regression decomposes $\log(\frac{\text{VVIX}_{t+\Delta}}{\text{VIX}^{\mathfrak{s}}_{t+\Delta}})$ into its components in different economic states:

$$\log(\frac{\text{VVIX}_{t+\Delta}}{\text{VIX}^{\mathfrak{s}}_{t+\Delta}}) = \overline{\omega}_{\{\mathcal{F}_t \in \mathfrak{s}_{\text{bad}}\}} \times \mathbb{1}_{\{\mathcal{F}_t \in \mathfrak{s}_{\text{bad}}\}} + \overline{\omega}_{\{\mathcal{F}_t \in \mathfrak{s}_{\text{normal}}\}} \times \mathbb{1}_{\{\mathcal{F}_t \in \mathfrak{s}_{\text{normal}}\}} + \overline{\omega}_{\{\mathcal{F}_t \in \mathfrak{s}_{\text{good}}\}} \times \underbrace{\mathbb{1}_{\{\mathcal{F}_t \in \mathfrak{s}_{\text{good}}\}}}_{\text{indicator variable}} + \underbrace{\epsilon_{\{t+\Delta\}}}_{\text{error term}}.$$

The "Wald" column refers to the one-sided p-value from the test of the hypothesis $\overline{\omega}_{\{\mathcal{F}_t \in \mathfrak{s}_{\text{bad}}\}} = \overline{\omega}_{\{\mathcal{F}_t \in \mathfrak{s}_{\text{good}}\}}$ versus $\overline{\omega}_{\{\mathcal{F}_t \in \mathfrak{s}_{\text{bad}}\}} > \overline{\omega}_{\{\mathcal{F}_t \in \mathfrak{s}_{\text{good}}\}}$. The variable definitions for the predictive variables are described in the note to Table 6.

			Percentiles			MAE	Regression in logs		
		Mean	25th	50th	75th	$\lvert\log(\frac{\text{model}_t}{\text{actual}_t})\rvert$ (%)	$\mathbb{b}$	NW[p]	$\overline{R}^2_{\text{model}}$ (%)
$\log(\frac{\text{VVIX}_t}{\text{VIX}^{\mathfrak{s}}_t})$	actual	1.8 [1.6 1.9]	1.6	1.8	2.0				
	model	1.7	1.2	1.9	2.3	46	0.32	(0.00)	49
F_t^{vix}	actual	19.4 [16.2 22.7]	13.9	17.6	23.4				
	model	16.1	11.0	13.5	18.9	26	0.66	(0.00)	56

		Regression specification				Predictive regressions $\log(\frac{\text{VVIX}_{t+\Delta}}{\text{VIX}^{\mathfrak{s}}_{t+\Delta}}) = \mathsf{c}_0 + \mathsf{c} \times \mathcal{F}_t + e_{t+\Delta}$		
$\mathcal{F}_t$ variable		$\overline{\omega}_{\{\mathcal{F}_t \in \mathfrak{s}_{\text{bad}}\}}$	$\overline{\omega}_{\{\mathcal{F}_t \in \mathfrak{s}_{\text{normal}}\}}$	$\overline{\omega}_{\{\mathcal{F}_t \in \mathfrak{s}_{\text{good}}\}}$	Wald p-val.	c	NW[p]	$\overline{R}^2$ (%)
$\text{OFR}^{\text{credit}}$	actual	1.45	1.87	1.99	(0.00)	-0.48	(0.00)	45.2
	model	1.20	1.91	2.06	(0.00)	-0.86	(0.00)	30.3
log(VIX futures)	actual	1.63	1.85	2.06	(0.00)	-0.62	(0.00)	44.8
	model	1.40	1.87	2.33	(0.00)	-1.44	(0.00)	43.5
$\log(1/\text{CDX}^{\text{high yield}})$	actual	1.63	1.93	1.97	(0.00)	-4.61	(0.00)	29.6
	model	1.48	2.03	2.18	(0.00)	-10.76	(0.00)	29.9
$\log(\text{CDX}^{\text{investment grade}})$	actual	1.66	1.92	1.95	(0.00)	-0.73	(0.00)	28.5
	model	1.51	2.05	2.13	(0.00)	-1.64	(0.00)	26.4
$\text{OFR}^{\text{equity valuation}}$	actual	1.49	1.92	1.89	(0.00)	-0.33	(0.00)	15.5
	model	1.30	1.80	2.06	(0.00)	-0.76	(0.00)	17.5
Minus of inflation swap	actual	1.67	1.93	1.94	(0.00)	-0.10	(0.01)	11.2
	model	1.57	2.08	1.92	(0.04)	-0.12	(0.36)	2.4
$\text{Volatility}^{\text{vix futures}}$	actual	1.72	1.80	1.78	(0.38)	-0.17	(0.22)	1.1
	model	1.33	1.90	1.93	(0.00)	-1.36	(0.00)	18.2
$\text{OFR}^{\text{safe asset}}$	actual	1.74	1.90	1.67	(0.48)	0.10	(0.57)	0.1
	model	1.66	2.08	1.43	(0.23)	0.19	(0.63)	0.0

Table 12: **Model-based and actual stock-bond association**

All reported summary statistics are based on matched weekly expiring options (Friday PM initiation to subsequent Friday PM expiration) on futures on the 10-year Treasury bond and the S&P 500 index. The sample period is January 28, 2011, to February 24, 2023, comprising 630 expiration cycles. In this table, $e_t = \text{model}_t - \text{actual}_t$. The model calculations for $\rho_t^{r^{\mathbf{s}},r^{\mathbf{b}}}$ are based on (38)–(40). $\mathbb{1}_{\{\text{same}\}}$ is the frequency that the actual and model values have the same sign. We employ predictive regressions with actual (model) values as the dependent (explanatory) variable and report the $\overline{R}^2_{\text{model}}$. For the purpose of comparison, we perform respective predictability regression tests equivalent to those in Table 6. We use the actual $\rho_t^{r^{\mathbf{s}},r^{\mathbf{b}}}$ as the dependent variable and identify the highest $\overline{R}^2$ value (as $\overline{R}^2_{\text{highest}}$) amongst the 11 variables.

			Percentiles					Predictive regressions	
		Mean	25^{th}	50^{th}	75^{th}	$\lvert e_t \rvert$	$\mathbb{1}_{\{\text{same}\}}$ (%)	$\overline{R}^2_{\text{model}}$ (%)	$\overline{R}^2_{\text{highest}}$ (%)
$\rho_t^{r^{\mathbf{s}},r^{\mathbf{b}}}$	actual	-0.28 $[-0.35\ -0.21]$	-0.47	-0.32	-0.13				14.8
	model	-0.20	-0.25	-0.20	-0.16	0.24	86	5.3	

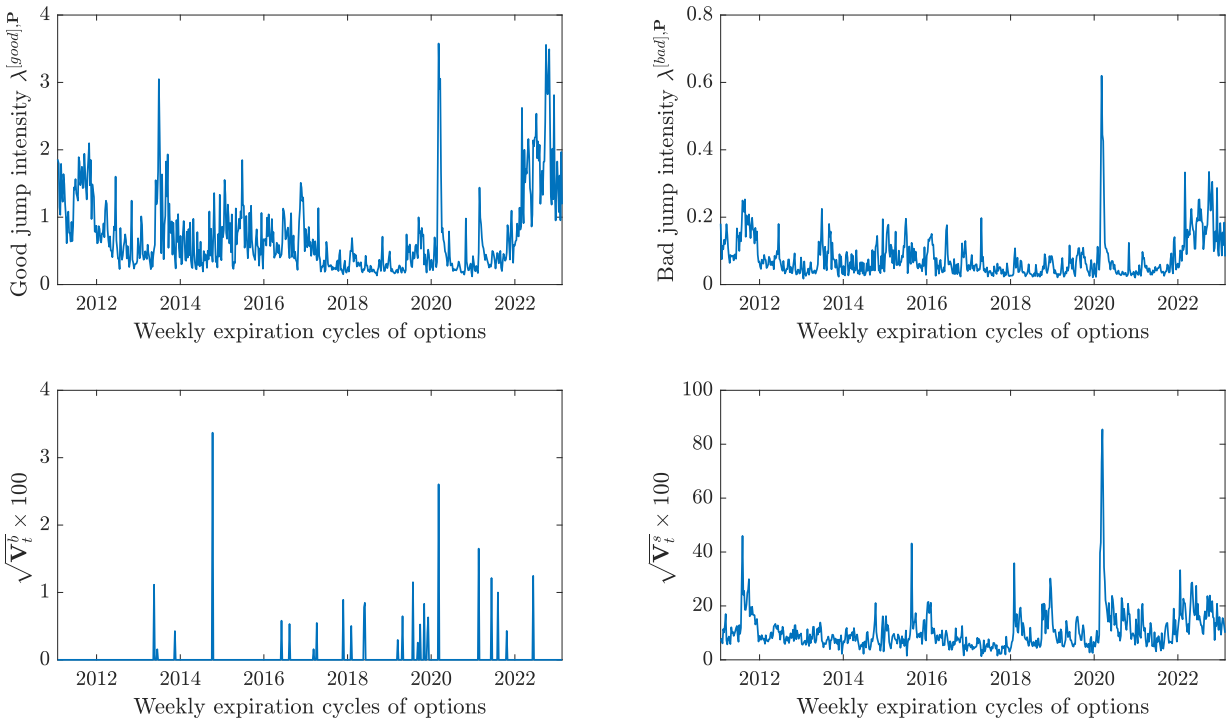

Figure 1: **Time-series of estimates of stochastic jump intensities and diffusive variances**

This plot is based on matched weekly options (Friday to Friday) on futures on the 10-year Treasury bond and the S&P 500 index. The sample period is January 28, 2011, to February 24, 2023, comprising 630 expiration cycles. The model in state-space form is presented in equation (29).

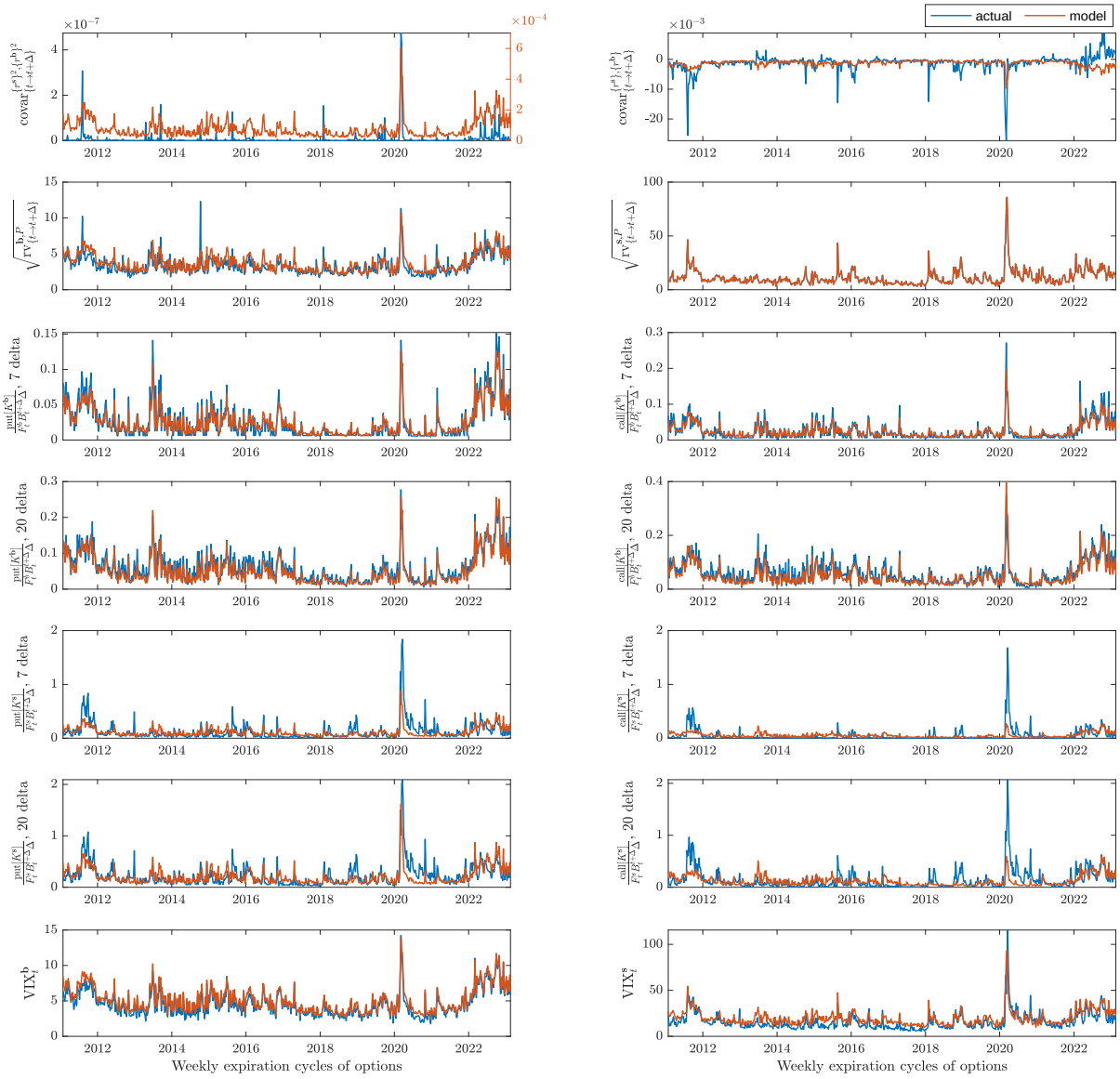

Figure 2: **Time-series of model fit to quantities in the measurement equations**

This plot is based on matched weekly options (Friday to Friday) on futures on the 10-year Treasury bond and the S&P 500 index. The sample period is January 28, 2011, to February 24, 2023, comprising 630 expiration cycles. The model in state-space form is presented in equation (29), and the corresponding model-based quantities are shown in equation (30).

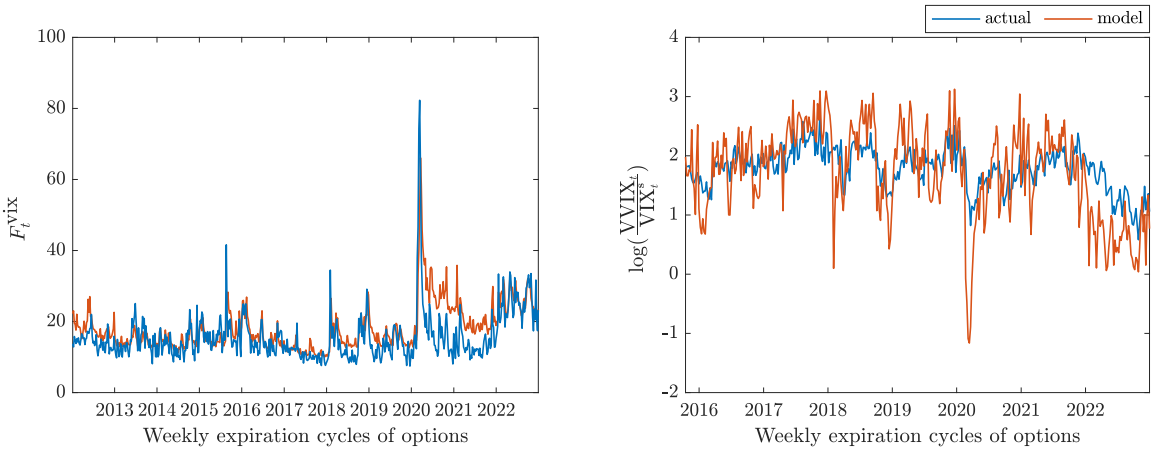

Figure 3: **Time-series of model fit to VIX futures price and** $\log(\frac{\text{VVIX}_t}{\text{VIX}_t^{\mathbf{s}}})$

This plot is based on 7DTE VIX futures and $\log(\frac{\text{VVIX}_t}{\text{VIX}_t^{\mathbf{s}}})$. The actual VVIX_t calculation is based on 11-day VIX option prices. We compute model-based F_t^{vix} and $\{\text{VVIX}_t\}^2$ according to (33) and (35), respectively.

Internet Appendix: Not for Publication

Abstract

Section I analyzes a setup that modifies the Merton (1976) model to allow for stochastic jump intensity. We show that this model is unable to capture the dynamic nature of small maturity stock and bond options markets (Table 3). Specifically, a single-jump intensity rate drives both puts and call prices for both stock and bond. This is inconsistent with Table 7 (Panel B).

I Merton (1976) model modified for stochastic intensity rates

We assume that the dynamics of $F_t^{\mathbf{s}}$ and $F_t^{\mathbf{b}}$ are as depicted in equation (11). Then, the covariance between bond call payoff and stock put payoff, for small option maturity Δ, is

$$\mathrm{Cov}_t^{\mathbb{P}}([\frac{F_{t+\Delta}^{\mathbf{b}}}{F_t^{\mathbf{b}}}-k^{\mathbf{b}}]^+,[k^{\mathbf{s}}-\frac{F_{t+\Delta}^{\mathbf{s}}}{F_t^{\mathbf{s}}}]^+) \sim \lambda_t^{\mathbb{P}}\,\Delta\int_{\log(k^{\mathbf{b}})}^{\infty}\int_{-\infty}^{\log(k^{\mathbf{s}})}(e^{x^{\mathbf{b}}}-k^{\mathbf{b}})(k^{\mathbf{s}}-e^{x^{\mathbf{s}}})\,\mathbb{p}[x^{\mathbf{s}},x^{\mathbf{b}}]\,dx^{\mathbf{s}}\,dx^{\mathbf{b}}. \tag{I-1}$$

The term $\int_{\log(k^{\mathbf{b}})}^{\infty}\int_{-\infty}^{\log(k^{\mathbf{s}})}(e^{x^{\mathbf{b}}}-k^{\mathbf{b}})(k^{\mathbf{s}}-e^{x^{\mathbf{s}}})\,\mathbb{p}[x^{\mathbf{s}},x^{\mathbf{b}}]\,dx^{\mathbf{s}}\,dx^{\mathbf{b}}$ is of one sign since it is a constant.

Assuming that the jump size is distributed normal with mean $\mu_x-\frac{1}{2}\sigma_x^2$ and variance σ_x^2, the analog of our Result 1 for OTM options, for small option maturity Δ, is

$$\mathrm{put}_t[K^{\mathbf{b}}] \;\sim\; F_t^{\mathbf{b}}\,B_t^{t+\Delta}\,\lambda_t^{\mathbb{Q}}\,\Delta\,\{k^{\mathbf{b}}\,\mathcal{N}(-d_2[k^{\mathbf{b}}])-e^{\mu_x}\mathcal{N}(-d_1[k^{\mathbf{b}}])\} \qquad \text{and} \tag{I-2}$$

$$\mathrm{call}_t[K^{\mathbf{b}}] \;\sim\; F_t^{\mathbf{b}}\,B_t^{t+\Delta}\,\lambda_t^{\mathbb{Q}}\,\Delta\,\{e^{\mu_x}\mathcal{N}(d_1[k^{\mathbf{b}}])-k^{\mathbf{b}}\,\mathcal{N}(d_2[k^{\mathbf{b}}])\}, \tag{I-3}$$

where $\mathcal{N}(.)$ denotes the standard normal cumulative distribution function, and

$$d_1[k^{\mathbf{b}}] \;=\; \frac{-\log(k^{\mathbf{b}})+\mu_x+\frac{1}{2}(\sigma_x)^2}{\sigma_x} \qquad \text{and} \qquad d_2[k^{\mathbf{b}}] \;=\; d_1[k^{\mathbf{b}}]\;-\;\sigma_x. \tag{I-4}$$

Analogously for options on stock. Both OTM bond and stock option prices are driven by $\lambda_t^{\mathbb{Q}}$. This implies, for example, that $\mathrm{call}_t[K^{\mathbf{b}}]/F_t^{\mathbf{b}}$ and $\mathrm{put}_t[K^{\mathbf{s}}]/F_t^{\mathbf{s}}$ are perfectly correlated, which contradicts the evidence in Table 7 (Panel B). ■

Table I-1: **Properties of excess returns of buying one-day options on the 10-year Treasury bond futures and the S&P 500 index**

This table is based on matched one-day options (Thursday to Friday) on futures on the 10-year Treasury bond and the S&P 500 index. The sample period is January 28, 2011, to February 24, 2023, comprising 630 expiration cycles. Excess returns for buying options on the S&P 500 index (and bond futures) are calculated according to equations (1)–(2). Option returns are based on one-day holding period. Reported 95% stationary bootstrap confidence intervals rely on 10,000 bootstrap draws. The unit of reported average option excess return is one-day percentage. We compute the excess returns of buying OTM options on bond (stock) with fixed-option delta, denoted $\delta^{\mathbf{b}}$ ($\delta^{\mathbf{s}}$). Reported $\mathbb{1}_{\{r>0\}}$ refers to the number of one-day expiration cycles in which the excess return of the option is positive. σ is the average option-implied volatility computed at the beginning of the expiration cycle. The reported dollar open interest (respectively, volume) is the number of contracts outstanding (respectively, traded) multiplied by the underlier on Thursday close, averaged across the 630 expiration cycles. Stationary bootstrap confidence intervals that do not bracket zero are indicated by "*."

Panel A: Buying one-day options on the 10-year Treasury bond futures

	Puts on bond		Bond	Calls on bond	
Bond option delta: $\delta^{\mathbf{b}}$ (%)	-7	-20	straddle	20	7
OTM moneyness (%)	1	0.5		0.5	1
Average options excess return (one-day, %)	-77*	-73*	-29*	-21*	-31*
Bootstrap CI: [Lower Upper]	[-89 -62]	[-84 -60]	[-40 -16]	[-35 -5]	[-44 -16]
$\mathbb{1}_{\{r>0\}}$ (out of 630)	21	35	170	166	141
Average option price	\$18.8	\$29.5		\$116.2	\$106.8
Dollar open interest (Thursday, million)	\$2149	\$1866		\$1807	\$1906
Dollar volume (Thursday, million)	\$1306	\$1495		\$1478	\$1236
Option-implied volatility (σ, %)	8.1	8.0	6.4	4.8	5.0

Panel B: Buying one-day options on the S&P 500 index

	Puts on stock		Stock	Calls on stock	
Stock option delta: $\delta^{\mathbf{s}}$ (%)	-7	-20	straddle	20	7
OTM moneyness (%)	3	1.5		1.5	3
Average options excess return (one-day, %)	-49*	-40*	-20*	-20	-60*
Bootstrap CI: [Lower Upper]	[-74 -20]	[-59 -18]	[-29 -10]	[-39 0]	[-81 -37]
$\mathbb{1}_{\{r>0\}}$ (out of 630)	35	67	211	94	34
Average option price	\$2.2	\$4.3		\$3.2	\$1.3
Dollar open interest (Thursday, million)	\$1640	\$1476		\$1728	\$1689
Dollar volume (Thursday, million)	\$1403	\$1674		\$1732	\$1068
Option-implied volatility (σ, %)	23.3	20.5	18.2	17.3	18.2